THE DEVELOPMENT AND CHARACTERIZATION OF A CONTRACTILE, COMPOSITE SCAFFOLD FOR SKELETAL MUSCLE TISSUE ENGINEERING

By

DANIEL PATRICK BROWE

A dissertation submitted to the

School of Graduate Students

Rutgers, The State University of New Jersey

In partial fulfillment of the requirements

For the degree of

Doctor of Philosophy

Graduate program in Biomedical Engineering

Written under the direction of

Joseph W. Freeman, Ph.D.

And approved by

_____

_____

_____

_____

New Brunswick, New Jersey

October, 2018

ABSTRACT OF THE DISSERTATION

The Development and Characterization of a Contractile, Composite Scaffold for Skeletal Muscle Tissue Engineering

By DANIEL PATRICK BROWE

Dissertation Director:

Joseph W. Freeman, Ph.D.

Current treatments for large volume deficiencies in skeletal muscle tissue have significant drawbacks, and patients suffering from these defects would greatly benefit from a superior solution. Tissue engineers seek to develop a three-dimensional matrix that can serve as a scaffold for muscle cells to regenerate lost tissue. Although substantial progress has been made in growing myoblasts on various scaffolds and promoting fusion into myotubes, plenty of hurdles remain before these scaffolds can be considered the new gold standard treatment. Principally, current scaffolds fail to produce myotubes that are optimally organized and fully differentiated, leading to limited force production. Despite the fusion of myoblasts into myotubes, the tissue lacks some form of stimulation which occurs in the native *in vivo* environment. This stimulation may be provided by supplementing muscle force with artificial muscles, which are capable of actuation and force production with similar contractile stress to native muscle tissue.

The goal of this project is to utilize a specific type of artificial muscle, called ionic electroactive polymers, to provide electrical and mechanical stimulation to developing myoblasts on a fibrous, conductive scaffold that can provide topographical guidance cues. Thus, this contractile, composite scaffold would seek to closely mimic the *in vivo* environment of developing skeletal muscle, producing highly organized and

differentiated muscle tissue. This project has the following aims: 1) Develop and characterize a biocompatible, ionic electroactive polymer which actuates in an electric field; 2) Develop, characterize, and evaluate the ability of a conductive, fibrous scaffold to promote the organization and differentiation of myoblasts into myotubes; 3) Characterize the *in vitro* response and evaluate the effect on myoblast differentiation of combined electrical and mechanical stimulation provided by the contractile, composite scaffold resulting from the first two aims.

The movement speed and contractile force of hydrogels made from poly(ethylene glycol) diacrylate and acrylic acid were optimized, but the maximum contractile stress produced fell short of the estimated contractile stress of native muscle fibers. The biocompatibility of the hydrogels was boosted through the addition of a fibrous scaffold synthesized from a copolymer of polycaprolactone (PCL) and polypyrrole (PPy). Cell studies indicated that myoblasts have a clear preference for scaffolds with PPy-PCL compared with scaffolds made from only PCL. Myoblasts exhibited higher attachment, more proliferation, higher numbers of myotubes formed, and a higher fusion index on scaffolds made with PPy-PCL as compared with scaffolds made of PCL. The developed composite scaffold was seeded with myoblasts, and electrical stimulation was applied while the myoblasts were developing. The electrical stimulation patterns seemed to have a net negative effect on the survival of myoblasts, and there was no difference in the progress of differentiation between groups exposed to electrical stimulation and the control groups which received no stimulation. Further experiments are needed to fully control for the complexity of the stimulation patterns use, but this project provides a framework for evaluating the effects of combined stimulation on myoblast development.

ACKNOWLEDGEMENTS

As with any doctoral project, there are plenty of people and organizations that contributed to the progress of this work in different ways. First, I would like to acknowledge and thank my thesis advisor, Dr. Joseph Freeman, for allowing me to work in his lab on this project and providing guidance along the way. Thank you for your patience as I learned all of the skills needed to complete this work. I'm impressed with your ability to remain kind and understanding in the face of stress, and I'm also impressed with your basketball skills.

Next, I would also like to thank my committee members, Dr. Ronke Olabisi, Dr. Laleh Najafizadeh, and Dr. Kenneth Paradiso. To Dr. Olabisi, thank you for your candid feedback on everything from my dissertation to my ability (or lack of ability) to write a letter of recommendation. To Dr. Najafizadeh, your professionalism and expertise during our collaboration has been impressive and much appreciated. To Dr. Paradiso, thank you for your perspective, sincere feedback, and interesting conversation along the way.

Furthermore, I am grateful for the encouragement and assistance from my fellow coworkers in the musculoskeletal tissue regeneration lab and all of our collaborators and technicians. My fellow lab-mates past and present, including Emmanuel Ekwueme, Brittany Taylor, Rohit Rao, Mike Pellegrini, Push Patel, Devika Joglekar, and Shreya Rao, Brandon Newton, Amin Khalili, Adhithi Kanthan, James Cipriano, Michael D'Ecclessis, Jay Shah and others have all been excellent coworkers and friends. I appreciate the supplemental mentorship provided by the post-docs Dr. Kristin McKeon-Fischer and Dr. Tracy Scott. A number of undergraduates and summer students also provided a helping hand including Caroline Wood, Matthew Sze, Sudeepti Vedula, Swati

Patel, Caresse Simmonds, Jay Shah, Mahir Mohiuddin, Lydia Liu, and Zhilin Liu. Our collaborators greatly accelerated the progress of this project by contributing knowledge and techniques including but not limited to Dr. Nicholas Stebbins and the Uhrich Lab, Dr. Dunbar Birnie from the Materials Science Department, SEM Technician Val Starovoytov, Dr. Rick Cohen, Kris White from the Olabisi lab in the BME Department, and Yi Huang and Dr. Najafizadeh in the Electrical Engineering Department.

I am also very grateful for all of the funding received from various organizations including Rutgers University, the National Institute of Health, the National Science Foundation, and our industry partner in research, Myos Corporation. I'm especially grateful for the Biotechnology Training Program at Rutgers under grant under the Ruth L. Kirschstein National Research Service Award T32 GM8339 from the NIGMS (NIH) which was administered by Dr. Martin Yarmush and Dr. Ann Stock. For my final years of funding, I want to thank Teresa M. Delcorso-Ellmann for providing me the opportunity to work at GradFund.

For tolerating hundreds of distraught phone calls over the years and providing emotional support, I have to acknowledge my parents, Paula and Andrew Browe. They kept me stable and supported throughout the tough times and intermittent isolation of graduate school. I love you both and appreciate all you have done for me.

Finally, for all of my friends and family not already mentioned, thank you for helping me in whatever ways that you could. There were many times when the little things truly got me through the day.

DEDICATION

This dissertation is dedicated to my parents, Paula and Andrew Browe, for their unwavering love and support. You will probably never read this dissertation, and I wouldn't wish that upon you anyway!

ACKNOWLEDGEMENT OF PREVIOUS PUBLICATIONS

Sections of this dissertation have been previously published or are being prepared for publication, as listed below. In each case, permission was obtained from the authors and the publisher to reproduce the content as an academic work.

Parts of chapter 1 have been reproduced from the following book chapter:

Brown JL, Kumbar SG, Banik BL. Bio-Instructive Scaffolds for Musculoskeletal Tissue Engineering and Regenerative Medicine. Elsevier Inc: Academic Press; 2017. Chapter 8: Bio-Instructive Scaffolds for Skeletal Muscle Regeneration: Conductive Materials. Freeman JW, Browe DP. ISBN: 978-0-12-803394-4.

Chapter 2 has been published in its entirety:

Browe DP, Wood C, Sze MT, White KA, Scott T, Olabisi RM, Freeman JW. Characterization and optimization of actuating poly(ethylene glycol) diacrylate/acrylic acid hydrogels as artificial muscles. Polymer 2017; 117: 331-341.

Chapter 3 has been submitted in its entirety for publication in 'Journal of Biomedical Materials Research Part A', but was under review when this dissertation was submitted:

Browe DP, Freeman JW. Optimizing C2C12 myoblast differentiation using Polycaprolactone-Polypyrrole copolymer scaffolds. Submitted to Journal of Biomedical Materials Research Part A. (Under review).

TABLE OF CONTENTS

LIST OF TABLES

LIST OF ILLUSTRATIONS

CHAPTER 1: BACKGROUND AND INTRODUCTION

Note: Part of this chapter has been reproduced with permission from the authors as an academic work from the following publication [1]:

Brown JL, Kumbar SG, Banik BL. Bio-Instructive Scaffolds for Musculoskeletal Tissue Engineering and Regenerative Medicine. Elsevier Inc: Academic Press; 2017. Chapter 8: Bio-Instructive Scaffolds for Skeletal Muscle Regeneration: Conductive Materials. Freeman JW, Browe DP. ISBN: 978-0-12-803394-4.

1.1 Skeletal Muscle Anatomy and Physiology

Skeletal muscle accounts for roughly 35-45% of total body mass in adult humans and is responsible for voluntary body movements and the maintenance of posture [2]. Skeletal muscle is composed of muscle fibers, also called myocytes, which are created during the fusion of individual myoblasts [3]. These muscle fibers are arranged in a hierarchical organization, as shown in Figure 1.1 (below) [4]. Individual muscle fibers, with endomysium between them, are wrapped in connective tissue, called perimysium, and packaged into fascicles. These fascicles together make the whole muscle, which is sheathed in epimysium [4]. Muscles exert their force on the skeletal system through tendons, which connect muscles to bone. Blood vessels and nerves are intertwined throughout muscle between the fascicles. This hierarchical organization allows for precise, voluntary control of movement, since different nerve signals can potentially be sent to each individual fascicle [2, 3].

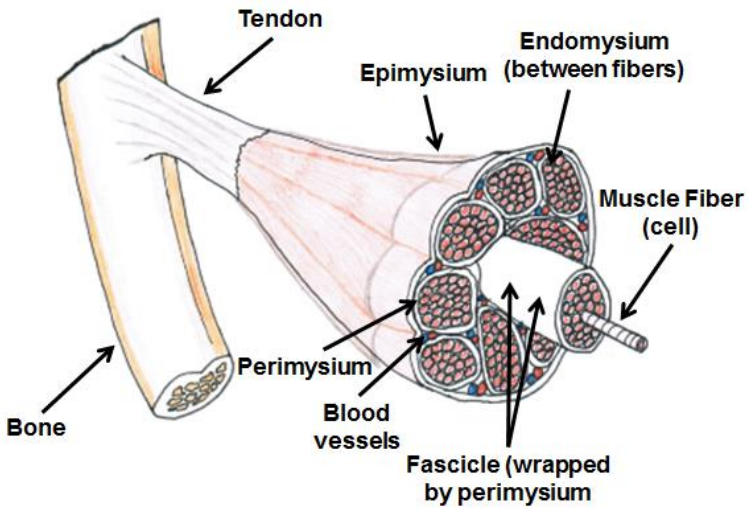

Figure 1.1: Anatomy of skeletal muscle tissue. Based on a figure from Shier and coworkers [4].

Each muscle fiber is made up of many myofibrils which contain sarcomeres, or the basic contractile unit of muscle [2, 3]. Sarcomeres have thin filaments, actin, and thick filaments, myosin, which allow contraction and relaxation by controlled binding of myosin heads to actin filaments. When a muscle is at rest, troponin and tropomyosin molecules interact with actin to prevent it from binding to myosin. Upon the excitation of skeletal muscle, motor neurons release acetylcholine across neuromuscular junctions, resulting in the depolarization of muscle tissue. The sarcoplasmic reticulum of each muscle fiber then releases ionic calcium (Ca^{2+}) into the sarcoplasm (muscle cytoplasm), which binds to troponin and leads to a conformational change in the protein. Finally, this refolding of troponin moves tropomyosin and exposes actin for myosin to bind. This entire process initiates the ATP-dependent cross-bridge cycling of actin and myosin filaments and contraction of the entire muscle on the macroscale [2, 3].

After minor injury, skeletal muscle is capable of rapidly regenerating and avoiding the loss of muscle mass [5]. Figure 1.2 (below) illustrates the stages of muscle

regeneration after a shearing injury [6]. Initially, necrosis occurs at the site of damaged fibers, and the inflammatory response is activated. During this phase, adult satellite cells become active and travel to the injury site. These muscle progenitor cells proliferate, differentiate, and fuse at the site of injury, closing the gap between fiber ends. Depending on the size of the injury, some scar tissue may remain between the newly reformed fiber ends, but for most exercise induced injuries, the entire contractile apparatus is reconstituted and functional [5, 6]. However, in the case of large volume injuries to skeletal muscle, which may be caused by trauma or aggressive tumor ablation, this regeneration process is insufficient to fully restore function [7, 8]. Satellite cells, which only comprise roughly 2-7% of all cells in adult muscle, do not have the capability to fill large voids [9, 10]. Instead, large amounts of scar tissue are formed, which interferes with muscle function.

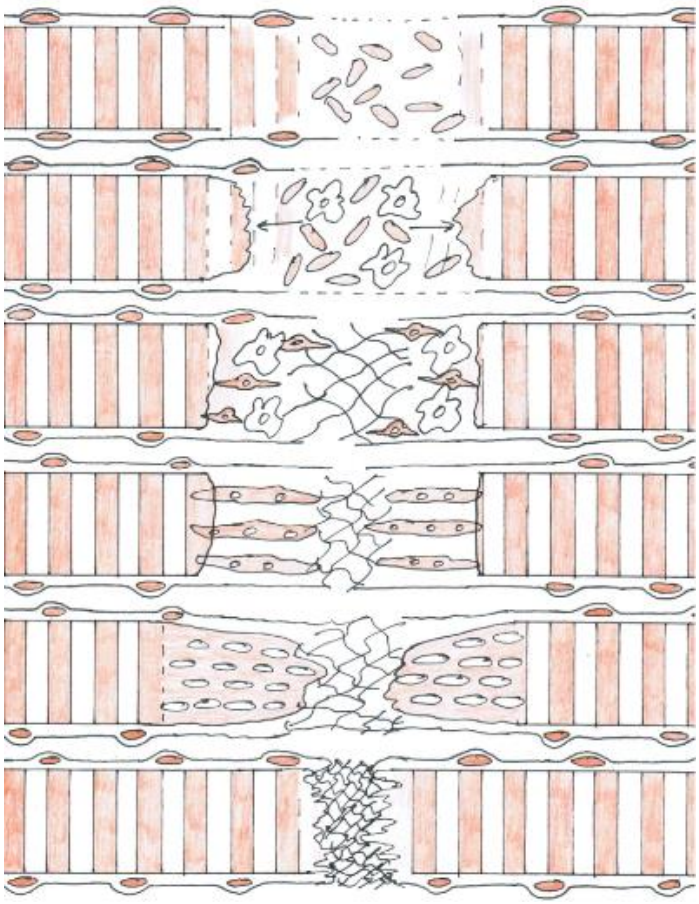

Figure 1.2: Muscle injury response. The regeneration process after a myofiber tear. Progressive images show the healing process from the initial tear, to satellite cell proliferation, differentiation to myoblasts, and fusion to the damaged fiber ends. Based on a figure from Järvinen, et al [6].

1.2 Epidemiology of Major Skeletal Muscle Injury and Current Treatment Methods

Major skeletal muscle injuries and deficiencies arise from three main sources, including traumatic injury, aggressive surgical tumor ablation, and a range of myopathies. Estimating the prevalence of major injuries to skeletal muscle due to trauma and tumor ablation is difficult because these types of injuries often result in limb amputations, which may or may not be labeled as the result of skeletal muscle injury only. Thus, using limb

amputations as an estimate of skeletal muscle injury will result in an overestimate, but it may be the best way to assess the incidence of these injuries.

In the United States alone, about 185,000 people must have a major amputation of an upper or lower limb each year [11]. The contributing factors to this number include diabetes mellitus, dysvascular disease, malignant tumors in bones, and trauma [12]. It is estimated that about 45% of these amputations are due to trauma, which amounts to about 83,000 amputations per year [12]. It is not known exactly what percentage of these amputations are due solely to skeletal muscle deficiencies, but this number still provides a reasonable estimate of skeletal muscle defects resulting from trauma.

Muscular dystrophies are a set of genetically inherited diseases distinguished by a gradual atrophying of skeletal muscle and replacement of muscle tissue by fat and fibrosis [13]. Two of the most common types of muscular dystrophy are Duchenne muscular dystrophy and Becker muscular dystrophy, which primarily affect males and have a prevalence of 1 in 3,500 male births and 1 in 18,518 male births, respectively [14, 15]. Given the population and birthrate in the United States, there are approximately 700 individuals born with these diseases each year in the United State alone [16, 17].

The current gold standard of care for large volume deficiencies in skeletal muscle is autologous transfer of muscle tissue from the donor. These can be free flaps of muscle tissue or pedicle flaps in the original blood supply is left intact while the tissue is transplanted. Good outcomes and functional recovery have been described in the forearm and elbow, but the prognosis is poor for larger defects in muscles the support the body while standing, walking, and running [18, 19]. Further, any autologous graft carries the risk of donor site morbidity and increased infection rate due to longer surgical time. For

muscular dystrophies, there are currently no viable treatments, although physical therapy and medications can slow the progression of the diseases. Thus, there is a great need for better treatment options for large volume defects in skeletal muscle tissue.

1.3 Progress of Skeletal Muscle Tissue Engineering

Tissue engineering has the potential to provide a superior treatment for large volume defects in skeletal muscle without the need for autologous tissue transfer. The field of tissue engineering focuses on regenerating tissues and organs through a process that mimics neoorganogenesis [20]. Although the ideal process is not agreed upon, the general tissue engineering paradigm is illustrated in figure 1.3 (below) [21]. First, a small quantity of muscle tissue is taken from the donor for the purpose of muscle progenitor cell isolation and expansion in culture. These cells are then seeded on some three-dimensional scaffold designed to fill the void existing in the patient. While the cells are proliferating, a variety of stimulation can be applied to the graft with the goal of providing the cells with the necessary cues to differentiate, proliferate, and organize into mature muscle tissue. Finally, the scaffold/tissue construct is implanted back into the patient to restore function [21].

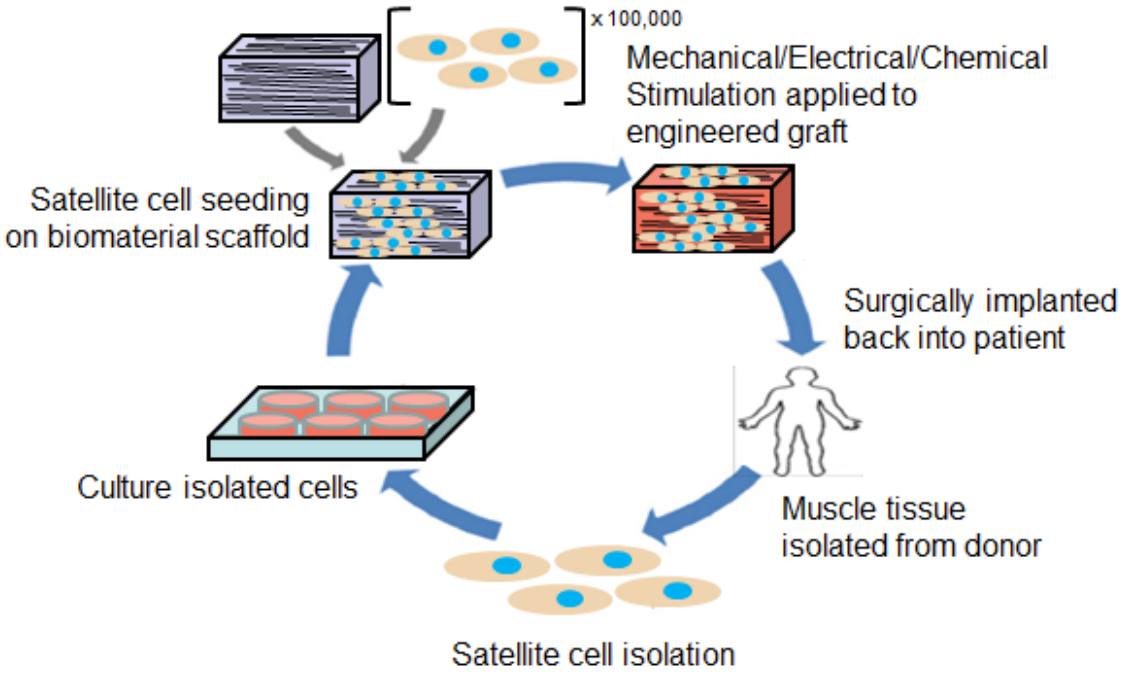

Figure 1.3: Tissue engineering paradigm. The tissue engineering paradigm for regenerating skeletal muscle tissue. Several variations on this theme exist. Based on a figure from Seidi and coworkers [21].

Regardless of the exact process used, skeletal muscle tissue engineers must meet several criteria for engineered muscle tissue [22]. The scaffold/graft must contain or facilitate the formation of a parallel alignment of muscle fibers with functioning sarcomeres. These muscle fibers must have ample intracellular calcium storage and functioning acetylcholine receptors for innervation. The *de novo* tissue must not invoke a host immune response, must integrate with surrounding muscle tissue, and needs to have functioning vasculature and peripheral nerves [22, 23]. To be considered a fully functional replacement, the new tissue must reproduce the contractile stress of native skeletal muscle and regenerate after minor, exercise-induced injuries. Although a scaffold/graft that meets all of these criteria has yet to be produced, researchers have made significant progress in meeting a subset of these criteria.

Myotubes have been grown into three-dimensional constructs as early as 1988, when primary avian myoblasts were seeded within a collagen gel matrix and fused into myotubes over the course of 3-4 weeks [24]. Many subsequent researchers have utilized a similar cells-in-gel technique in which myoblasts are embedded within a solution of extracellular matrix, typically ether collagen I or Matrigel, and then set within a mold [25-27]. Although the resulting tissue was thicker than a simple monolayer of cells, the center of the construct became necrotic when the diameter was greater than 500 μm due to limited diffusion of waste and nutrients [25]. Further, none of these constructs have been able to create measureable force when electrically stimulated [22]. This may have been due to the stiffness of the set gels or the relatively low concentration of mature myotubes.

The organization and structure of the extracellular matrix (ECM) plays an important role in the attachment, proliferation, alignment, and differentiation of myoblasts [28, 29]. Thus, many researchers have investigated aligned, fibrous scaffolds which attempt to duplicate the parallel alignment of muscle fibers in native skeletal muscle fascicles. Many studies have shown that aligned fibrous meshes are capable of providing topographical guidance cues for developing myoblasts [30-34]. Multiple studies have shown improved myoblast alignment and myotube formation on aligned fibers of various materials as compared to randomly aligned fibers of the same material [32, 33]. Significantly higher myotube alignment and length have been seen on composite collagen/poly(ε-caprolactone) meshes with aligned fibers as opposed to randomly aligned fibers [32]. Furthermore, a study utilizing composite, fibrous scaffolds of conductive polyaniline and poly(ε-caprolactone) showed enhanced myotube formation and

maturation on scaffolds of aligned polyaniline/poly(ε-caprolactone) fibers compared to both randomly aligned scaffolds and aligned poly(ε-caprolactone) scaffolds [33]. This indicates that electrical cues provided by conductive materials also influences myoblast differentiation. However, these studies fail to measure the contractile stress produced upon excitation of the resulting tissue. Similar studies that measure contractile stress in tissue engineered constructs found that these constructs can only produce about 1% of the contractile stress produced in adult muscle tissue [35, 36]. Thus, it seems that these constructs lack some form of stimulation which allows the resulting tissue to develop into more mature muscle tissue capable of greater contractile stress.

An exciting and complex area of current research in skeletal muscle tissue engineering involves investigating the application of various forms of stimulation to developing skeletal muscle tissue *in vitro*. Various mechanical stretch protocols have been examined for their effect on myoblast differentiation [37-39]. It seems that developing myoblasts are very sensitive to mechanical stretch, since many studies report negative effects on myoblast differentiation [38, 39]. However, it has been reported that a stretch protocol of 10% cyclic uniaxial strain at a frequency of 1 Hz for 24 hours has promoted myogenic differentiation on bone marrow-derived human mesenchymal stem cells [37]. Electrical stimulation has also been explored as a means of promoting myoblast differentiation with much success [40, 41]. High frequency stimulation of approximately 100 Hz with voltages of up to 50 V has been shown to increase the rate of protein production in C2C12 myoblasts, as well as improve force production and excitability [41]. In another study, lower frequency stimulation of about 1 Hz was shown to speed the production of sarcomeres, but they were unable to replicate the results at

higher frequencies (10 Hz) [40]. Continuing research focuses on finding the ideal chemical, mechanical, and electrical stimulation protocol for optimal muscle fiber differentiation and maximal force production.

1.4 Artificial Muscles: Non-Surgical Treatments for Skeletal Muscle Deficiencies

For the purposes of this document, the term "artificial muscle" refers to a group of electroactive polymers that are capable of functioning as soft actuators (actuators that have a relatively low density). Electroactive polymers respond to electrical stimulation by changing in size or shape [42]. Thus, they have potential to serve as both sensors and artificial muscles. Although there are many different types of electroactive polymers with different mechanisms of action, this project will consider only ionic electroactive polymers. Furthermore, the two subtypes of ionic electroactive polymers that will be discussed are electroactive hydrogels (EAHs) and ionic polymer-metal composites (IPMCs).

Both EAHs and IPMCs have a similar pattern and mechanism of movement when placed in an electric field (figure 1.4, below) [43]. Inside of the ionic polymer, or hydrogel, there are fixed negative charges that are attached to the polymer backbone. When swelled with water, positively-charged cations associate with water molecules by hydrogen bonds and are evenly dispersed through the hydrogel. When an electric field is applied, the positively-charged cations and associated water molecules move towards the negative electrode, causing one side of the hydrogel to swell. This swelling leads to an overall bending actuation in the construct [44]. The only difference between an EAH and an IPMC is that the IPMC has the electrodes attached directly to the ionic polymer/hydrogel while an EAH relies on external electrodes to apply the electric field.

The actuations produced by both are reversible by reversing the electric field, and the movements are repeatable [42].

Ionic electroactive polymers, especially IPMCs, have been researched for their potential to supplement muscle force in patients with skeletal muscle deficiencies. Electroactive polymers can obtain contractile forces in the range of 0.1 – 40 MPa, which is sufficient to mimic adult muscle tissue [42]. In addition, IPMCs have a low power requirement, with actuation occurring under an applied voltage as low as 1 V [42]. However, ionic electroactive polymers have a few hurdles to overcome before they can be clinically relevant. IPMCs and EAHs each suffer from the following drawbacks: a lack of consistent processing, the bending mode of actuation doesn't perfectly mimic contraction, and it will be difficult to scale-up current experimental models (typically 1-10 mm wide) to the relevant size for prosthetics [42].

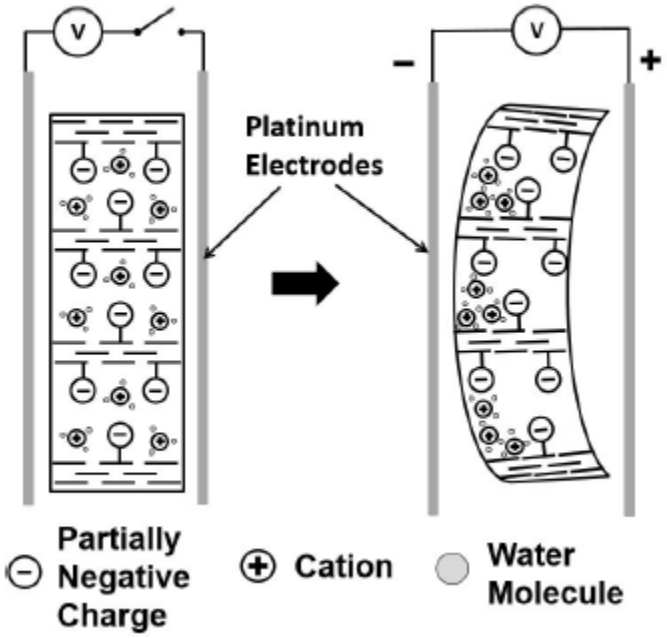

Figure 1.4: Mechanism of electroactive polymer actuation. The mechanism of operation of electroactive hydrogels and ionic polymer-metal composites. The application

of an electric field causes the flow of free ions and water towards the oppositely charged electrode, swelling one side of the hydrogel more than the other and leading to a bending actuation. Taken from a paper by Huang and coworkers with permission from the authors to reuse in an academic work [43].

1.5 Merging Artificial Muscles with Tissue Engineering

The potential application of artificial muscles within the field of skeletal muscle tissue engineering has not yet been explored. Ionic electroactive polymers function in much the same way as native muscle tissue; in both cases, the flow of ions in solution caused by some external source of depolarization or potential leads to conformational changes and actuation (bending or contraction). Given these similarities, there is plenty of potential for integrating ionic electroactive polymers with tissue engineered constructs.

In order to utilize ionic electroactive polymers to simultaneously deliver electrical and mechanical stimulation, this proposal aims to develop a biocompatible IPMC that can support cell growth while actuating in response to an electric field. The concept for this contractile, composite scaffold is illustrated in figure 1.5 below. Conductive fibers will act as electrodes in the device, and an external power source will supply the potential needed for contraction. Cells can be seeded on the conductive fibers, and the entire device can operate in culture. Thus, a combination of electrical and mechanical stimulation can be applied simultaneously to developing myoblasts while they develop *in vitro*.

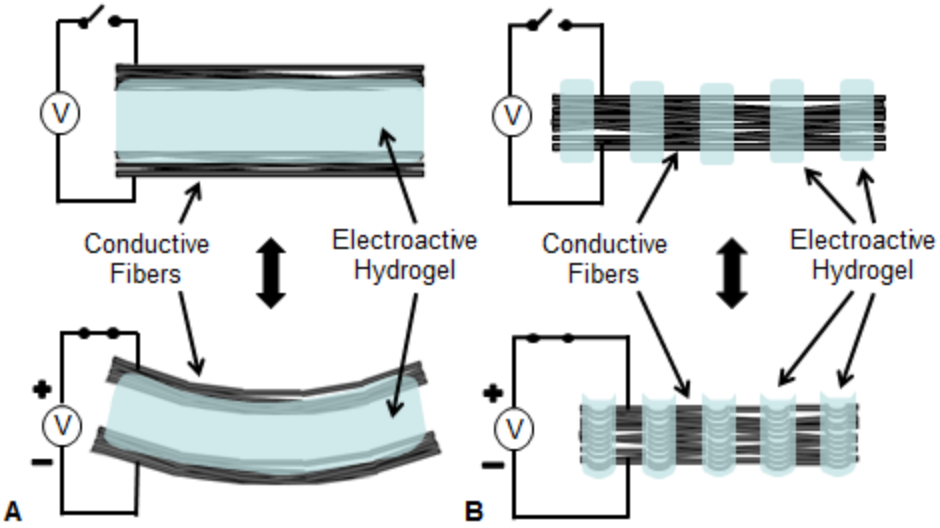

Figure 1.5: Proposed composite scaffold. Mechanism of movement in the proposed biocompatible, electroactive hydrogel. **A)** This composite scaffold works in a similar manner to the ionic polymer-metal composites described earlier, but the electrodes have been replaced by conductive polymer fibers, which can be seeded with cells and operated *in vitro*. **B)** This variation of the composite scaffold illustrates how the orientation of the electroactive hydrogel component can be adjusted to achieve different forms of movement upon electrical stimulation.

The central hypothesis of this project is that the electrical and mechanical stimulation provided by this scaffold will promote the proliferation, fusion, differentiation, and maturation of myoblasts into mature muscle fibers. A successful implementation of this project will lead to a highly novel method for applying coupled electrical and mechanical stimulation to cells *in vitro*, and will advance the field of skeletal muscle tissue engineering. Furthermore, when this contractile, composite scaffold is eventually implanted *in vivo*, it can immediately supplement muscle force production by utilizing an external power source. Although the process of designing and

optimizing the function of this composite device will be somewhat complex, there is ample literature on the construction of each scaffold component, and there are vast potential benefits to the field of tissue engineering and individuals suffering from skeletal muscle deficiencies.

1.6 Project Goal and Specific Aims

The overall goal of this project is to develop and characterize a contractile, composite scaffold for skeletal muscle regeneration that provides simultaneous electrical and mechanical stimulation and topographical cues for the purpose of facilitating differentiation and organization of muscle progenitor cells into mature muscle fibers. To accomplish this goal, this project will be divided into the following specific aims:

Specific Aim 1: Develop and characterize a biocompatible, electroactive hydrogel which actuates in an electric field. We hypothesize that an electroactive hydrogel composed of a biocompatible polymer can mimic the amount and speed of actuation of other electroactive hydrogels and provide a biocompatible environment for cells. We will test this hypothesis using crosslinked copolymers of poly(acrylic acid) (PAA) and poly(ethylene glycol) (PEG).

Specific Aim 2: Develop, characterize, and evaluate the ability of a conductive, nanofibrous scaffold to promote the organization and differentiation of myoblasts into myotubes. We hypothesize that a fibrous scaffold made with a conductive polymer will function as a synthetic extracellular matrix that will facilitate the differentiation of myoblasts into aligned myotubes. We will test this hypothesis using electrospun scaffolds made of a copolymer of poly(ε-caprolactone) (PCL) and polypyrrole (PPy).

Specific Aim 3: Characterize the *in vitro* response and evaluate the effect on myoblast differentiation of combined electrical and mechanical stimulation provided by the contractile, composite scaffold. We hypothesize that the combination of a biocompatible, electroactive hydrogel and a conductive, fibrous scaffold will create a contractile composite scaffold that will further enhance the differentiation of myoblasts by providing electrical, mechanical, and topographical cues. We will test this hypothesis by combining the scaffold components developed in the first two aims and performing a variety of *in vitro* assays.

1.7 References

[1] Brown JL, Kumbar SG, Banik BL. Bio-Instructive Scaffolds for Musculoskeletal Tissue Engineering and Regenerative Medicine. Elsevier Inc: Academic Press; 2017. Chapter 8: Bio-Instructive Scaffolds for Skeletal Muscle Regeneration: Conductive Materials. Freeman JW, Browe DP. ISBN: 978-0-12-803394-4.
[2] Marieb EN, Hoehn K. Human Anatomy & Physiology. 8th Edition. San Francisco, USA: Benjamin Cummings; 2010. page 312. ISBN: 978-0-8053-9569-3.
[3] Guyton AC, Hall JE. Textbook of Medical Physiology. 11th Edition. Philadelphia, USA: Elsevier Saunders; 2006. page 1116. ISBN: 0-7216-0240-1.
[4] Shier D, Butler JL, Lewis R. Hole's Human Anatomy and Physiology. 10th Edition. New York, USA: Glencoe/McGraw-Hill; 2003. ISBN-13: 9780072438901.
[5] Chargé SBP, Rudnicki MA. Cellular and Molecular Regulation of Muscle Regeneration. Physiol Rev 2004; 84: 209-238.
[6] Järvinen TAH, Järvinen M, Kalimo H. Regeneration of injured skeletal muscle after the injury. Muscles, Ligaments and Tendons Journal 2013; 3(4): 337-345.
[7] Bach AD, Beier JP, Stern-Staeter J, Horch RE. Skeletal muscle tissue engineering. J Cell Mol Med 2004; 8(4): 413-422.
[8] Kin S, Hagiwara A, et al. Regeneration of skeletal muscle using in situ tissue engineering on an acellular collagen sponge scaffold in a rabbit model. ASAIO J 2007; 53(4): 506-513.
[9] Hawke TJ, Garry DJ. Myogenic satellite cells: physiology to molecular biology. J Appl Physiol 2001; 91(2): 534-551.
[10] Halevy O, Piestun Y, Allouh MZ, Rosser BW, Rinkevich Y, Reshef R, Rozenboim I, Wleklinski-Lee M, Yablonka-Reuveni Z. Pattern of Pax7 expression during myogenesis in the posthatch chicken establishes a model for satellite cell differentiation and renewal. Dev Dyn 2004; 231(3): 489-502.
[11] Owings M, Kozak L. Ambulatory and inpatient procedures in the United States, 1996. Vital Health Stat 13 1998; 139: 1-119.

[12] Ziegler-Graham K, MacKenzie EJ, Ephraim PL, Travison TG, Brookmeyer R. Estimating the Prevalence of Limb Loss in the United States: 2005 to 2050. Achives of Physical Medicine and Rehabilitation 2008; 89(3): 422-429.
[13] Emery AE. The muscular dystrophies. Lancet. 2002; 359(9307): 687-695.
[14] Emery AE. Population frequencies of inherited neuromuscular diseases – a world survey. Neuromuscul Disord 1991; 1(1): 19-29.
[15] Romitti P, Puzhankara S, et al. Prevalence of Duchenne/Becker Muscular Dystrophy Among Males Aged 5-24 Years – Four States, 2007. Morbidity and Mortality Weekly Report (MMWR). Centers for Disease Control and Prevention (CDC) 2009; 58(40): 1119-1122.
[16] United States Birth Rate. Index Mundi. 2015. http://www.indexmundi.com/united_states/birth_rate.html. Accessed on December 5, 2015.
[17] QuickFacts: United States. United States Census Bureau. 2015. http://quickfacts.census.gov/qfd/states/00000.html. Accessed on December 5, 2015.
[18] Fan C, Jiang P, Fu L, Cai P, Sun L, Zeng B. Functional reconstruction of traumatic loss of flexors in forearm with gastrocnemius myocutaneous flap transfer. Microsurgery 2008; 28(1): 71-75.
[19] Vekris MD, Beris AE, Lykissas MG, Korompilias AV, Vekris AD, Soucacos PN. Restoration of elbow function in severe brachial plexus paralysis via muscle transfers. Injury 2008; 39 Suppl 3: S15-22.
[20] Mooney DJ, Mikos AG. Growing new organs. Sci Am 1999; 280(4): 60-65.
[21] Seidi A, Ramalingam M, Elloumi-Hannachi I, Ostrovidov S, Khademhosseini A. Gradient biomaterials for soft-to-hard interface tissue engineering. Acta Biomaterialia 2011; 7: 1441-1451.
[22] Liao H, Zhou GQ. Development and Progress of Engineering of Skeletal Muscle Tissue. Tissue Engineering: Part B 2009; 15(3): 319-331.
[23] Vandenburgh H. Functional assessment and tissue design of skeletal muscle. Ann N Y Acad Sci 2002; 961: 201-202.
[24] Vandenburgh HH, Karlisch P, Farr L. Maintenance of highly contractile tissue-cultured avian skeletal myotubes in collagen gel. In Vitro Cell Dev Biol 1988; 24(3): 166-174.
[25] Okano T, Matsuda T. Hybrid muscular tissues: preparation of skeletal muscle cell-incorporated collagen gels. Cell Transplant 1997; 6(2): 109-118.
[26] Shansky J, Creswick B, Lee P, Wang X, Vandenburgh H. Paracrine release of insulin-like growth factor 1 from a bioengineered tissue stimulates skeletal muscle growth *in vitro*. Tissue Eng 2006; 12(7): 1833-1841.
[27] Cheema U, Brown R, Mudera V, Yang SY, McGrouther G, Goldspink G. Mechanical signals and IGF-I gene splicing *in vitro* in relation to development of skeletal muscle. J Cell Physiol 2005; 202(1): 67-75.
[28] Okano T, Satoh S, Oka T, Matsuda T. Tissue engineering of skeletal muscle: highly dense, highly oriented hybrid muscular tissues biomimicking native tissues. ASAIO J 1997; 43(5): M749-753.
[29] Saxena AK, Willital GH, Vacanti JP. Vascularized three-dimensional skeletal muscle tissue-engineering. Biomed Mater Eng 2001; 11(4): 275-281.

[30] Kroehne V, Heschel I, Schugner F, Lasrich D, Bartsch JW, Jockusch H. Use of a novel collagen matrix with oriented pore structure for muscle cell differentiation in cell culture and in grafts. J Cell Mol Med 2008; 12(5a): 1640-1648.
[31] Yan W, George S, Fotadar U, et al. Tissue engineering of skeletal muscle. Tissue Eng 2007; 13(11): 2781-2790.
[32] Choi JS, Lee SJ, Christ GJ, Atala A, Yoo JJ. The influence of electrospun aligned poly(ε-caprolactone)/collagen nanofiber meshes on the formation of self-aligned skeletal muscle myotubes. Biomaterials 2008; 29: 2899-2906.
[33] Chen MC, Sun YC, Chen YH. Electrically conductive nanofibers with highly oriented structures and their potential application in skeletal muscle tissue engineering. Acta Biomaterialia 2013; 9: 5562-5572.
[34] Huang NF, Patel S, Thakar RG, Wu J, Hsiao BS, Chu B, Lee RJ, Li S. Myotube Assembly on Nanofibrous and Micropatterned Polymers. Nano Letters 2006; 6(3): 537-542.
[35] Dennis RG, Kosnik PE. Excitability and Isometric Contractile Properties of Mammalian Skeletal Muscle Constructs Engineered *In Vitro*. In Vitro Cell. Dev. Biol.—Animal 2000; 36: 327-335.
[36] Kosnik PE, Faulkner JA, Dennis RG. Functional Development of Engineered Skeletal Muscle from Adult and Neonatal Rats. Tissue Engineering 2001; 7(5): 573-584.
[37] Haghighipour N, Heidarian S, Shokrgozar MA, Amirizadeh N. Differential effects of cyclic uniaxial stretch on human mesenchymal stem cell into skeletal muscle cell. Cell Biology International 2012; 36: 669-675.
[38] Boonen KJM, Langelaan MLP, Polak RB, van der Schaft DWJ, Baaijens FPT, Post MJ. Effects of a combined mechanical stimulation protocol: Value for skeletal muscle tissue engineering. Journal of Biomechanics 2010; 43: 1514-1521.
[39] Akimoto T, Ushida T, Miyaki S, Tateishi T, Fukubayashi T. Mechanical stretch is a down-regulatory signal for differentiation of C2C12 myogenic cells. Materials Science and Engineering 2001; C 17: 75-78.
[40] Fujita H, Nedachi T, Kanzaki M. Accelerated *de novo* sarcomere assembly by electric pulse stimulation in C2C12 myotubes. Experimental Cell Research 2007; 313: 1853-1865.
[41] Donnelly K, Khodabukus A, Philp A, Deldicque L, Dennis RG, Baar K. A Novel Bioreactor for Stimulating Skeletal Muscle *In Vitro*. Tissue Engineering: Part C 2010; 16(4): 711-718.
[42] Bar-Cohen Y. Electroactive Polymer (EAP) Actuators as Artificial Muscles – Reality , Potential, and Challenges. 2nd Edition. Bellingham, USA: SPIE—The International Society for Optical Engineering; 2004. ISBN: 0-8194-5297-1.
[43] Huang Y, Browe D, Freeman J, Najafizadeh L. A Wirelessly Tunable Electrical Stimulator for Ionic Electroactive Polymers. IEEE Sensors Journal 2018; 18(5): 1930-1939.
[44] Shahinpoor M, Kim KJ. Ionic polymer-metal composites: I. Fundamentals. Smart Mater. Struct 2001; 10: 819-833.

CHAPTER 2: THE DEVELOPMENT AND CHARACTERIZATION OF A BIOCOMPATIBLE, IONIC ELECTROACTIVE POLYMER WHICH ACTUATES IN AN ELECTRIC FIELD

Note: This chapter has been reproduced in its entirety (with some modifications to the introduction) with permission as an academic work from the following publication [1]: Browe DP, Wood C, Sze MT, White KA, Scott T, Olabisi RM, Freeman JW. Characterization and optimization of actuating poly(ethylene glycol) diacrylate/acrylic acid hydrogels as artificial muscles. Polymer 2017; 117: 331-341.

2.1 Introduction

Ionic electroactive polymers (iEPs) are capable of moving when exposed to an electric field due to the flow of ions throughout a hydrogel layer [2]. Both iEPs and IPMCs have a very similar mechanism of movement, as shown in figure 2.1 below [3]. When an electric field is applied, free ions in the hydrogel portion move toward the oppositely charged electrode, which leads to asymmetric swelling [2]. This creates an overall bending actuation in the construct.

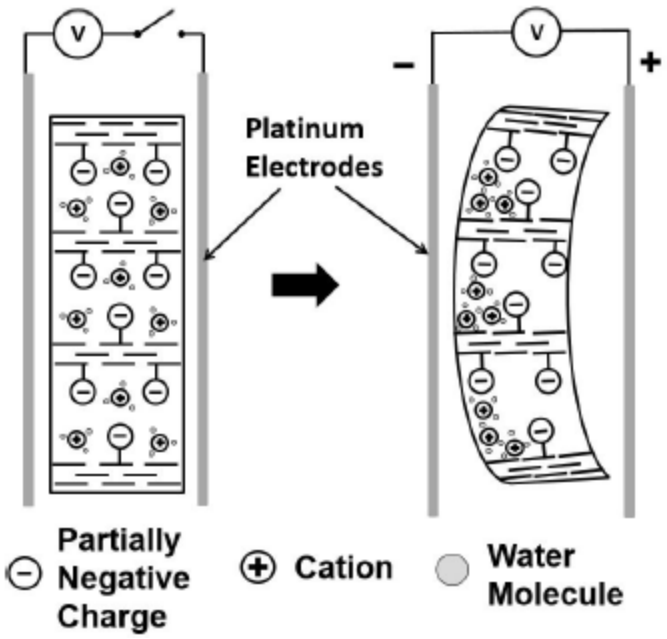

Figure 2.1: Mechanism of IPMC actuation. The electric field causes mobile ions in solution to aggregate on one side of the construct leading to asymmetric swelling of the gel, which causes a bending actuation. Taken from a paper by Huang and coworkers with permission from the authors to reuse in an academic work [3].

Hydrogels are commonly used in a variety of biomedical applications because they provide an environment that is similar to the extracellular matrix of many tissues due to their permeable and highly hydrated structure. In addition, their material properties have enormous flexibility depending on their composition and method of preparation. Electroactive polymers, a type of stimuli-responsive hydrogel, respond to an electric field by changing in size or shape. These polymers have been investigated for use as artificial muscles, biosensors, and other applications [4, 5]. Ionic electroactive polymers are typically hydrogels which have been swelled with an ionic solution. When an electric field is applied, the ions in solution will move towards the oppositely charged electrode and pull water molecules in the same direction. This rearrangement of ions and water

leads to a conformational change in the polymer chains of the material, which results in a bending movement [6]. The mechanical response to the movement of ions can be similar to muscle contraction in native tissue. In addition, these polymers are relatively light-weight and can produce contractile stresses comparable to native muscle tissue [2]. Thus, ionic electroactive polymers may provide a favorable environment for muscle cell development by mimicking the electro-mechanical environment of developing muscle.

In an attempt to develop a biocompatible ionic electroactive polymer, we have explored the use of poly(ethylene glycol) diacrylate (PEGDA) and poly(acrylic acid) (PAA) in crosslinked networks. PEGDA and PAA have been used together in biocompatible hydrogels for a variety of applications including drug carriers [7] and actuators [8]. Previous experiments in our laboratory have found reversible and repeatable movement in hydrogels incorporating PAA [9]. PEGDA has been heavily used in biomedical research, and it allows for precise control of the exact chemical structure of the resulting material [10]. The combination of PEGDA and PAA has the potential to produce a biocompatible actuating hydrogel with immense potential for future modification.

We hypothesize that reproducing the environment of developing muscle tissue in a cell culture system will produce mature muscle tissue, which will result in a muscle graft that can be used to replace large voids in muscle tissue. In this study, we investigate and characterize the ability of hydrogels made of PEGDA and acrylic acid (AA) to actuate in an electric field. In an attempt to optimize the extent and speed of actuation, we investigated the following parameters for their effect on hydrogel movement in rectangular prism samples: molecular weight of PEGDA, ratio of PEGDA to AA, overall

polymer concentration, and sample geometry (thickness). Further, we gauged the biocompatibility of these samples by measuring the proliferation and morphology of C2C12 mouse myoblasts seeded on hydrogel samples with various ratios of PEGDA to AA.

2.2 Materials and Methods

2.2.1 Hydrogel Crosslinking and Swelling

Poly(ethylene glycol) diacrylate (PEGDA) samples with molecular weights of 1000 Da, 4000 Da, and 10,000 Da were purchased from Monomer-Polymer and Dajac Labs (an MPD Chemicals Company). Acrylic acid (AA) monomer (anhydrous), 2,2-Dimethoxy-2-phenylacetophenone, and 1-Vinyl-2-pyrrolidinone were purchased from Sigma Aldrich. All phosphate buffered saline (PBS) used in this study was made with the following formulation per 1 L of deionized water: 8.765 g/L sodium chloride; 2.455 g/L sodium phosphate dibasic heptahydrate; 0.138 g/L monosodium phosphate. The pH of all PBS was adjusted to 7.4 using 1 M hydrogen chloride. A photo-initiator solution of 300 mg/mL of 2,2-Dimethoxy-2-phenylacetophenone in 1-Vinyl-2-pyrrolidinone was prepared using a vortex mixer.

All hydrogel solutions were prepared by dissolving PEGDA and AA in PBS using a vortex mixer. The photo-initiator solution described above was added to the hydrogel solutions at a concentration of 50 μL of photo-initiator solution per 1 mL of hydrogel solution (5% v/v) just prior to applying UV radiation. The mixture of hydrogel solution and photo-initiator solution was then injected into a glass mold with pre-measured dimensions in the shape of a rectangular prism, and UV radiation at a wavelength of 365 nm was applied using a 3UV™ Lamp (UVP: Ultra-Violet Products S/N 100306-001, P/N 95-0343-01; 8 Watt. Upland, CA, USA). UV radiation was applied in 30 second intervals until the solution solidified and failed to flow. Free radical polymerization occurred, which created a random 3-dimensional polymer network, as shown in Figure 2.2.

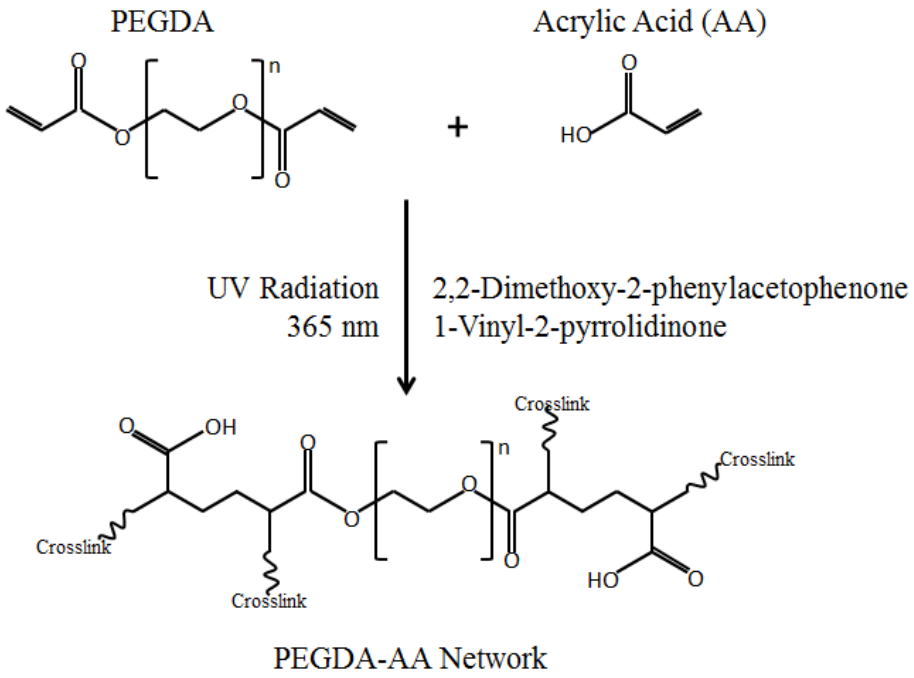

Figure 2.2: PEGDA and AA crosslinking reaction. PEGDA and acrylic acid (AA) react in the presence of photo-initiator solution (2,2-dimethoxy-2-phenylacetophenone in 1-vinyl-2-pyrrolidinone) with UV radiation (365 nm). The resulting polymer network of PEGDA and AA is random, but the unit structure shown is representative of the whole network. The potential locations for additional crosslinks are marked.

Immediately after UV radiation was applied, the length, width, and thickness of the hydrogel samples were measured, and the samples were allowed to soak in PBS solution. After 3 days in PBS, the samples had reached their final size, and the dimensions of the sample were measured again. Table 2.1 below shows all of the samples that were used in this study and the abbreviations that will be used from this point forward.

Group Abbreviation	Molecular Weight of PEGDA (Da)	Concentration of PEGDA (g/mL of PBS)	Concentration of AA (g/mL of PBS)	Thickness of Mold for Crosslinking (mm)
100% PEGDA	4000	0.1	**0**	0.75
1:4 PEGDA:AA	4000	0.1	**0.4**	0.75
1:8 PEGDA:AA	4000	0.1	**0.8**	0.75
1:12 PEGDA:AA	4000	0.1	**1.2**	0.75
1:16 PEGDA:AA	4000	0.1	**1.6**	0.75
0.9 g/mL	4000	**0.1**	**0.8**	0.75
1.8 g/mL	4000	**0.2**	**1.6**	0.75
2.7 g/mL	4000	**0.3**	**2.4**	0.75
3.6 g/mL	4000	**0.4**	**3.2**	0.75
1000 Da	**1000**	0.1	0.8	0.75
4000 Da	**4000**	0.1	0.8	0.75
10,000 Da	**10,000**	0.1	0.8	0.75
0.3 mm	4000	0.1	0.8	**0.25**
0.7 mm	4000	0.1	0.8	**0.5**
1.0 mm	4000	0.1	0.8	**0.75**
1.4 mm	4000	0.1	0.8	**1.0**
1.7 mm	4000	0.1	0.8	**1.25**
2.1 mm	4000	0.1	0.8	**1.5**

Table 2.1: Electroactive hydrogel sample identification. The abbreviations, composition, and geometry of all of the hydrogel samples used in this study. The abbreviations for the groups are meant to emphasize the differences in composition and structure that are being investigated in each experiment.

In order to calculate crosslinking density and equilibrium volumetric swelling ratio, the following procedure was performed. Hydrogel samples were fabricated as previously mentioned and allowed to swell in PBS for at least 3 days. The samples were weighed to determine the swelled mass (M_s) and frozen then lyophilized overnight to obtain the dry mass (M_d). The equilibrium volumetric swelling ratio (Q) was calculated using the following equation:

$$Q = 1 + \frac{\rho_{poly}}{\rho_{solv}}\left(\frac{M_s}{M_d} - 1\right)$$

where ρ_{poly} is the density of the polymer solution and ρ_{solv} is the density of the solvent. The cross-linking density (ρ_x) was calculated using an adjusted form of the Flory-Rehner equation (neglecting chain ends) as shown below [11, 12]:

$$\rho_x = \frac{-1}{V_{solv}}\left(\frac{In(1-\upsilon_p) + \upsilon_p + \chi{\upsilon_p}^2}{{\upsilon_p}^{1/3} - (1/2)\upsilon_p}\right)$$

where V_{solv} is the molar volume of the solvent, χ is the solvent-polymer interaction parameter, and υ_p is the equilibrium polymer volume fraction (1/Q). The value of χ was taken from the literature to be 0.426 [11, 13].

2.2.2 FTIR Spectroscopy

Fourier Transform Infrared (FTIR) spectroscopy was used to characterize the hydrogels and verify the presence of specific functional groups. FTIR spectra were collected in the range of 4000 and 500 cm^{-1} (Thermo Scientific, Nicolet iS10). Samples were prepared by lyophilization before being placed in the machine and 32 scans were acquired at 2 cm^{-1} resolution with the subtraction of background (air).

2.2.3 Mechanical Testing

Hydrogel samples were cut into 2 cm x 5 cm strips for mechanical testing (n = 4). All samples were soaked in PBS prior to being placed in the soft tissue grips of an Instron 5869 mechanical testing machine. The gauge length was 3.0 cm, and the samples were strained at a rate of 1.5 mm/min (5% strain/minute) until failure. The elastic modulus and ultimate tensile stress for each sample were calculated from the generated stress vs. strain graph. The elastic moduli and ultimate tensile stresses are reported as an average with a standard deviation for each group.

2.2.4 Actuation Testing

Hydrogel samples were cut into 20 mm x 4 mm strips for actuation testing (n = 4). The strips were suspended in the device depicted in Figure 2.3 to measure the response to an electric field (view from above). The device consisted of a small well filled with PBS and two platinum electrodes submerged in the PBS at a distance of 3.0 cm apart. Each platinum electrode consisted of four twisted platinum wires (99.5% pure, 0.20 mm diameter). The sample was held up using two small pegs in the middle of the electrodes to prevent the sample from translating in the well. A DC voltage of 20 V, equivalent to 6.67 V/cm, was applied for 1 minute at a time using an Agilent Dual Output DC Power Supply (E3646A Agilent Technologies, Santa Clara, CA, USA). The DC voltage was applied to the hydrogel strips two times in each direction, with each application lasting 1 minute. Thus, 4 total minutes of stimulation were applied to each hydrogel strip. All actuation tests were recorded with a digital camera in video mode, and the videos were replayed and analyzed to determine the angular movement and speed of the hydrogel strip for each movement. The data are reported as an average for the movement in each direction (forward and reserve) with the standard deviation.

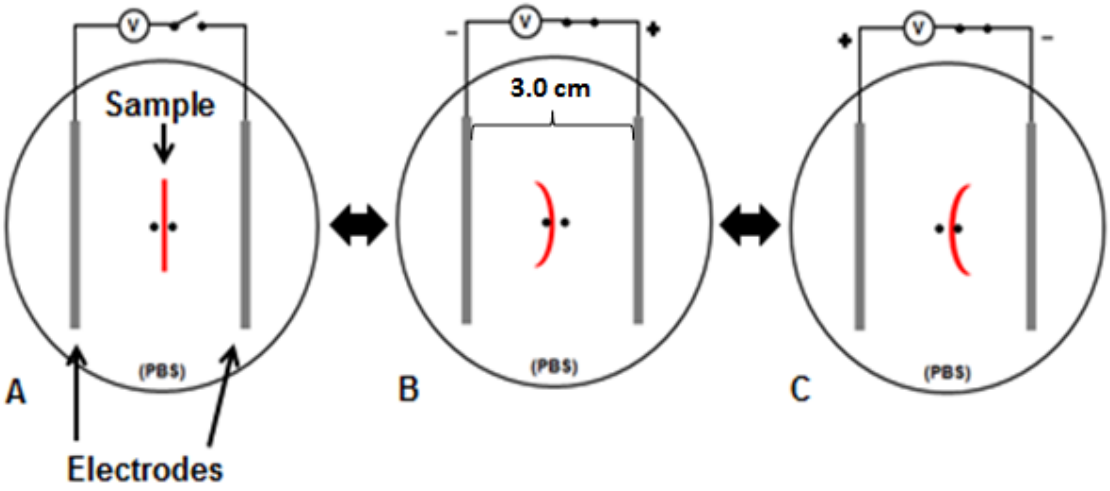

Figure 2.3: Actuation apparatus. Design of device used for actuation testing (view

from above). 20 V of DC voltage was applied to the hydrogel strips in a PBS bath across two platinum electrodes that were 3.0 cm apart (6.67 V/cm). **A)** The sample was held up by two small pegs in the middle of the electrodes which prevented the sample from translating. **B)** When the voltage is applied, the sample will bend towards the negative electrode. **C)** When the he polarity of the voltage is reversed, the sample will bend in the opposite direction.

When testing longevity of actuation, the same hydrogel strips were tested using the above procedure at time-points of 1 week, 4 weeks, 8 weeks, and 12 weeks after initial crosslinking (n = 4). In between testing, the hydrogel strips were kept at room temperature in PBS solution, which was changed every week. If necessary, the hydrogel strips were trimmed to maintain a 20 mm x 4 mm size prior to the actuation tests.

2.2.5 Contractile Strength

Hydrogel samples were cut into 20 mm x 4 mm strips for evaluating their contractile strength (n = 4). The mechanism of measuring the contractile strength is shown in Figure 2.4 (view from the side). Hydrogel strips were suspended in a vertical bath of PBS between two platinum electrodes each consisting of four twisted platinum wires (99.5% pure, 0.20 mm diameter) that were 3.0 cm apart. A DC voltage of 20 V (6.67 V/cm) was applied for up to 1 minute using the same Agilent Dual Output DC Power Supply. Increasing aluminum foil weights were added to the bottom of the samples until an applied voltage no longer resulted in movement of the weight. If the bottom of the sample increased in height by at least 5 mm, then the hydrogel strip was deemed to have lifted the weight.

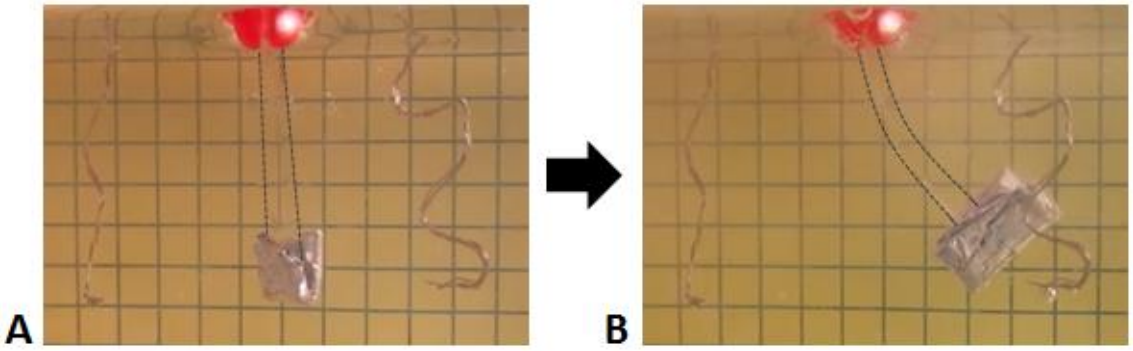

Figure 2.4: Contractile strength measurement method. Contractile strength measurements in a PBS bath (side view). **A)** Prior to the application of voltage, the hydrogel sample hangs vertically with an aluminum weight at the end. **B)** After application of the voltage, the sample starts to bend towards the negative electrode, lifting the aluminum weight in the process. The hydrogel sample is outlined for visibility.

The contractile stresses of the hydrogel strips were calculated using the equation below where $\sigma_{Contraction}$= contractile stress, m_H= mass of hydrogel strip, m_{Al}= mass of aluminum, V_H= volume of hydrogel strip, V_{Al}= volume of aluminum, ρ_{H_2O}= density of water, g = acceleration due to gravity, and A_H= cross-sectional area of the hydrogel strip. This equation accounts for the buoyancy of the hydrogel samples and aluminum weights.

$$\sigma_{Contraction} = \frac{\left[(m_H + m_{Al}) - (V_H + V_{Al})\rho_{H_2O}\right]g}{A_H}$$

2.2.6 C2C12 Cell Study

Hydrogel samples were cut to fit inside a 24-well plate and sterilized by briefly rinsing in ethanol and applying UV radiation for 30 minutes on each side (n = 4). The hydrogel samples were then washed with sterile PBS before soaking overnight in DMEM media with 10% fetal bovine serum (FBS) and 1% penicillin/streptomycin (P/S). Each hydrogel sample was seeded with approximately 50,000 C2C12 mouse myoblast cells

(25,000 cells/cm^2), which were purchased from the American type culture collection (ATCC). Blank wells (tissue culture plastic, TCP) served as a positive control and were subjected to the same conditions as the hydrogel samples. For the first three days, all wells were fed daily with DMEM media with 10% FBS and 1% P/S to encourage proliferation. For the next seven days, all wells were fed daily with DMEM media with 1% FBS and 1% P/S to encourage differentiation.

Metabolic activity and cellular attachment were assessed using a PrestoBlue® cell viability assay on day 3, day 6, and day 10 after cell seeding according to the manufacturer's instructions (n = 4). Briefly, the media from all wells was removed and replaced with PrestoBlue® cell viability reagent diluted 1:10 with media for a 1 hour incubation. At the end of the incubation period, the absorbance was read on a plate reader at 570 nm. The absorbance value was proportional to the metabolic activity of the cells. On day 10 after cell seeding, the cells were fixed with a 4% paraformaldehyde solution and prepared for staining to visualize cell morphology. Cells were stained with NucBlue® fixed cell ReadyProbes® reagent (Thermo Fisher Scientific) for DNA and Fluorescein Phalloidin (Thermo Fisher Scientific) for F-actin.

2.2.7 Statistics

The average and standard deviation of the data for each group were calculated. All data were evaluated with a one-way ANOVA with a Tukey's post-hoc test and significance was set at $\alpha = 0.05$ (denoted by *).

2.3 Results

2.3.1 Hydrogel Crosslinking and Swelling

After application of UV radiation, the hydrogel solutions changed from a liquid to a solid state. Immediately after crosslinking, the samples were generally transparent with some appearing a semi-opaque white color. After swelling in PBS solution for a period of 3 days, all the hydrogel samples became transparent and maintained their aspect ratio as they increased in volume.

Swelling was proportional to AA concentration, as shown in Figure 2.5A. Hydrogel samples without AA barely swelled in the PBS, but samples with a 1:16 ratio of PEGDA to AA swelled to more than 200% of their original size. Increasing the overall concentration of polymer in the hydrogel solutions from 0.9 g/mL to 1.8 g/mL caused a significant increase in swelling as shown in Figure 2.5B. However, further increasing the concentration of polymer resulted in a decrease in swelling.

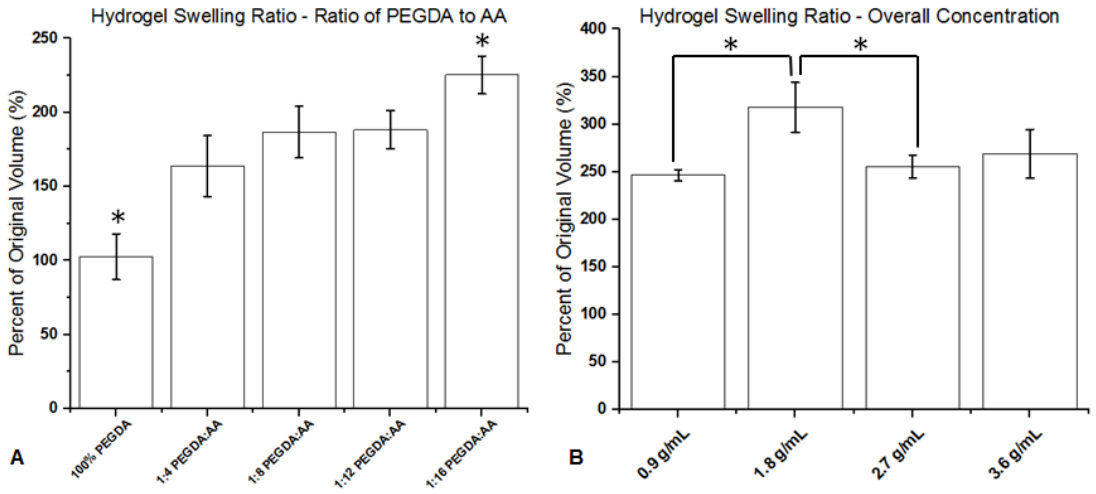

Figure 2.5: Hydrogel swelling ratio. Percent change in swelling of hydrogel samples after crosslinking (n = 6). **A)** Different ratios of PEGDA to AA. **B)** Different overall polymer concentrations. (* indicates a statistically significant difference with $p < 0.05$)

The cross-linking density and equilibrium volumetric swelling ratio were calculated for the 1:4 PEGDA:AA and 1:16 PEGDA:AA groups to approximate the ranges of these parameters in this paper, as shown in Table 2.2 (n = 6). Cross-linking density increased with increasing concentration of AA. When increasing the ratio of AA to PEGDA from 1:4 to 1:16 (a four-fold increase), the cross-linking density increased nearly three-fold. The equilibrium volumetric swelling ratio was almost twice as high for the 1:4 PEGDA:AA group as the 1:16 PEGDA:AA group. The lower cross-link density in the 1:4 PEGDA:AA group likely allowed these samples to swell more than the 1:16 PEGDA:AA group.

Hydrogel Sample	Cross-linking Density (mmol/L)	Equilibrium volumetric swelling ratio
1:4 PEGDA:AA	41 ± 2	19.0 ± 0.5
1:16 PEGDA:AA	113 ± 15	11.4 ± 0.7

Table 2.2: Crosslinking density and swelling ratio. The cross-linking density (mmol/L) and equilibrium volumetric swelling ratio are shown for the 1:4 PEGDA:AA and 1:16 PEGDA:AA groups. Data are shown as average ± standard deviation (n = 6).

2.3.2 FTIR Spectroscopy

The FTIR spectra for 1:4 PEGDA:AA, 1:16 PEGDA:AA, and 100% PEGDA shown in Figure 2.6 verify the structure of the resulting hydrogels. The peaks for alkane C-H bonds and ether C-O bonds are found in all three spectra. However, peaks for carboxylic acid O-H bonds and C=O bonds are found only in the 1:4 PEGDA:AA and 1:16 PEGDA:AA groups. This verifies that AA is being incorporated into the structure of the hydrogel.

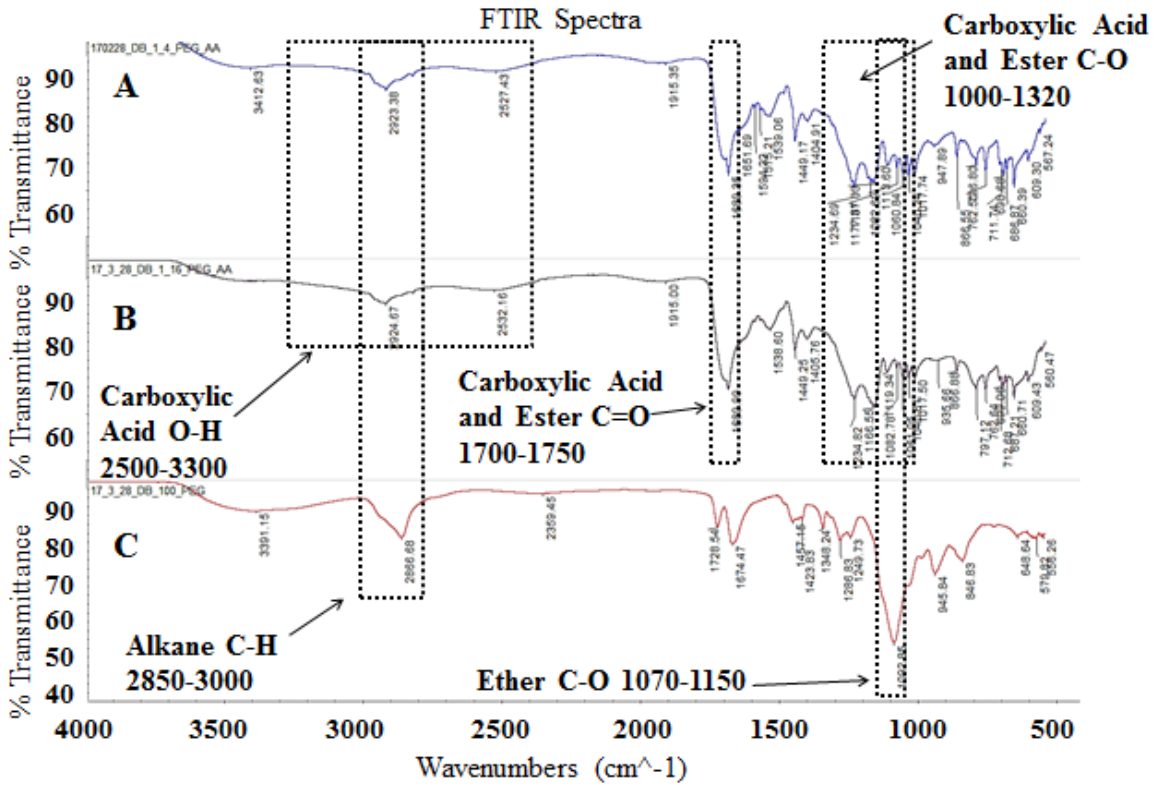

Figure 2.6: FTIR spectra. The FTIR spectra of A) 1:4 PEGDA:AA, B) 1:16 PEGDA:AA, and C) 100% PEGDA. Important peaks are labeled.

2.3.3 Mechanical Testing

After applying tensile stress to the hydrogel samples to failure, the elastic moduli and ultimate tensile stresses were calculated from the resulting stress-strain graphs as shown in Table 2.3. The samples generally failed in the mid-substance, but some samples failed right on the edge of the clamps. The elastic moduli of the hydrogel samples ranged from 65 kPa to 219 kPa for all samples, and the ultimate tensile stresses ranged from 16 kPa to 77 kPa. There were no significant differences in the elastic moduli from the groups with different ratios of PEGDA to AA; however, the elastic modulus increased with increasing overall polymer concentration. The 2.7 g/mL and 3.6 g/mL groups produced significantly higher moduli than the 0.9 g/mL and 1.8 g/mL groups. The 100% PEGDA

group had a significantly lower ultimate tensile stress than groups with different ratios of PEGDA to AA, but there were no other significant differences in ultimate tensile stress based on overall polymer concentration.

Hydrogel Sample	Elastic Modulus (kPa)	Ultimate Tensile Stress (kPa)
100% PEGDA	96.3 ± 18.7	26.0 ± 5.6*
1:4 PEGDA:AA	78.4 ± 7.3	56.2 ± 4.5
1:8 PEGDA:AA	89.1 ± 8.8	47.0 ± 11.2
1:12 PEGDA:AA	90.0 ± 13.4	61.4 ± 13.7
1:16 PEGDA:AA	77.8 ± 7.0	44.9 ± 9.5
0.9 g/mL	67.3 ± 4.3*	22.7 ± 8.7
1.8 g/mL	96.2 ± 6.1*	23.0 ± 3.9
2.7 g/mL	191.8 ± 20.3	36.6 ± 3.4
3.6 g/mL	213.6 ± 7.0	42.9 ± 23.0

Table 2.3: Mechanical properties of electroactive hydrogels. Mechanical properties data including elastic modulus (kPa) and ultimate tensile stress (kPa) with n = 4. Samples are grouped by the ratio of PEGDA to AA and by the overall concentration for statistical comparisons. (* indicates a statistically significant difference with $p < 0.05$)

2.3.4 Actuation Testing

All actuation tests showed that the hydrogel samples exhibited reversible and repeatable movement when exposed to an electric field. The samples always bent towards the negative electrode, although at different speeds. The forward and reverse movements were roughly the same for all samples tested.

The relationship between movement and the molecular weight of the PEGDA molecule used is shown in Figure 2.7. Although the 4000 Da group produced the most angular movement, there were no significant differences in the movement between the

three different molecular weights of PEGDA. The average angular movement was between 74 and 93 degrees for all groups, and samples moved roughly the same in the forward and reverse directions. A maximum movement speed of 1.9 degrees/s was obtained by a sample in the 4000 Da group.

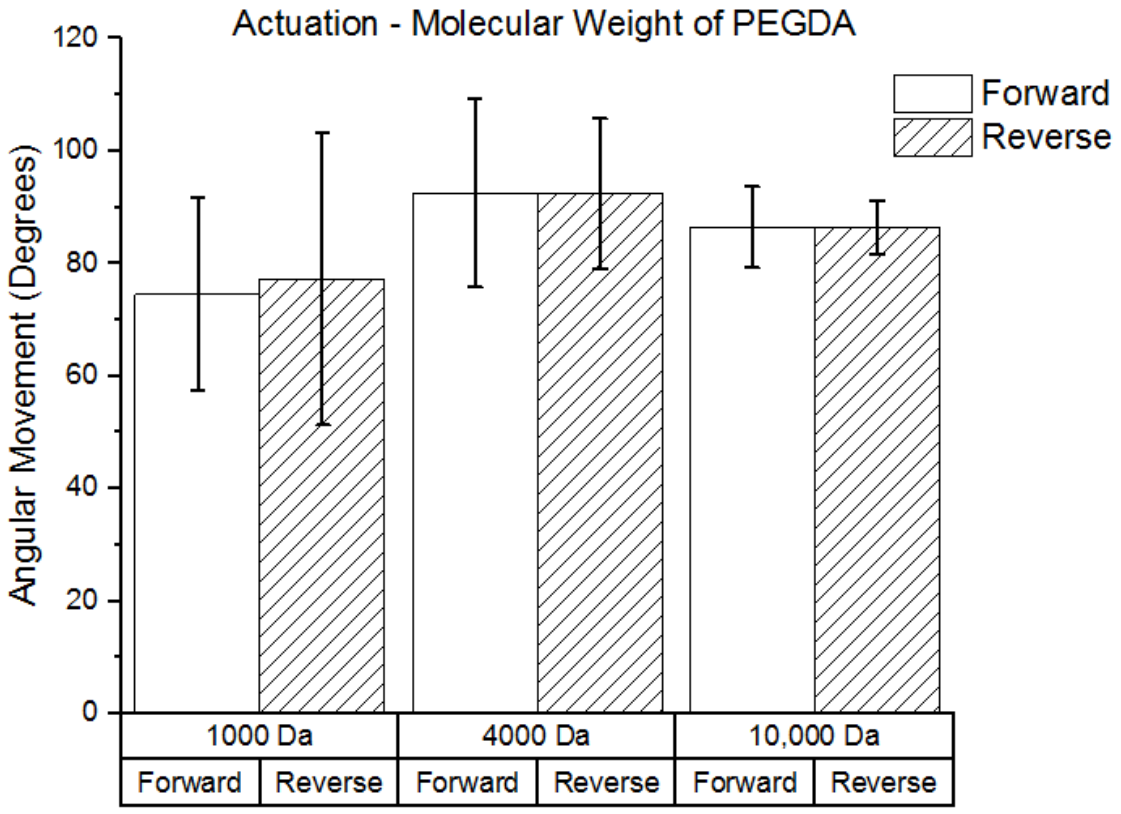

Figure 2.7: Actuation: PEGDA molecular weight. Effect of molecular weight of PEGDA on angular movement (n = 4). The movements in the forward and reverse directions are shown for each group.

The relationship between angular movement and the thickness of the hydrogel samples is shown in Figure 2.8. The results show a bell-shaped curve with movement increasing as thickness increases from 0.3 mm to 1.4 mm and movement decreasing as thickness increases from 1.4 mm to 2.1 mm. The 0.3 mm group produced the lowest

angular movement with 17.1 and 14.4 degrees of average forward and reverse movement, respectively. The 1.4 mm group produced the greatest angular movement with 113.2 and 114.5 degrees of average forward and reverse movement respectively, which was over 6 times the movement seen in the 0.3 mm group. The 1.4 mm group also produced the maximum movement speed at 2.1 degrees/s. The thickest group tested (2.1 mm) produced only 37.7 and 42.1 degrees of forward and reverse movement, respectively.

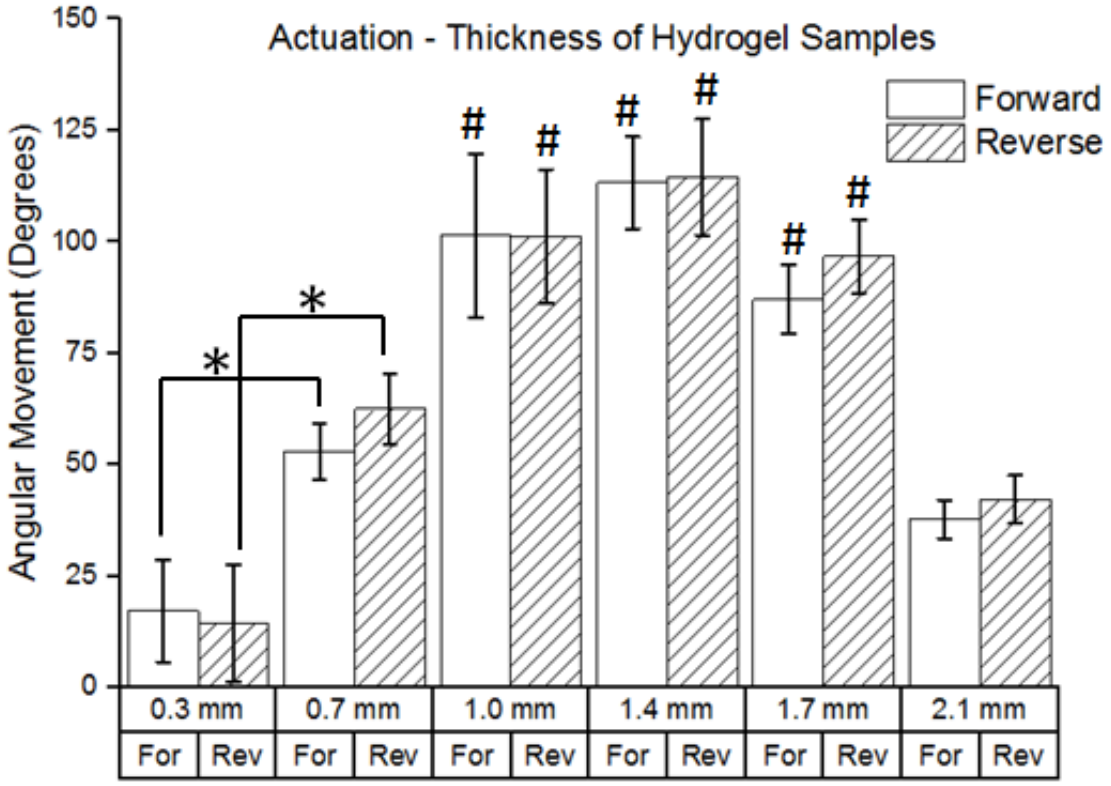

Figure 2.8: Actuation: Aspect ratio. Effect of hydrogel sample thickness on angular movement (n = 4). The movements in the forward and reverse directions are shown for each group. (* indicates a statistically significant difference from the corresponding movements in other groups with $p < 0.05$; # indicates statistically significant from the corresponding movement in the 0.3 mm, 0.7 mm, and 2.1 mm groups with $p < 0.05$).

The relationship between angular movement and the overall hydrogel concentration in the hydrogel samples is shown in Figure 2.9. The 0.9 g/mL group produced significantly lower angular movement than the other three groups. There were no statistically significant differences between the 1.8 g/mL, 2.7 g/mL, and 3.6 g/mL groups. A maximum movement speed of 2.4 degrees/s was obtained by a sample in the 3.6 g/mL group.

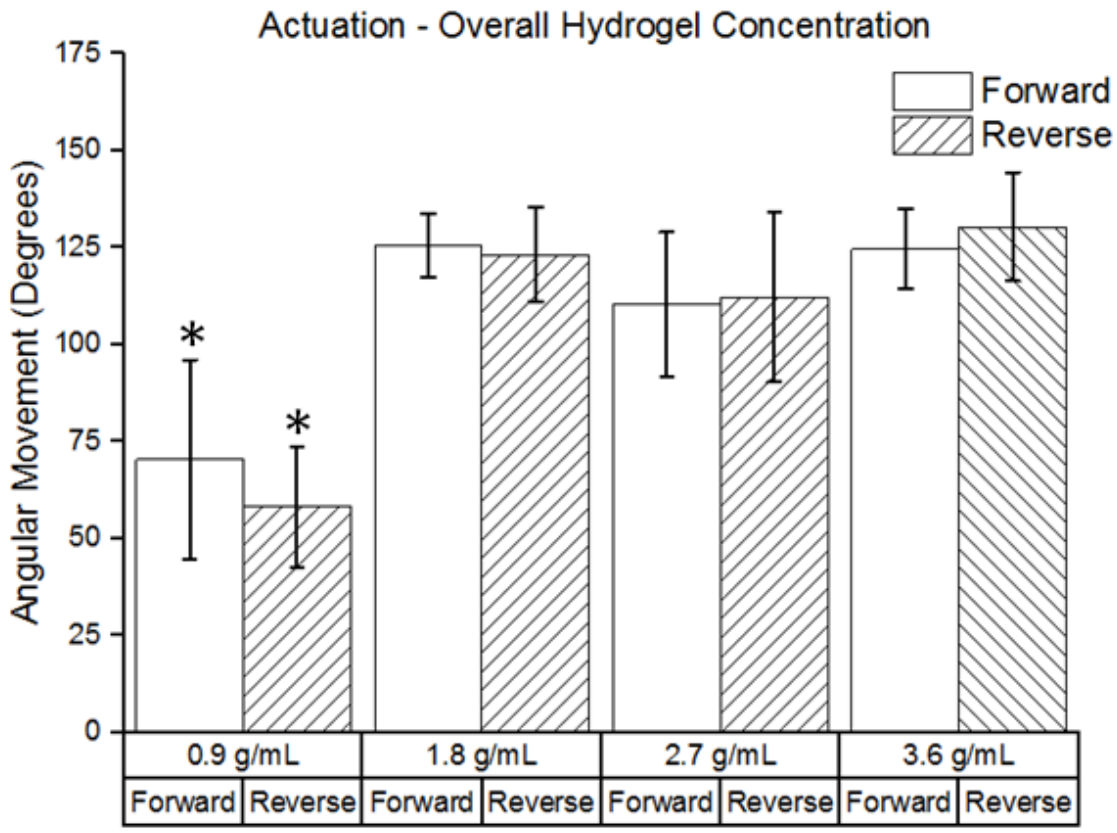

Figure 2.9: Actuation: Overall concentration. Effect of overall polymer concentration on angular movement (n = 4). The movements in the forward and reverse directions are shown for each group. (* indicates a statistically significant difference from the corresponding movements in other groups with $p < 0.05$)

The relationship between movement and the ratio of PEGDA to AA in the hydrogel samples is shown in Figure 2.10. The forward and reverse movements in the 1:4 PEGDA:AA group were significantly lower than the corresponding movements in the other three groups. Although the amount of angular movement generally increased with increasing AA concentration, there were no significant differences between the 1:8 PEGDA:AA, 1:12 PEGDA:AA, and 1:16 PEGDA:AA groups. A maximum movement speed of 1.6 degrees/s was obtained by a sample in the 1:16 PEGDA:AA group. The 100% PEGDA group is not shown because it did not produce any movement.

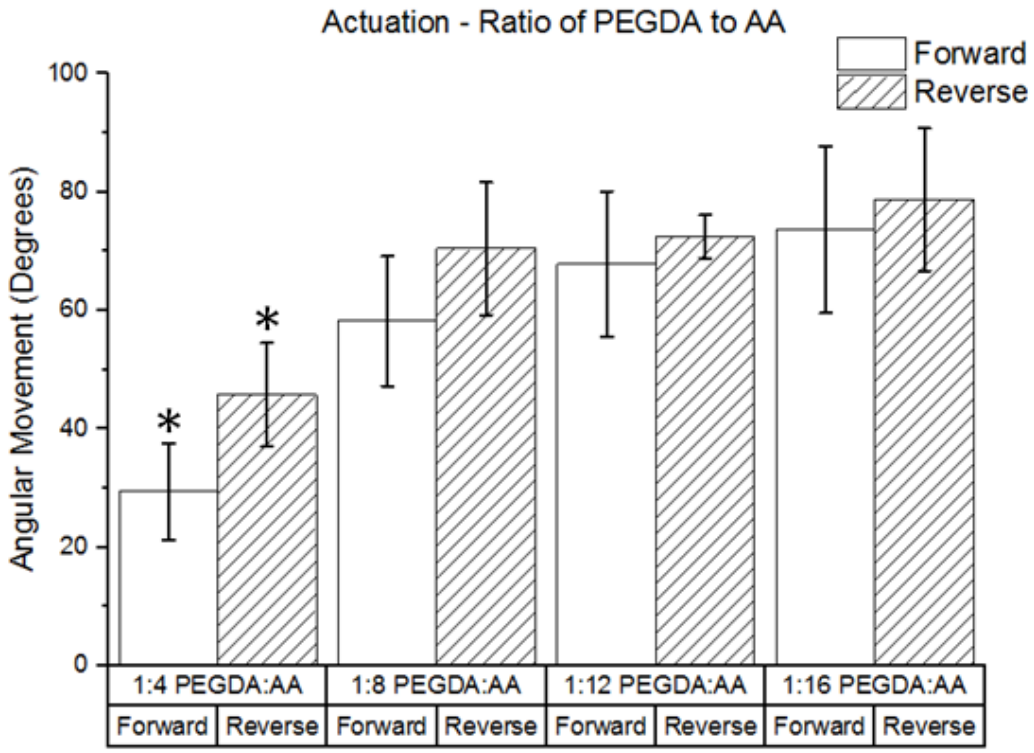

Figure 2.10: Actuation: Ratio of PEGDA to AA. Effect of ratio of PEGDA to AA on angular movement (n = 4). The movements in the forward and reverse directions are shown for each group. (* indicates a statistically significant difference from the corresponding movements in other groups with $p < 0.05$)

Hydrogel samples with various ratios of PEGDA to AA were able to actuate in an electric field for up to 12 weeks after crosslinking, as shown in Figure 2.11. For all groups tested, the greatest angular movement was recorded 4 weeks after the hydrogel samples were crosslinked. The least angular movement was recorded 12 weeks after the hydrogel samples were crosslinked. Further, there was a greater drop in the angular movement from week 4 to week 12 for the groups with a higher concentration of AA. For instance, the angular movement in the 1:4 PEGDA:AA group dropped 51% from week 4 to week 12, but the angular movement in the 1:16 PEGDA:AA group dropped 71% across the same time period.

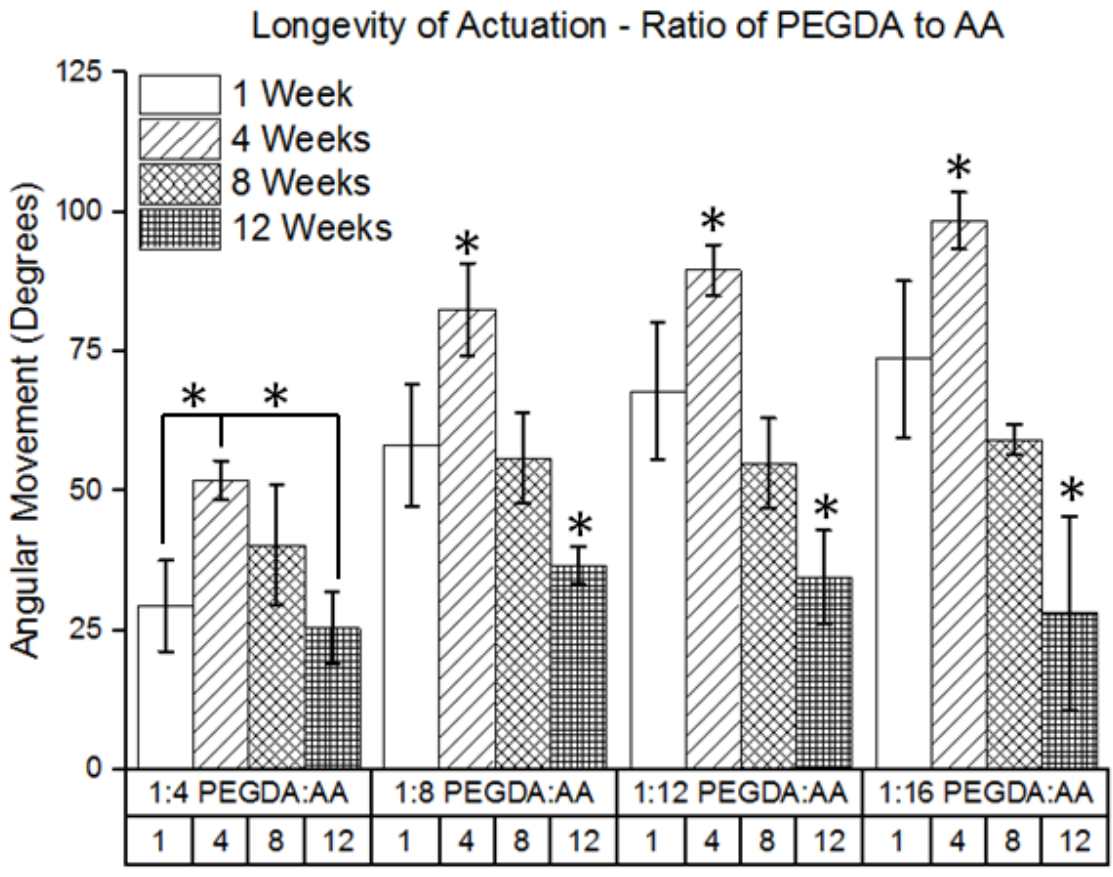

Figure 2.11: Actuation: Longevity. Longevity of angular movement for hydrogel samples with different ratios of PEGDA to AA (n = 4). For simplicity, only movements

in the forward direction are shown. (* indicates a statistically significant difference from the time-points in same group with $p < 0.05$)

2.3.5 Contractile Strength

Hydrogel samples were tested for their ability to move aluminum weights in a submerged system, and the resulting contractile stress measurements are shown in Table 2.4. The contractile stresses ranged from 297 Pa and 821 Pa for all hydrogel samples shown. There were no significant differences in contractile stress between the four hydrogel sample groups with different overall polymer concentrations. Contractile stress generally increased with increasing concentration of AA; the 1:12 PEGDA:AA and 1:16 PEGDA:AA groups produced significantly higher contractile stress than the 1:4 PEGDA:AA and 1:8 PEGDA:AA groups. Data for the 100% PEGDA samples is not shown because these samples produced no contractile stress.

Hydrogel Sample	Contractile Stress (Pa)	Hydrogel Sample	Contractile Stress (Pa)
1:4 PEGDA:AA	347 ± 43	0.9 g/mL	536 ± 152
1:8 PEGDA:AA	461 ± 88	1.8 g/mL	699 ± 131
1:12 PEGDA:AA	594 ± 71*	2.7 g/mL	612 ± 88
1:16 PEGDA:AA	592 ± 47*	3.6 g/mL	646 ± 111

Table 2.4: Contractile Stress. Contractile strength of hydrogel samples with n = 4. Samples are grouped by the ratio of PEGDA to AA and by the overall concentration for statistical comparisons. (* indicates a statistically significant difference when compared to the 1:4 PEGDA:AA and 1:8 PEGDA:AA groups with $p < 0.05$)

2.3.6 C2C12 Cell Study

C2C12 cells were seeded on hydrogel samples with different ratios of PEGDA to AA, and the cells survived and were metabolically active through 10 days, as shown in Figure 2.12. Tissue culture polystyrene (TCP) was used as a positive control. The cells

seeded on TCP and the 1:4 PEGDA:AA hydrogel sample had significantly higher metabolic activity than all other groups at all time-points. There was a trend of decreasing metabolic activity with increasing concentration of AA at all time-points. While most groups had relatively constant or increasing metabolic activity throughout the study period, the 100% PEGDA group had decreasing metabolic activity over time with the lowest metabolic activity occurring on day 10.

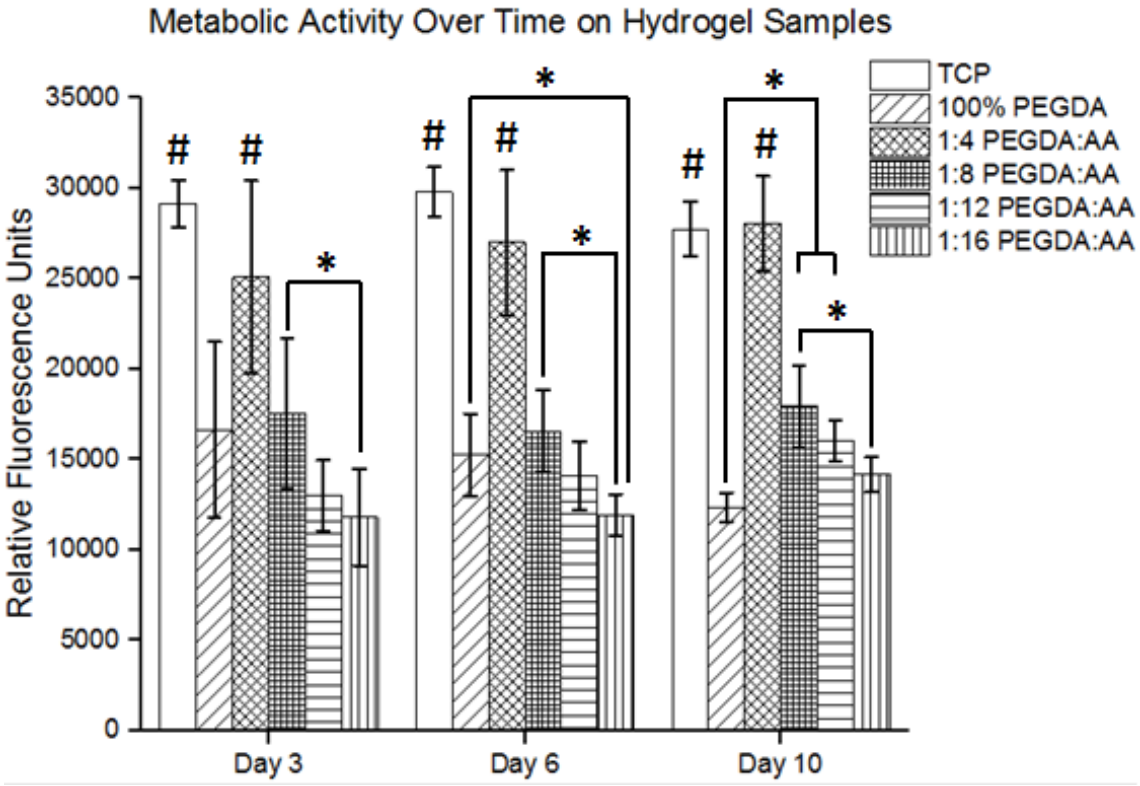

Figure 2.12: Metabolic activity on hydrogel samples. Metabolic activity data with C2C12 cells as measured by a PrestoBlue® cell viability assay n = 4. (* indicates a statistically significant difference from the corresponding movements in other groups with $p < 0.05$; # indicates statistically significant from the 100% PEGDA, 1:8 PEGDA:AA, 1:12 PEGDA:AA, and 1:16 PEGDA:AA groups at the same time-point with $p < 0.05$).

Cellular attachment and morphology were assessed by staining the cells for actin and DNA on day 10, as shown in Figure 2.13. Cells were present on all hydrogel samples, although intracellular matrix production varied widely between groups. On the 100% PEGDA samples, the cells seemed to stick together and not expand much on the hydrogel (Figure 10A). The 1:4 PEGDA:AA samples had the highest level of intracellular matrix production and attachment (Figure 10B). In addition, there was some evidence of cell fusion, but it was difficult to find myotubes, or immature muscle fibers, that were both distinct and linear. From the 1:8 PEGDA:AA sample to the 1:16 PEGDA:AA sample, there was a trend of decreasing intracellular matrix production and lower cell attachment.

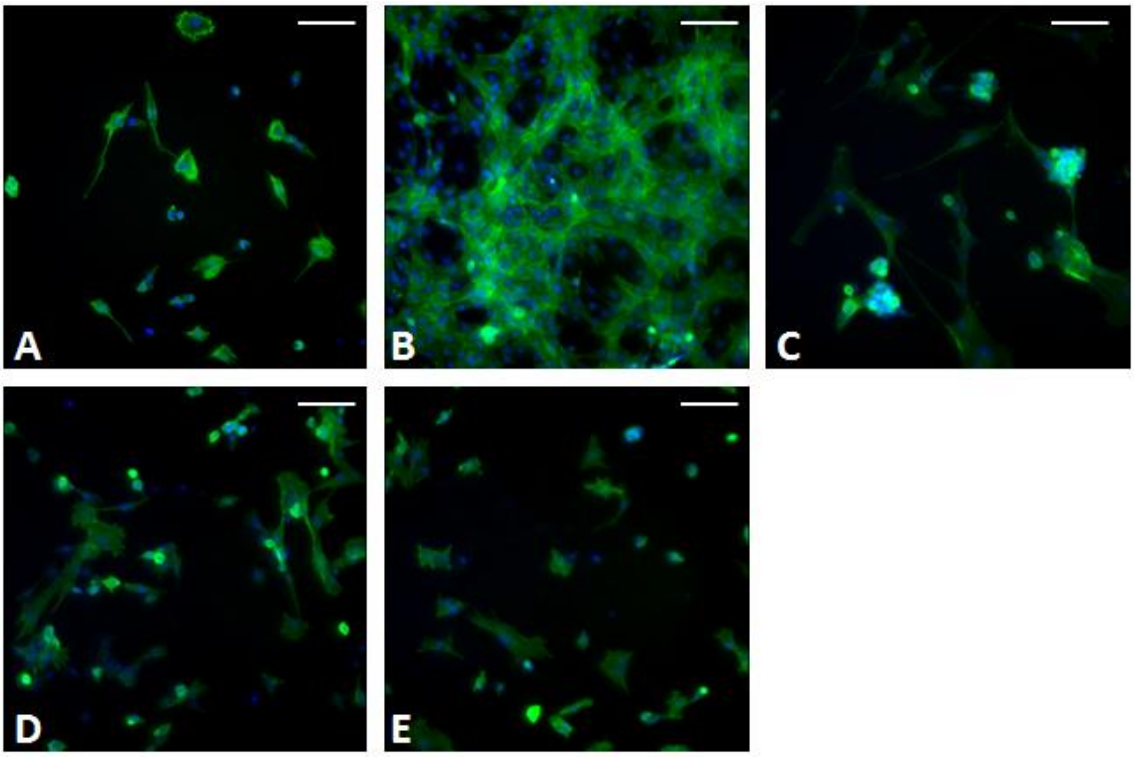

Figure 2.13: Actin and DNA staining on hydrogel samples. Cells were stained with phalloidin for actin (green) and DAPI for DNA (blue) and imaged at 10x magnification.

A) 100% PEGDA. **B)** 1:4 PEGDA:AA. **C)** 1:8 PEGDA:AA. **D)** 1:12 PEGDA:AA. **E)** 1:16 PEGDA:AA. The scale bars are all 100 μm.

2.4 Discussion

Despite comparisons of electroactive polymers to muscles, there has been relatively little research on the implementation of electroactive polymers in skeletal muscle tissue engineering. In this paper, we developed and characterized a biocompatible ionic electroactive polymer made of PEGDA and AA in a chemically crosslinked network with the ultimate goal of providing a unique stimulus to developing muscle cells. In order to measure the extent of actuation in an electric field, we devised a highly precise method of applying electrical stimulation and measuring the resulting angular displacement. This method was used to investigate multiple parameters for their effect on the angular movement of hydrogel samples in the shape of rectangular prisms. Finally, we utilized a 10 day cell study with C2C12 mouse myoblasts to judge the biocompatibility of these hydrogel samples with various ratios of PEGDA to AA.

Hydrogels made of various compositions of PEGDA and AA were crosslinked using a photo-initiator solution of 2,2-Dimethoxy-2-phenylacetophenone in 1-Vinyl-2-pyrrolidinone and UV radiation with a wavelength of 365 nm. The resulting hydrogel samples were swelled in PBS and retained their original aspect ratio. Overall, the percentage increase in volume after swelling was proportional to AA concentration, as shown in Figure 2.4A. The carboxyl groups of the AA monomers have a high polarity compared to the ether groups present in PEGDA, and the high polarity of the carboxyl groups draws water into the crosslinked polymer network. Predictably, the 100% PEGDA group swelled very little. However, there may be a limit to how much acrylic acid can be packed into a given volume, as suggested by Figure 2.4B. At higher overall polymer concentrations, the amount of swelling actually decreased as compared to lower overall

polymer concentrations. This may be due to a high chemical crosslink density and a larger number of physical entanglements in the 2.7 g/mL and 3.6 g/mL hydrogel samples which prevents additional water molecules from penetrating the polymer network.

Tensile testing to failure was completed by subjecting hydrogel samples to 5% strain/min, as shown in Table 2.2. Hydrogel samples with a greater overall polymer concentration were able to form more crosslinks with the surrounding molecules when subjected to UV radiation. Thus, both elastic modulus and ultimate tensile stress were proportional to overall polymer concentration. The ultimate tensile stress of the hydrogel samples was fairly variable, which was likely due to the tendency of some samples to fail within the grips and the variation in the exact structure of the hydrogel polymer network. It was expected that the samples with a higher concentration of AA would produce higher elastic moduli and ultimate tensile stresses, but there were no significant differences in these parameters between any of the groups with different ratios of PEGDA to AA. This trend may be explained by fewer crosslinks being formed in hydrogel samples with a higher concentration of AA. Even though there were was more opportunity for crosslinks in the hydrogel samples with a higher concentration of AA, a lower percentage of available crosslinking sites were activated by the UV radiation due to competition between crosslinking sites. Overall, the elastic moduli found in the hydrogel samples compare favorably to the elastic modulus of native muscle tissue. The elastic modulus of rat vastus lateralis muscle has been reported as 51.27 ± 28.48 kPa, and the elastic modulus of pig medial muscle has been reported as 141.12 ± 42.34 kPa [14]. These values overlap with the values that we found for most hydrogel groups with various ratios of PEGDA to AA and various overall concentrations, respectively (Table 2.2). Thus,

hydrogel samples made of PEGDA and AA are capable of reproducing the mechanical environment of native muscle tissue with respect to elastic modulus.

The response of the hydrogel samples to an electric field of 6.67 V/cm in PBS was measured as an angular displacement. All actuation tests were performed in PBS because PBS approximates the ion concentrations in the extracellular fluid of the human body. The data show that this angular movement is reversible, consistent in both directions, and repeatable. We investigated the effect of various parameters on the actuation response including PEGDA molecular weight, thickness of hydrogel samples, overall polymer concentration, and ratio of PEGDA to AA. It was found that the molecular weight of PEGDA had little effect on the actuation response. This may be due to the fact that the relative concentration of ethylene glycol and AA monomers was roughly the same between groups. In contrast, the thickness of hydrogel samples, overall polymer concentration, and the ratio of PEGDA to AA were all found to significantly affect the actuation response. It was found that the relationship between hydrogel sample thickness and actuation response formed a bell curve. Very thin hydrogel samples had a low number of polar carboxyl groups, which bring in a low amount of water and ions, leading to a small actuation response. However, in very thick hydrogel samples, the stiffness of the sample impeded the actuation response. Thus, with samples that were roughly 1.4 mm thick, the balance of low stiffness and high number of polar carboxyl groups produced the optimal actuation response. For both overall polymer concentration and the ratio of PEGDA to AA, we saw a similar trend in the actuation data. Initially, the actuation response increased with both increasing AA concentration and increasing overall polymer concentration. However, the actuation response reached a plateau at a 1:8

ratio of PEGDA:AA and an overall polymer concentration of 1.8 g/mL. This phenomenon may be explained by the interplay between concentration of water and ions in the samples and the stiffness of the samples. As the overall polymer concentration and AA concentration increase, the number of polar carboxyl groups per unit volume increases, which initially brings in more water and ions. The mechanism of movement in these samples is powered by the movement or ions, so a greater concentration of ions inside the hydrogel should lead to more movement. However, after a certain point, there are diminishing returns in terms of bringing in more water and ions because a more densely packed hydrogel sample has less room for water and ions to permeate. In addition, the increasing stiffness of hydrogel samples with a higher overall concentration or higher AA concentration eventually impedes movement. Thus, the actuation response was not improved by adding more AA beyond a ratio of PEGDA to AA of 1:8 or increasing the overall polymer concentration above 1.8 g/mL.

The degradation of the actuation response over time in hydrogel samples with various ratios of PEGDA to AA was measured by repeating the actuation tests at 1, 4, 8, and 12 weeks after initial crosslinking. A reversible actuation response was recorded at all time-points for all groups. It was expected that there would be a gradual decrease in the actuation response over time, and that is what was observed from week 4 through week 12. This decreased angular movement in response to an electric field was likely due to the gradual degradation of the hydrogel samples, which did not hold as high of a concentration of water and ions as freshly crosslinked samples. However, an unexpected increase in the actuation response was observed from 1 week to 4 weeks after crosslinking. This may be due to increased swelling in the samples over time prior to

eventual degradation that occurs after 4 weeks. These results suggest that altering the swelling conditions of the hydrogel samples may improve the actuation response. In any case, these results show that the hydrogel samples will provide some movement in response to an electric field for at least 12 weeks after crosslinking in a simulated *in vitro* environment.

The contractile stress of a range of hydrogel samples was measured by applying increasing aluminum weights to the end of the samples as they bent against gravity. The contractile stress measurements were collected with samples submerged in PBS and exposed to 20 V. Because the measurements were collected underwater, the buoyancy of the system was taken into account. Although there was no significant difference between groups with different overall polymer concentrations, the 1.8 g/mL group produced the highest contractile stress. When comparing samples with different ratios of PEGDA to AA, a higher concentration of AA produced greater contractile stress due to the presence of a greater concentration of polar carboxyl groups. The values of contractile stress measured in these experiments (297 Pa to 821 Pa) are lower than the contractile stress of native muscle tissue, which is estimated at around 60 kPa to 380 kPa [15-18]. The contractile stress of these hydrogel samples may increase with increasing voltage, but high levels of voltage are detrimental to cell growth. Indeed, 20 V is well above the threshold for electrolysis to occur, which creates a harsh environment for cells. However, in some preliminary actuation experiments in which hydrogel samples were exposed to voltages as low as 1 V (below the threshold for electrolysis), angular movement was still observed, and this mechanical response may provide a beneficial stimulus for developing muscle tissue.

To test the biocompatibility of the developed hydrogel samples, C2C12 mouse myoblast cells were seeded on hydrogel samples with various ratios of PEGDA to AA. The cell study was designed to have a period of cell proliferation, where the C2C12 cells divided until they were confluent on the hydrogel samples, and a period of cell differentiation, where the cells fused together to form myotubes, or immature muscle fibers. Metabolic activity, which can be used as an approximation of relative cell number, was measured at the end of the proliferation phase and at two points in the differentiation phase – 3 and 7 days after differentiation media was first applied. The metabolic activity on the 1:4 PEGDA:AA group was just as high as the TCP control at all time-points, but all other groups were significantly lower than TCP at all time-points. These findings can be explained by considering the functional groups on the hydrogel samples and their effect on the acidity of the surrounding media. On the 100% PEGDA samples, the presence of ether groups did not affect the pH of the media, but they did not provide adequate sites for cellular attachment. Thus, the cells seemed to form clusters together rather than spreading out on the samples (Figure 2.11A). On the 1:4 PEGDA:AA samples, the presence of carboxyl groups provided polar functional groups to facilitate cell attachment and spreading. However, as the concentration of AA increased, the pH of the media decreased, which created an increasingly hostile environment for cells. Pre-soaking the hydrogel samples in media likely improved cell attachment by allowing proteins in the media to associate to the surface of the samples. However, the C2C12 cells failed to form long, linear myotubes on any of the hydrogel groups, and the hydrogels in this study did not provide optimal sites for cell attachment. This may be caused by a lack of guidance cues on the surface of the hydrogel samples to provide

support for attachment and fusion. In future experiments, linear guidance cues will be patterned or attached to the surface of the hydrogel samples to improve both cell attachment and alignment of developed myotubes. These cues may be physical channels and nanofibers or the use of hydrogel actuation to create strain in the substrate and on the cells.

2.5 Conclusion

In this study, we produced biocompatible, actuating hydrogels made of PEGDA and AA. It was found that the mechanical properties of these hydrogels are in the same range as skeletal muscle, which may provide a beneficial mechanical environment for developing cells. The actuation response was reversible and repeatable, and was found to depend on sample thickness, overall polymer concentration, and ratio of PEGDA to AA. The actuation response decreased over time, but angular movement occurred in a range of samples at 12 weeks after initial crosslinking. Although the contractile stress of these hydrogel samples was below that of native muscle tissue, this system can still be used to apply mechanical stress to cells in an *in vitro* environment. Cells attached and proliferated on hydrogel samples with a range of ratios of PEGDA to AA, but the 1:4 PEGDA:AA group produced the highest metabolic activity and matrix deposition. In the future, we will produce these hydrogel samples with guidance cues on the surface in the form of electrospun nanofibers and also investigate the effect of hydrogel movement on cellular behavior. The combination of fibrous guidance cues to a strain-inducing, electroactive scaffold should provide beneficial stimulation in the form of electrical, mechanical, and topographical cues. This system has the potential to produce a scaffold that reproduces the environment of developing muscle tissue *in vitro*, which will then result in a highly mature graft to be used to replace large voids in muscle tissue.

2.6 Acknowledgements

I would like to thank Dr. Koustubh Dube for assisting with FTIR spectroscopy.

2.7 References

[1] Browe DP, Wood C, Sze MT, White KA, Scott T, Olabisi RM, Freeman JW. Characterization and optimization of actuating poly(ethylene glycol) diacrylate/acrylic acid hydrogels as artificial muscles. Polymer 2017; 117: 331-341.
[2] Bar-Cohen Y. Electroactive Polymer (EAP) Actuators as Artificial Muscles – Reality, Potential, and Challenges. 2nd Edition. Bellingham, USA: SPIE—The International Society for Optical Engineering; 2004. ISBN: 0-8194-5297-1.
[3] Huang Y, Browe D, Freeman J, Najafizadeh L. A Wirelessly Tunable Electrical Stimulator for Ionic Electroactive Polymers. IEEE Sensors Journal 2018; 18(5): 1930-1939.
[4] Shahinpoor M, Bar-Cohen Y, Simpson JO, Smith J. Ionic polymer-metal composites (IPMCs) as biomimetic sensors, actuators and artificial muscles – a review. Smart Materials and Structures 1998; 7(6): R15-R30.
[5] Kim KJ, Tadokoro S. Electroactive Polymers for Robotic Applications: Artificial Muscles and Sensors. London, UK: Springer-Verlag; 2007.
[6] Shahinpoor M, Kim KJ. Ionic polymer-metal composites: I. Fundamentals. Smart Mater. Struct 2001; 10: 819-833.
[7] Serra L, Domenech J, Peppas NA. Drug transport mechanisms and release kinetics from molecularly designed poly(acrylic acid-g-ethylene glycol) hydrogels. Biomaterials 2006; 27: 5440-5451.
[8] Wang L-P, Ren J, Yao M-Q, Yang X-C, Yang W, Li Y. Synthesis and characterization of self-oscillating P(AA-co-AM)PEG semi-IPN hydrogels based on a pH oscillator in closed system. Chinese Journal of Polymer Science 2014; 32(12): 1581-1589.
[9] McKeon-Fischer KD, Flagg DH, Freeman JW. Poly(acrylic acid)/poly(vinyl alcohol) compositions coaxially electrospun with poly(ε-caprolactone) and multi-walled carbon nanotubes to create nanoactuating scaffolds. Polymer 2011; 52: 4736-4743.
[10] Inada Y, Furukawa M, Sasaki H, Kodera Y, Hiroto M, Nishimura H, Matsushima A. Biomedical and biotechnological application of PEG- and PM-modified proteins. Trends in Biotechnology 1995; 13(3): 86-91.
[11] Bryant SJ, Chowdhury TT, Lee DA, Bader DL, Anseth KS. Crosslinking Density Influences Chondrocyte Metabolism in Dynamically Loaded Photocrosslinked Poly(ethylene glycol) Hydrogels. Annals of Biomedical Engineering 2004; 32(3): 407-417.
[12] Flory PJ. Principles of Polymer Chemistry. Ithaca, USA: Cornell University Press; 1953.
[13] Merrill EW, Dennison KA, Sung C. Partitioning and diffusion of solutes in hydrogels of poly(ethylene oxide). Biomaterials 1993; 14: 1117-1126.
[14] McKeon-Fischer KD, Flagg DH, Freeman JW. Coaxial electrospun poly(ε-caprolactone), multiwalled carbon nanotubes, and polyacrylic acid/polyvinyl alcohol scaffold for skeletal muscle tissue engineering. Journal of Biomedical Materials Research Part A 2011; 99A: 493-499.
[15] Close RI. Dynamic properties of fast and slow skeletal muscle of the rat after nerve cross-union. J. Physiol. (London) 1969; 204: 331-46.

[16] Burke RE, Tsairis P. Anatomy and innervation ratios in the motor units in cat gastrocnemius. J. Physiol. 1973; 234: 769-5.
[17] Lannergren J, Westerblad H. The temperature dependence of isometric contraction of single, intact fibres dissected from a mouse foot muscle. J. Physiol 1987; 390: 285-93.
[18] Kanda K, Hashizume K. Factors causing difference in force output among motor units in the rat medial gastrocnemius muscle. J. Physiol 1992; 448: 677-95.

CHAPTER 3: THE PROCESS OF ELECTROSPINNING CONDUCTIVE NANOFIBERS IN A HIGHLY ALIGNED ORIENTATION: MORPHOLOGY AND BIOLOGICAL RESPONSE

Note: At the time of submission of this dissertation, this chapter had been submitted in its entirety to the journal, 'Journal of Biomedical Materials Research Part A', and was under review.

3.1 Introduction

The fields of tissue engineering and biomaterials have the potential to provide a scalable solution to the problem of large volume defects in skeletal muscle. Tissue engineers and biomaterials scientists aim to develop mature skeletal muscle tissue using a combination of biomaterials, cells, and a variety of stimuli including growth factors, mechanical stretching, and electrical pulses to promote differentiation of the tissue [1, 2]. The paradigm followed by researchers usually involves isolating some type of muscle progenitor cell (satellite cells or mesenchymal stem cells), expanding the cells in culture, allowing them to attach to some biomaterial scaffold, and administering the proper stimulation (chemical, mechanical, electrical, etc.) to differentiate the cells. Satellite cells are the closest precursor cells to muscle, and C2C12 mouse myoblasts are a common satellite cell line used by researchers [3, 4]. Numerous biomaterial scaffolds have been shown to facilitate the development of C2C12 cells into myotubes, the early stage of muscle fibers [5-7]. However, previous scaffold research falls short of aiding the development of highly mature muscle tissue capable of contracting with the same force as native muscle tissue. Part of addressing this gap involves determining the characteristics of an ideal scaffold for regenerating skeletal muscle. Researchers have

posited that the properties of the ideal scaffold include a fibrous architecture, a highly aligned orientation of those fibers, and a biodegradable and conductive substrate among others [3-7].

Previous research has focused on the role of conductivity in promoting cell attachment and differentiation on muscle scaffolds. Chen and coworkers utilized polyaniline, a conductive polymer, to demonstrate that C2C12 myoblasts will mature to a greater extent on electrically conductive scaffolds than non-conductive scaffolds even when guidance cues are constant [6]. Jun and coworkers also used polyaniline to investigate whether the level of conductivity impacted the differentiation of satellite cells, but they found that the scaffolds with two different concentrations of polyaniline produced roughly the same myotube number, length, and area [7]. However, this study also found that polyaniline increased the Young's modulus of the scaffolds. Other studies have used Gold nanoparticles, multi-walled carbon nanotubes, and other conductive polymers have usually increased conductivity at the expense of increasing mechanical properties [8-10]. Given that other studies have found that the mechanical properties of a substrate can have a large impact on the myogenic potential of progenitor cells [11-12], it is possible that the extent of C2C12 differentiation could be improved by accounting for the mechanical properties of the scaffold while increasing conductivity.

Our goal is to find a combination of materials that can be fabricated into a biocompatible, biodegradable, fibrous, conductive scaffold which has mechanical properties similar to native muscle tissue. We have previously determined that electrospun scaffolds made of polycaprolactone (PCL) have similar mechanical properties to rat muscle tissue [9]. In addition, PCL has been used extensively in tissue

engineering research as a biocompatible and biodegradable polymer [9, 13-15]. Since PCL is not conductive, we sought to increase the conductivity of the resulting scaffolds through the use of a conductive polymer. Polypyrrole (PPy) is a biocompatible, biodegradable, conductive polymer that has been used as a biomaterial for nerve tissue electrodes [16]. In addition, PPy has previously been polymerized with PCL to form a copolymer [17]. Thus, in an attempt to arrive at a suitable material to increase conductivity without significantly increasing mechanical properties, we have synthesized a copolymer of PPy and PCL (PPy-PCL) to use in the fabrication of fibrous scaffolds for skeletal muscle regeneration via electrospinning.

Electrospinning has been utilized extensively for fabricating scaffolds for tissue engineering. The basic set-up for electrospinning is shown below in figure 3.1. First, the polymer solution inside of a syringe with a metal needle is placed within a syringe-pump aimed at a collection plate or spinning mandrel [18]. While the syringe-pump expels the solution, a voltage potential between the metal needle and the collection device drives the solution through the air in a spinning pattern, which draws the solution into a thin fiber. After collection, the solvent evaporates and leaves a fibrous scaffold of polymer. A spinning mandrel may be used to collect fibers in a highly aligned orientation [18].

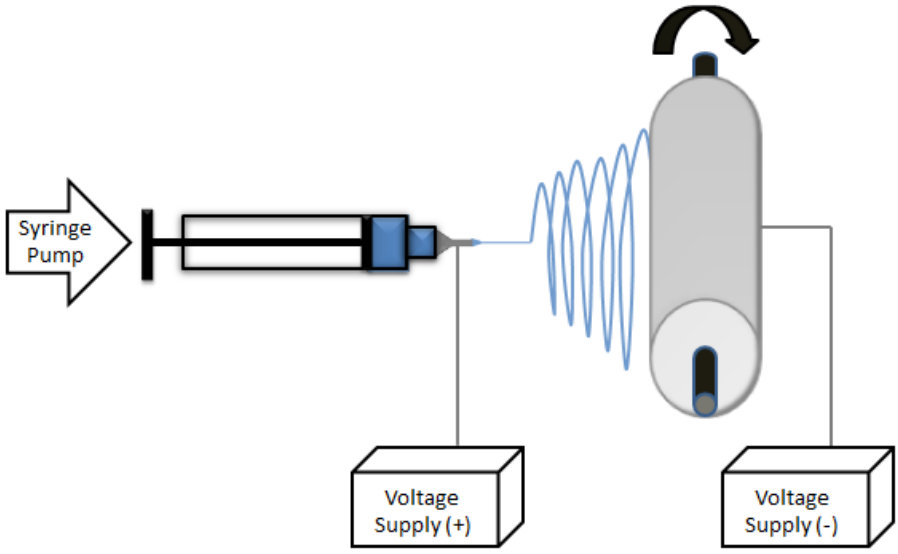

Figure 3.1: Electrospinning diagram. Basic diagram of the electrospinning process for producing aligned scaffolds on a spinning mandrel.

The objective of this paper is to fabricate and characterize an electrospun PPy-PCL scaffold and evaluate its potential as a scaffold for skeletal muscle regeneration. After synthesizing a PPy-PCL copolymer, solutions with three different blends of PCL and PPy-PCL copolymer (at different concentrations) plus a control solution of pure PCL are electrospun into fibrous scaffolds with an aligned and random orientation. These scaffolds are evaluated for their conductivity, mechanical properties, and morphology on the nano-scale. Further, we evaluate the ability of the scaffolds to promote the attachment, proliferation, and differentiation of C2C12 myoblasts. Through these experiments, we seek to provide insight on the optimal properties of a scaffold for skeletal muscle regeneration.

3.2 Materials and Methods

3.2.1 Synthesis of Polypyrrole-Polycaprolactone (PPy-PCL) Copolymer

A copolymer of polycaprolactone (PCL) and polypyrrole (PPy) was synthesized in a similar manner to Nguyen and coworkers [17]. All chemicals were purchased from Sigma-Aldrich (St. Louis, MO) and used as received. PCL diols (27.8 g) having an average molecular weight of 2000 Daltons were purged with nitrogen for 10 minutes then dissolved in 100 mL of anhydrous tetrahydrofuran (THF). The solution was cooled with an isopropanol/liquid nitrogen bath, and then butyl lithium (2.5 M, 10 mL) was added drop-wise. After addition of the butyl lithium, the bath was removed, and the reaction mixture was stirred for 20 minutes. A solution of 2-(trichloroacetyl)pyrrole (5.9 g) in 30 mL of anhydrous THF was mixed in a separate container. After allowing the lithiated-Capa (PCL diols in THF treated with butyl lithium) to cool within the isopropanol/liquid nitrogen bath, the 2-(trichloroacetyl)pyrrole solution was added drop-wise to the reaction flask. The bath was removed after all of the solution was added, and the reaction mixture was stirred for 1 hour at room temperature. The reaction was then quenched with cold 1M HCl solution to lower the pH to 7. Under vacuum, the THF was removed and the organic residue was extracted with dichloromethane with two washings. The combined extracts were washed with 5% $NaHCO_3$ three times, then with deionized water two times to achieve a pH of 7. The organic layer was dried over anhydrous $MgSO_4$ and the solvent was removed under vacuum. The intermediate product (Polycaprolactone2000diPyrrole) was verified with ^1H NMR analysis.

Iron (III) p-toluenesulfonate ($Fe[PTS]_3$, 23.67 g) and acetonitrile (300 mL) were mixed in a 1 L round bottom flask by an overhead stirrer for 5 minutes. Pyrrole (1.2 g)

and Polycaprolactone2000diPryrrole (2.4 g) in acetonitrile (300 mL) were added to the reaction flask. The copolymerization mixture was stirred for 2 days. During this time, the conducting copolymer aggregated and flocculated to form a black particulate suspension. The reaction mixture was centrifuged at 5000 RPM for 25 minutes to isolate the product. The supernatant was removed and the precipitate, a black gel, was washed with ethanol and centrifuged an additional three times. The final product, polypyrrole-co-polycaprolactone (PPy-PCL), was dried and verified with ^{1}H NMR analysis.

3.2.2 Solution Preparation and Electrospinning

Solutions were prepared by sonicating the PPy-PCL copolymer component in solvent before adding the appropriate amount of pure PCL (MW 70,000 – 90,000 Daltons) to achieve the proper viscosity for electrospinning. For all solutions, the solvent was a 1:1 (volume:volume) mixture of dichloromethane (DCM) and dimethylformamide (DMF). . The PPy-PCL component was sonicated in the DCM/DMF solution using a Branson Digital Sonifier 450 (Danburg, CT, USA) prior to adding the PCL component. Solutions were sonicated for a total of 6:00 minutes at 20% amplitude using pulses that lasted 2 seconds with 3 seconds between pulses. The PCL component was added immediately after sonicating, and the final solution was rotated for at least 12 hours to mix homogenously. The total concentration of polymer in the solution was 20% (weight/volume), and the relative ratio of PCL and PPy-PCL was adjusted to obtain scaffolds with different relative concentrations.

The solution was electrospun in a similar method to McKeon-Fisher and coworkers [8-9]. A diagram of the electrospinning set-up can be seen in Figure 3.2. A fibrous scaffold was formed at an extrusion rate of 0.50 mL/hour or 0.25 mL/hour and a

distance of 12 cm between the needle and the collection device. A negative voltage of -10 kV and a positive voltage in the range of 10-25 kV was used to obtain a stable stream of solution. The aligned scaffolds were collected on a spinning mandrel with a 9 cm diameter rotating at 3,000 RPM (± 100 RPM), as seen in Figure 3.2A. The random scaffolds were collected on a flat plate, as seen in Figure 3.2B. The abbreviations for all of the groups used in this paper along with the electrospinning parameters can be found in Table 3.1.

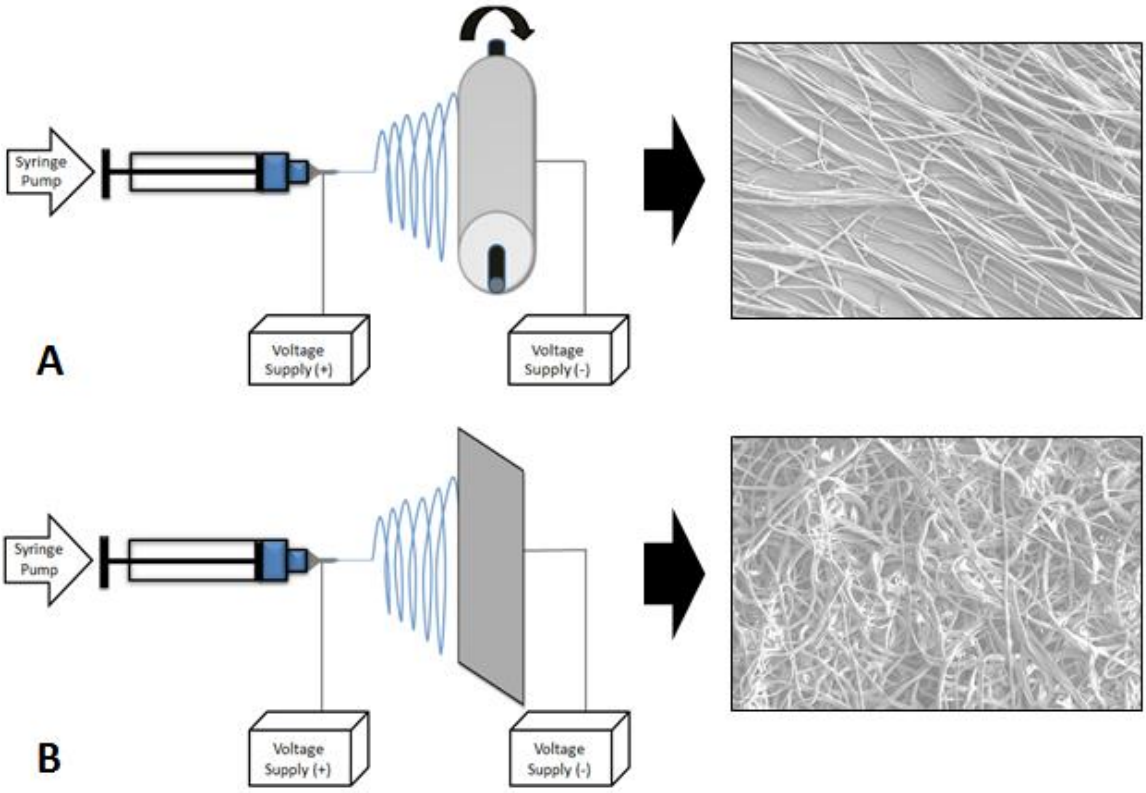

Figure 3.2: Influence of collection method on electrospinning. Schematic of the two set-ups for electrospinning. **A**) A spinning mandrel (3,000 RPM) is used to collect fibers in an aligned orientation. **B**) When fibers are collected on a flat plate, a random orientation results.

Group Name	Ratio PPy-PCL copolymer (%)	Ratio PCL (%)	Collection Method	Flow Rate (mL/hour)
PCL - R	0%	100%	Flat Plate	0.5 mL/hour
PCL - A	0%	100%	Spinning Mandrel (3,000 RPM)	0.5 mL/hour
10% PPy-PCL - R	10%	90%	Flat Plate	0.5 mL/hour
10% PPy-PCL - A	10%	90%	Spinning Mandrel (3,000 RPM)	0.5 mL/hour
20% PPy-PCL - R	20%	80%	Flat Plate	0.5 mL/hour
20% PPy-PCL - A	20%	80%	Spinning Mandrel (3,000 RPM)	0.5 mL/hour
40% PPy-PCL - R	40%	60%	Flat Plate	0.25 mL/hour
40% PPy-PCL - A	40%	60%	Spinning Mandrel (3,000 RPM)	0.25 mL/hour

Table 3.1: Copolymer scaffold sample identification. The different scaffold groups fabricated for this study with the relevant electrospinning parameters. The two main fiber orientations are random (R) and aligned (A).

3.2.3 Scanning Electron Microscopy (SEM) and Morphological Characterization

All fibrous scaffolds were examined under a Scanning Electron Microscope (SEM) [Zeiss Sigma Field Emission SEM with Oxford INCA PentaFETx3 EDS system (Model 8100)] and evaluated for their fiber morphology using ImageJ software [version 1.46r/Java 1.6.0_25 (32-bit)]. Fiber orientation was quantified by measuring the angle formed by the fibers from each scaffold group relative to the vertical axis of each image (n = 105). The fiber angles were normalized to an average value of 0 degrees for each scaffold group and plotted in histograms. Fiber diameter was quantified by measuring the width of the fibers perpendicular to the long axis of each fiber and comparing to the scale bar for each image (n = 25).

3.2.4 Conductivity Measurements

Each of the aligned scaffold groups was cut into 1 cm x 1 cm squares to test their conductivity under a DC voltage of 20 V (n = 4). The voltage was applied and the current output was measured with an E3646A dual output DC power supply (Agilent Technologies, Santa Clara, CA). The conductivity of each sample was determined with the equation, C = L/[(V/I) x A], where C is the conductance of the scaffold, L is the length of the scaffold, V is the voltage, I is the current, and A is the cross-sectional area of the scaffold (width x thickness).

3.2.5 Mechanical Testing

Scaffold samples were cut into 1 cm x 4 cm strips for mechanical testing in tension (n = 4). Samples were secured in the soft tissue grips of an Instron 5869 mechanical testing machine. The gauge length was 2.0 cm, and the samples were pulled in tension at a rate of 2.0 mm/min (10% strain/minute) until failure. A stress versus strain graph was used to calculate the elastic modulus and ultimate tensile stress for each sample.

3.2.6 Cell Studies with C2C12 Myoblasts, Measuring Metabolic Activity, and Fluorescence Imaging

Scaffold samples were cropped to the size of a 24-well plate (ultra low attachment) and sterilized by soaking in ethanol for 30 minutes and administering UV radiation for 30 minutes on both sides (n = 8). The samples were washed with sterile phosphate buffered saline (PBS) before soaking in DMEM media with 10% fetal bovine serum (FBS) and 1% penicillin/streptomycin (P/S) for 12 hours. The scaffold samples were seeded with C2C12 mouse myoblasts at a density of 25,000 cells/cm^2 (purchased from ATCC). Tissue culture plastic (TCP), i.e. blank wells, served as a positive control.

During the proliferation phase (day 0 to day 3), all samples were fed with DMEM media with 10% FBS and 1% P/S every other day. During the differentiation phase (day 4 to day 10), all samples were fed with DMEM media with 1% FBS and 1% P/S once per day.

The metabolic activity of the cells on the scaffold samples was measured using a PrestoBlue® cell viability assay on day 1, day 3, and day 7 after applying the differentiation media using the instructions provided by the manufacturer (n = 8). Briefly, the media from the wells was aspirated, and PrestoBlue® cell viability reagent diluted to a ratio of 1:10 with differentiation media was applied for a 1 hour incubation period. The reagent-media mixture was removed at the end of the incubation period, and the absorbance was analyzed by a plate reader at a wavelength of 570 nm. After subtracting a blank control, the absorbance value produced by this assay is directly proportional to the metabolic activity of the cells on each sample.

On day 10, the cells on the scaffold samples were fixed with a 4% paraformaldehyde solution to prepare for staining (n = 4). Cells were stained with NucBlue® fixed cell ReadyProbes® reagent (Thermo Fisher Scientific) for DNA (Blue) and Fluorescein Phalloidin (Thermo Fisher Scientific) for F-actin (Green).

3.2.7 Morphological Analysis of Fluorescent Images

A representative sample of five images for each group was used to quantify the morphology of the cells on the scaffold groups. ImageJ software [version 1.46r/Java 1.6.0_25 (32-bit)] was used to quantify the total number of nuclei, the total number of myotubes, and the number of nuclei inside of myotubes for each image. Myotubes were defined as clearly distinguishable, linear structures which contained two or more nuclei. These parameters were used to calculate the fusion index (nuclei inside of myotubes/total

number of nuclei) and the average number of nuclei per myotubes (nuclei inside of myotubes/total number of myotubes).

3.2.8 Quantitative Polymerase Chain Reaction (qPCR)

Expression of myogenic markers was evaluated using quantitative polymerase chain reaction (qPCR) on day 10 (n = 4). Total RNA was isolated and filtered by spin protocol using a RNeasy Plus Mini Kit (Qiagen, Valencia, CA, USA) according to the manufacturer's protocol. The RNA concentrations were quantified using a ND100 spectrophotometer (Thermo Fisher Scientific, Cambridge, MA, USA). The total RNA was normalized across all groups before being reverse transcribed to obtain the cDNA library using a High-Capacity cDNA Reverse Transcription kit (Applied Biosystems, Foster City, CA, USA) according to the manufacturer's protocol. The cDNA was subjected to qPCR using a SYBR Green PCR Master Mix (Applied Biosystems, Foster City, CA, USA) on a Real-time PikoReal™ PCR Detection System (Thermo Fisher, St Louis, MO, USA). All primers used in this paper are listed in Table 3.2. The relative gene expression was determined using the ΔΔCT method and normalized to glyceraldehyde 3-phosphate dehydrogenase (GAPDH) as the endogenous control (housekeeping gene).

Primer	Primer Abbreviation	Forward Sequence	Reverse Sequence	PrimerBank ID
Mus Musculus glyceraldehyde-3-phosphate dehydrogenase	GAPDH	AGG TCG GTG TGA ACG GAT TTG	GGG GTC GTT GAT GGC AAC A	126012538c1
Mus Musculus Myogenic Differentiation 1 (MyoD1)	MyoD	CGG GAC ATA GAC TTG ACA GGC	TCG AAA CAC GGG TCA TCA TAG A	170172578c1
Mus Musculus Myogenin	Myogenin	GAG ACA TCC CCC TAT TTC TAC CA	GCT CAG TCC GCT CAT AGC C	13654247a1
Mus Musculus Myosin, Heavy Chain 15 (Myh15)	MHC	TGT CAA TGC TGC TTT ACC TCA A	GCA TAT CCT GAA AGG CAC GAT	261245015c1

Table 3.2: List of primer sequences. All primer sequences were taken from the Harvard PrimerBank.

3.2.9 Statistical Analysis

The fiber orientation data are expressed in histograms, and all other data are expressed as averages with the error bars corresponding to the standard deviation. Significance between groups was evaluated using a one-way ANOVA with a Tukey's post-hoc test. Significance was set at $\alpha = 0.05$ (denoted by * unless otherwise noted).

3.3 Results

3.3.1 Solution Preparation and Electrospinning

The electrospinning procedure was successful for all groups, but different parameters were required for each group. In general, a higher voltage difference between the metal needle and the collection device was needed for solutions with a higher concentration of PPy-PCL copolymer. In addition, for solutions with a higher concentration of PPy-PCL, the Taylor cone and stream of polymer were less stable and required more fine tuning to keep the process going. The pure PCL solutions produced the most stable electrospinning processes, and resulted in a white scaffold. The scaffolds got darker in color with increasing concentration of PPy-PCL. The 40% PPy-PCL solutions made the electrospinning process difficult to stabilize, so a change to a slower flow rate (0.25 mL/hour) was implemented. All scaffolds were removed from the collection devices without much labor; although, the scaffolds with PPy-PCL seemed to stick to the collection device to a greater extent.

3.3.2 Scanning Electron Microscopy (SEM) and Morphological Characterization

Representative SEM images of the eight scaffold groups are shown in Figure 3.3. Beading, or the tendency of the polymer stream to pool instead of depositing in a clear fiber, was more common on the random scaffolds than the aligned scaffolds. In addition, beading increased in frequency with an increase in the concentration of PPy-PCL. There is a clear distinction in the orientation of the fibers between the scaffolds collected on the spinning mandrel (aligned) and the scaffolds collected on the flat plate (random). A quantification of the fiber orientation is shown in the histograms of fiber angle shown in Figure 3.4. The aligned scaffolds had 62.9% of their fibers within 20 degrees of the mean

direction on average, and the random scaffolds had only 32.6% of their fibers within 20 degrees of the mean direction on average (a statistically significant difference). The fiber diameter data for all groups are shown in Figure 3.5. The 40% PPy-PCL – A group produced a significantly higher average fiber diameter than the groups. However, the average fiber diameter for all groups fell between 0.5 μm and 2.5 μm.

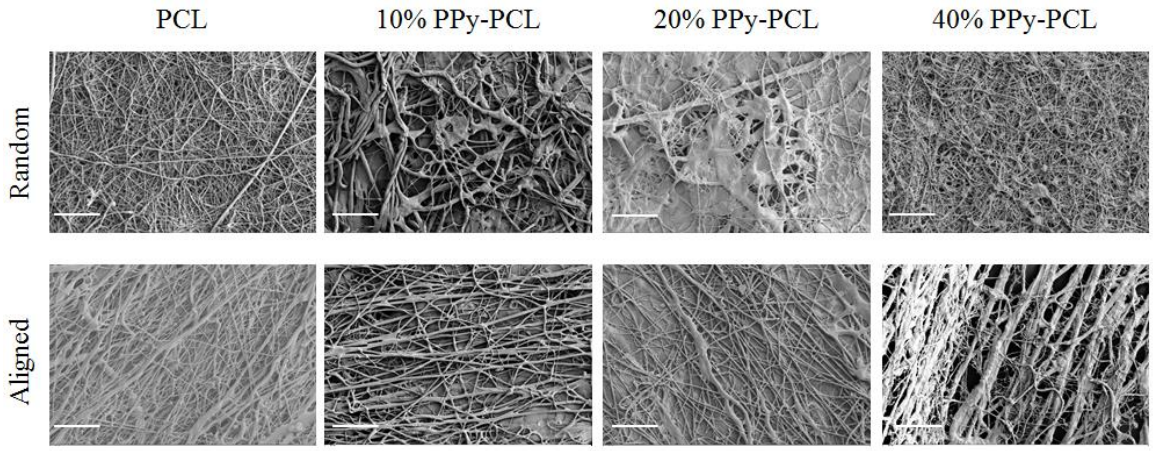

Figure 3.3: Scaffold SEM images. Representative SEM images of the different scaffolds. The scale bar in each image represents a length of 50 μm.

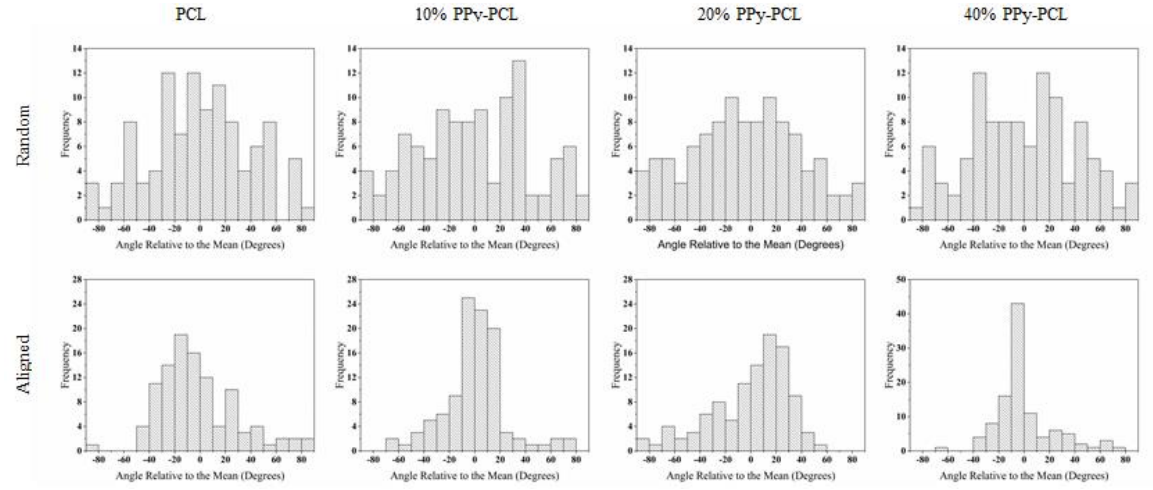

Figure 3.4: Histograms of fiber orientation. Histograms of the distribution of fiber angles for the different scaffolds (n = 105).

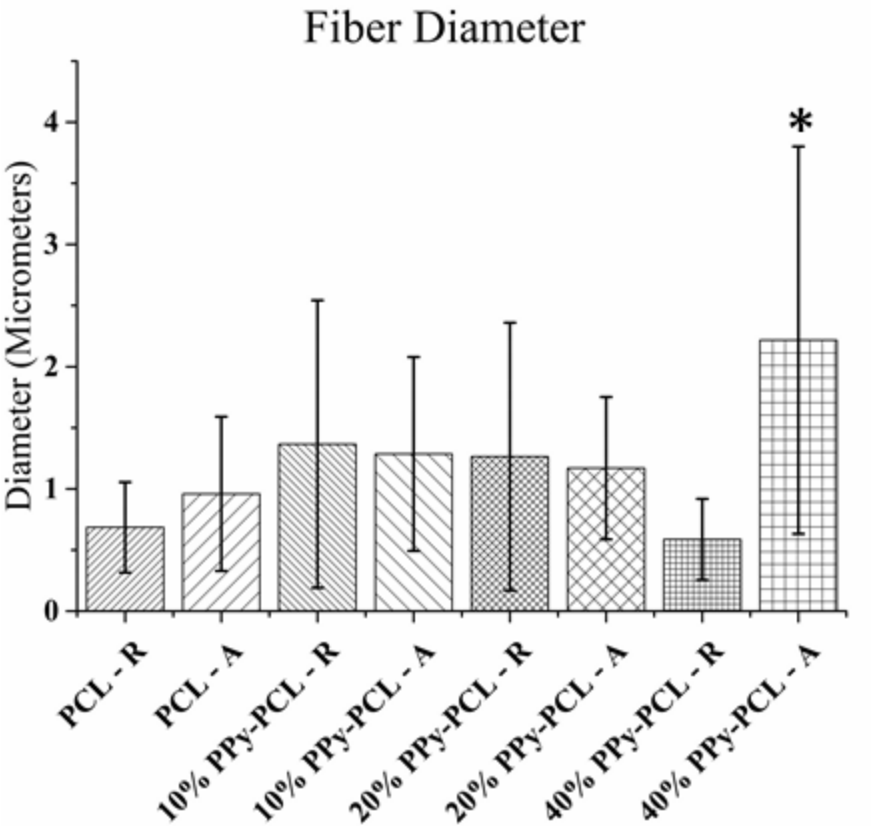

Figure 3.5: Copolymer scaffold fiber diameter. Fiber diameters of the different scaffolds (n = 25; * denotes statistical significance with $p < 0.05$).

3.3.3 Conductivity Measurements and Mechanical Testing

The conductivity data and the values for elastic modulus and ultimate tensile stress calculated from the mechanical testing experiments are shown in Table 3.3. The only scaffolds with a measureable conductivity were the 40% PPy-PCL scaffolds, which produced a conductivity of 1.1 mS/cm. All other scaffold groups did not post a measurable conductivity when tested. The highest elastic modulus was obtained with the PCL – A group, but there was no significant difference between any of the groups for elastic modulus. The PCL – A group produced a significantly higher ultimate tensile stress than the other groups, but there was no difference in ultimate tensile stress between

any of the groups with PPy-PCL. Only the aligned scaffolds were tested for their conductivity and mechanical properties.

Group Name	Elastic Modulus (kPa)	Ultimate Tensile Stress (kPa)	Conductivity (mS/cm)
PCL - A	10422 ± 2364	3367 ± 1131 *	0.0 ± 0.0
10% PPy-PCL - A	7433 ± 1502	1788 ± 159	0.0 ± 0.0
20% PPy-PCL - A	8509 ± 1304	1809 ± 465	0.0 ± 0.0
40% PPy-PCL - A	8685 ± 1397	1574 ± 370	1.1 ± 0.2 *

Table 3.3: Copolymer scaffold mechanical properties and conductivity. The elastic modulus, ultimate tensile stress, and conductivity of the different scaffolds (n = 4; * denotes statistical significance with $p < 0.05$).

3.3.4 Cell Studies with C2C12 Myoblasts, Measuring Metabolic Activity, and Fluorescence Imaging

The metabolic activity data for three time-points are shown in Figure 3.6. Cells on the PCL-R and PCL-A groups produced significantly lower metabolic activity than all scaffold groups containing PPy-PCL and the positive control (TCP) at all time-points. On day 1, four other groups (10% PPy-PCL – A, 20% PPy-PCL – R, 20% PPy-PCL – A, 40% PPy-PCL – A) produced significantly lower metabolic activity than the control. By day 3, only one group with PPy-PCL (20% PPy-PCL – A) produced metabolic activity lower than the control, and none of the groups with PPy-PCL were below the control on day 7. The metabolic activity on the 40% PPy-PCL – R group was significantly higher than the control on day 7. Overall, metabolic activity gradually increased in the cells on scaffolds with PPy-PCL, and metabolic activity gradually decreased in cells on the pure PCL scaffolds.

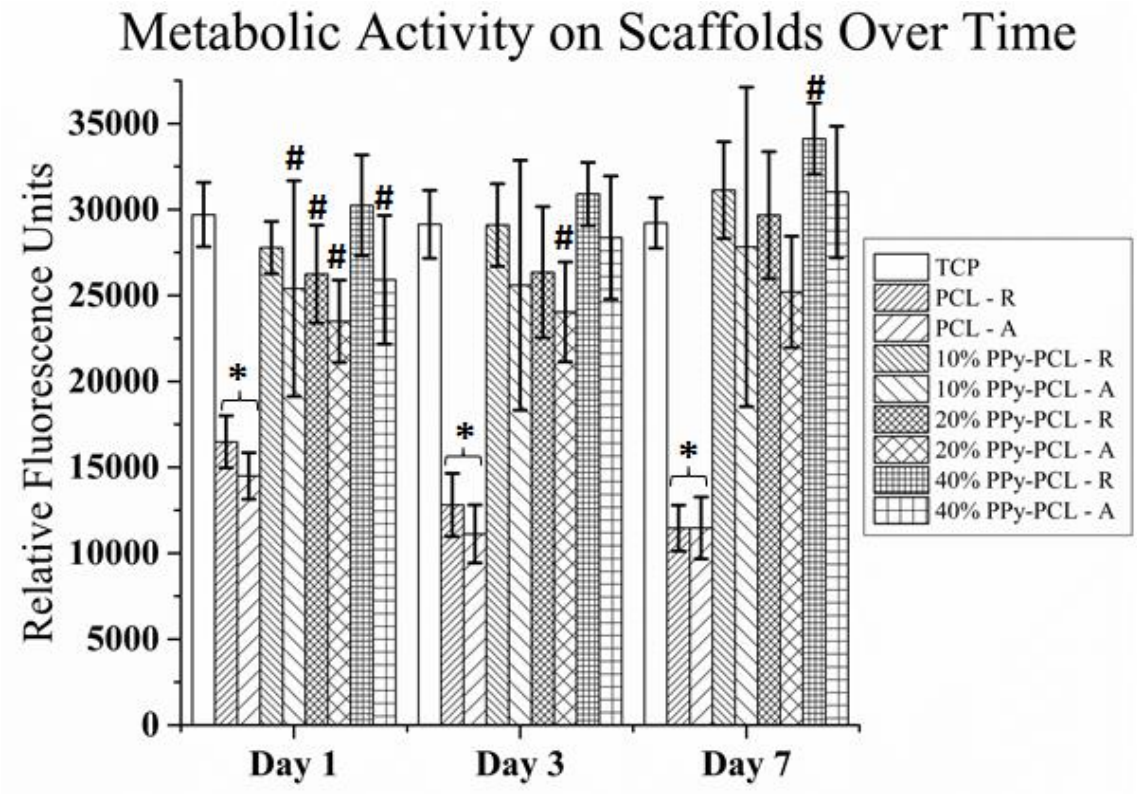

Figure 3.6: Metabolic activity on copolymer scaffolds. Metabolic activity of C2C12 cells seeded on the different scaffolds as measured by a PrestoBlue® cell viability assay on days 1, 3, and 7 of the differentiation protocol (n = 8; * denotes significantly different from all other groups at that time-point with $p < 0.05$; # denotes significantly different from the TCP control group at that time-point with $p < 0.05$).

Representative fluorescence images of the cells on the scaffolds are shown in Figure 3.7 for day 10 in culture. In general, there was less matrix deposition and cell adherence on the PCL scaffolds than on the scaffolds with any concentration of PPy-PCL. Although some myotubes formed on the random scaffolds, there were more myotubes on the corresponding aligned scaffolds, and the myotubes were much closer to parallel on the aligned scaffolds than the random scaffolds. In addition, the fluorescence

images of the aligned scaffolds were clearer and in better focus than the images of the random scaffolds.

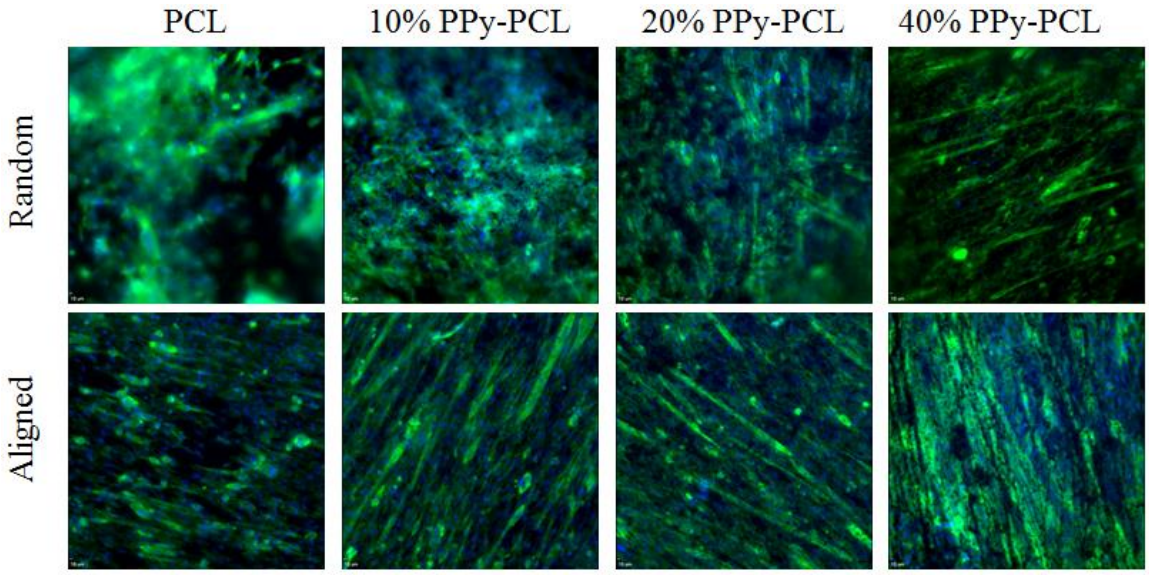

Figure 3.7: Actin and DNA staining on copolymer scaffolds. Representative fluorescence images taken to illustrate cell morphology on day 10. Actin is stained in green with Fluorescein Phalloidin, and DNA is stained in blue with NucBlue® fixed cell ReadyProbes® reagent.

3.3.5 Morphological Analysis of Fluorescent Images

The results of the morphological analysis are shown in the four parts of Figure 3.8. All scaffolds with randomly aligned fibers produced significantly lower numbers of nuclei and myotubes than the TCP control and all aligned groups with PPy-PCL (Figure 3.8A and 3.8B). There were no significant differences between any of the aligned groups for the number of nuclei or myotubes. The data for fusion index are shown in Figure 3.8C. The fusion index of the TCP control was significantly higher than all other groups. Generally, the aligned scaffold facilitated a greater fusion index than the corresponding random scaffold. All of the randomly aligned scaffolds also had a significantly lower

fusion index than the 10% PPy-PCL – A, 20% PPy-PCL – A, and 40% PPy-PCL – A groups. The 10% PPy-PCL – A and 40% PPy-PCL – A groups produced a significantly higher fusion index than the PCL – A and 20% PPy-PCL – A groups. The number of nuclei per myotube was higher in the aligned scaffolds than the corresponding random scaffolds except for the pure PCL groups where there was no significant difference (Figure 3.8D). As with the fusion index, the 10% PPy-PCL – A and 40% PPy-PCL – A groups had the highest average number of nuclei per myotube, and both of these groups were comparable to the positive control.

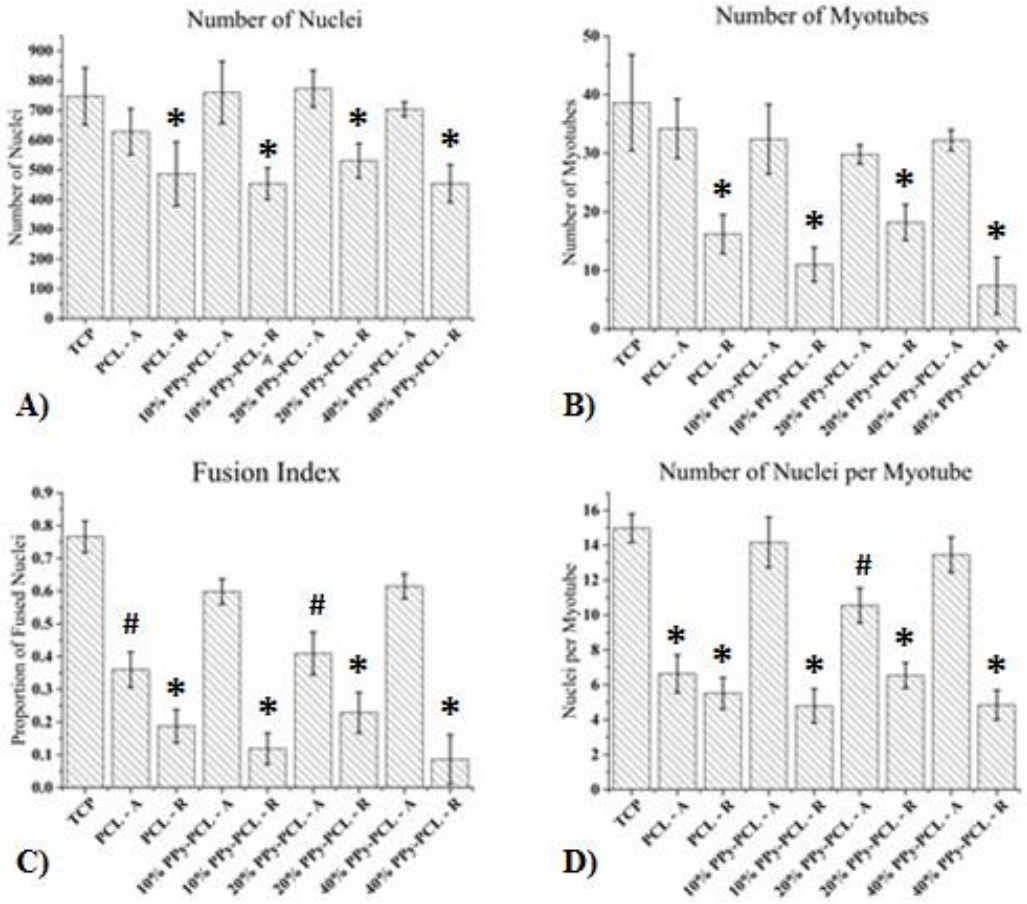

Figure 3.8: Myotube morphological analysis. Morphological analysis of the fluorescence images with the **A)** number of nuclei, **B)** number of myotubes, **C)** fusion index, and **D)** number of nuclei per myotube (n = 5; * denotes significantly different from

the TCP control, 10% PPy-PCL – A, 20% PPy-PCL – A, and 40% PPy-PCL – A groups with $p < 0.05$; # denotes significantly different from the TCP control, 10% PPy-PCL – A, and 40% PPy-PCL – A groups with $p < 0.05$).

3.3.6 Quantitative Polymerase Chain Reaction (qPCR)

The relative gene expression data for MyoD, MHC, and Myogenin on day 10 are shown in Figure 3.9. For the expression of MyoD, shown in Figure 3.9A, there was a small trend of the random scaffolds producing higher levels of MyoD expression than the corresponding aligned scaffolds. The highest MyoD expression was found in the PCL – R group, which was significantly higher than three other groups (20% PPy-PCL – A, 40% PPy-PCL – R, and 40% PPy-PCL – A). The relative Myogenin expression is shown in Figure 3.9B. The 20% PPy-PCL-A and 40% PPy-PCL-A groups produced significantly lower Myogenin expression than the control. Otherwise, Myogenin expression was fairly consistent between groups. The expression of Myosin Heavy Chain (MHC) was also fairly consistent across all groups (Figure 3.9C). The highest expression of MHC was found in the 10% PPy-PCL – A group, and the lowest MHC expression was found in the PCL – R group, but these differences were not significant.

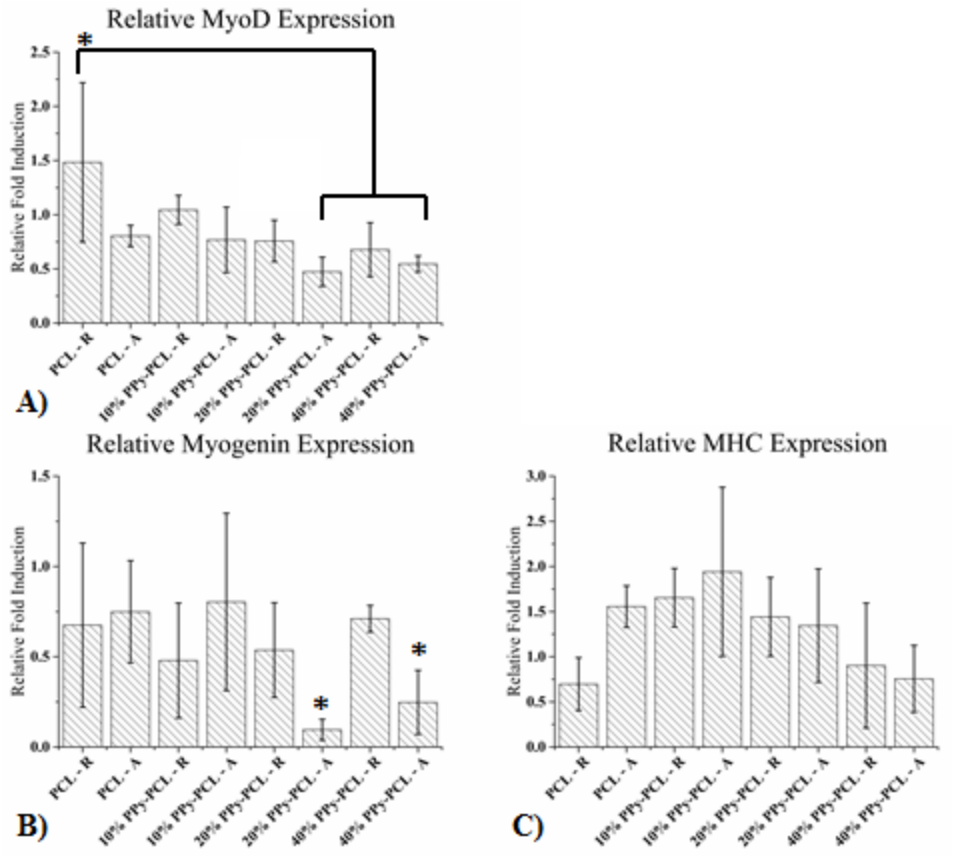

Figure 3.9: qPCR of C2C12 cells on copolymer scaffolds. Relative gene expression normalized to GAPDH expression on the TCP control for **A)** MyoD, **B)** Myogenin, and **C)** MHC on day 7 after differentiation (n = 4; * denotes significantly different from the TCP control group with $p < 0.05$, and brackets are used to specify differences between groups).

3.4 Discussion

There is still debate on what scaffold properties are optimal to aid in regenerating skeletal muscle tissue. This study has investigated the use of a conductive copolymer to enhance scaffold conductivity without significantly increasing mechanical properties. Several versions of the resulting scaffolds were characterized and evaluated for their ability to promote myoblast attachment and differentiation using C2C12 myoblasts as a model of muscle progenitor cells. In the process, this paper also provides information on how to incorporate more complex materials, such as copolymers and composites, into scaffolds using existing fabrication techniques like electrospinning.

When fabricating the scaffolds, sonication was used to disperse the PPy-PCL copolymer homogenously within solution prior to electrospinning. We utilized this approach since we were unable to find a solvent that dissolves both the PPy-PCL copolymer and PCL. Sonication only disperses particles for a limited period of time, but it was long enough to successfully incorporate the PPy-PCL copolymer into an electrospun scaffold. However, the electrospinning process itself was somewhat complicated by the addition of PPy-PCL. In general, a greater voltage difference between the metal needle and the collection device was needed for greater concentrations of PPy-PCL, and it was difficult to obtain a stable flow of solution for the 40% PPy-PCL groups. We previously had difficulty with electrospinning another conductive polymer, poly(3,4-ethylenedioxythiophene) (PEDOT), that was dispersed using sonication and combined with PCL [19]. While sonication allows particles to be dispersed in solution for electrospinning, we have found that there is a limit to the concentration of particles that will stay dispersed without affecting the electrospinning procedure. We were unable to

perform the electrospinning procedure with solutions with a concentration of greater than 40% copolymer. Other studies dispersing conductive elements in solution have also found difficulty with electrospinning at higher concentrations [9, 20-21]. Part of this difficulty may be a result of partially charged areas on the PPy-PCL molecules (or conductive particles in general) interacting strongly with the applied voltage and disrupting the electrospinning process. We suspect that using conductive copolymers which are fully soluble in a solvent that is compatible with electrospinning may avoid these issues by avoiding sonication as a dispersal method.

The SEM images and subsequent morphological characterization show that collecting fibers on a spinning mandrel had a large impact on the final orientation of the fibers as compared to the flat plate. There was no discernable pattern to how the concentration of PPy-PCL copolymer affected the orientation of the fibers. However, there seemed to be a greater incidence of beading, or the tendency for the collecting solution to pool instead of forming a fiber, with a higher concentration of PPy-PCL. It is possible that the higher conductivity of the solutions with a higher concentration of PPy-PCL makes the stream more sensitive to the electric field. In this case, the solution leaves the electrospinning needle faster and travels to the collection device faster, not allowing it to dry as quickly as the less conductive solutions. This phenomenon was especially evident with the scaffolds that were collected on a flat plate. It is possible that the spinning mandrel facilitated fiber formation by allowing solvent to evaporate more quickly than the fibers collected on the flat plate, reducing the frequency of beading in scaffolds collected on a spinning mandrel. The average fiber diameter for all groups fell between 0.5 μm and 2.5 μm, and there were some notable trends. First, the fibers formed

from solutions with PPy-PCL had a greater standard deviation in fiber diameter than the fibers formed from solutions with pure PCL. Second, the 40% PPy-PCL-A scaffolds had fibers that were larger than the other groups. Both of these trends can be attributed to greater variability in the electrospinning process caused by the addition of PPy-PCL, which may have caused the solution stream to travel faster during the electrospinning process. Previous studies that electrospun conductive particles have obtained similar fiber diameters [19, 22-23]. As we have found in our previous work, the addition of conductive particles may destabilize the electrospinning process [19], but it did not prevent a fibrous scaffold from being formed

A measureable conductivity was recorded for only the 40% PPy-PCL scaffolds. Part of the reason that the 10% PPy-PCL and 20% PPy-PCL groups did not register any conductivity can be attributed to the limitations of our machine. Our voltage supply can give a maximum Voltage of 20 V and can only measure a resulting current down to 1 mA. Therefore, it is possible that these scaffolds were weakly conductive, but it fell outside of the range of our machine. Based on a conservative calculation, the machine can only measure conductivities as low as 0.5 mS/cm for scaffolds with similar dimensions as those used in this study. It is also possible that the concentrations of PPy-PCL in the 10% PPy-PCL and 20% PPy-PCL scaffolds were below the percolation threshold needed to exhibit any measurable conductivity. The conductivity measured from the 40% PPy-PCL scaffolds in this study (1.1 ± 0.2 mS/cm) was significantly lower than the conductivity values from scaffolds in some comparable studies. Our previous studies with PEDOT/PCL fibers produced average conductivities in the range of 20-67 mS/cm [19]. In studies utilizing polyaniline as a conductive element, Chen and coworkers

reported average conductivities in the range of 16.2-63.6 mS/cm [6], and Jun and coworkers reported average conductivities in the range of 160-296 mS/cm [7]. The lower conductivity reported in this study as compared to other studies is likely explained by the fact that the copolymer itself was mostly PCL and that the copolymer was further diluted with pure PCL in order to provide the proper viscosity for electrospinning. On the other hand, some other studies have reported conductivity values in the same range or lower than the measured value for the 40% PPy-PCL scaffold. Sirivisoot and coworkers reported average conductivities in the range of 0.09-1.53 mS/cm for polyurethane scaffolds with single-walled or multi-walled carbon nanotubes [5]. Jeong and coworkers reported conductivites of 1.5 mS/cm up to 13.8 mS/cm for poly(L-lactide-co-ε-caprolactone) scaffolds combined with polyaniline [24]. All of these studies provide useful points of comparison for the impact of a specific value of conductivity on the resulting cell response.

Previous studies have found that substrate mechanical properties can have a large impact on the myogenic potential of muscle progenitor cells [11-12]. Further, myoblasts may require a scaffold stiffness typical of normal muscle in order to differentiate optimally into striated muscle tissue [11]. Reports of the passive Young's modulus of muscle tissue vary and include 51.27 ± 28.48 kPa for rat vastus lateralis muscle [9], 151.83 ± 50.30 kPa for pig medial muscle [9], 5-15 kPa for various types of muscle [25], and around 11,200 kPa for activated skeletal muscle [26]. The average Young's modulus in this study ranged from 7,433 to 10,422 kPa, which puts these scaffolds near the upper range for skeletal muscle Young's modulus. Perhaps more importantly, the addition of the conductive particles, PPy-PCL copolymer molecules, did not increase the modulus of

the scaffolds in this study. Other studies which design conductive fibrous scaffolds achieve a high conductivity at the expense of significantly increasing scaffold stiffness [5-9, 27]. Furthermore, the PPy-PCL copolymer used in this study can be incorporated into different versions of PCL with various molecular weights, allowing the scaffold stiffness to be tuned to the appropriate level for various types of muscle.

The scaffolds were tested for their biocompatibility and ability to promote myoblast differentiation using a protocol in which C2C12 myoblasts are seeded on the scaffolds, fed with proliferation media for the first few days, and then fed with differentiation media for the remainder of the study. The C2C12 cells attached and differentiated to some degree on all scaffolds. The PrestoBlue® viability assay, which is an indirect measure of cell attachment, shows that cells attached and proliferated more on scaffolds with PPy-PCL than the pure PCL scaffolds even from an early time point. However, the metabolic activity was generally not significantly different between random versus aligned scaffolds, and the scaffolds with three different concentrations of PPy-PCL did not significantly differ in metabolic activity. Thus, it seems that the orientation of the fibers does not affect how cells attach and proliferate nearly as much as the composition of the fibers, and there may be a critical concentration of PPy-PCL, around 10% or lower, that causes a significant increase in cell attachment over PCL alone. The differences between aligned and random scaffolds are brought to light when considering the morphological analysis of the fluorescent images. There were significant differences in number of myotubes, fusion index, and number of nuclei per myotube between the random and aligned scaffolds, and these findings are corroborated by previous research [6]. The morphological analysis also provides evidence for the superiority of PPy-PCL

scaffolds over scaffolds with PCL alone. While the number of myotubes was roughly the same between the aligned scaffolds made of PCL and those made of PPy-PCL, the fusion index and average number of nuclei per myotube were generally greater on aligned scaffolds with PPy-PCL than scaffolds with only PCL. Fusion index and number of nuclei per myotube are indicators of myoblast differentiation, so the presence of PPy-PCL seems to cause more myoblast differentiation, but the effect does not seem to be concentration dependent. Fusion index and average number of nuclei per myotube were roughly equal in the 10% PPy-PCL – A group and the 40% PPy-PCL – A group. The 20% PPy-PCL – A group was lower for both of these parameters while remaining higher than all random groups. Previous studies seem split on the ideal concentration of conductive particles (conductivity) for myoblast differentiation. Some studies show a proportional response between conductivity and myoblast differentiation parameters [5, 24], but other studies show no difference in myoblast differentiation between scaffolds of different conductivities as long as some conductive elements are present [7, 19, 23, 28]. This study provides more evidence for the latter group, and we suspect that chemical moieties which promote initial cell attachment may be the more important factor than scaffold conductivity when explaining differences in myoblast differentiation. Although, there are some theories which may explain how the conductive particles are promoting superior initial cell attachment. It is possible that a slight positive charge on the surface of conductive scaffolds attracts the negatively charged myoblast membrane, which results in a higher rate of cell attachment [29]. Also, the electrostatic charges on the scaffold surface may alter protein adsorption and improve cell attachment in the process [30].

Overall, the qPCR data did not show large differences in gene expression between the different groups. The relative expression of MyoD was higher in the PCL – R group than in three other groups, but there were no other significant differences in MyoD expression. The expression of MyoD is increased at the onset of myogenesis and the commitment of satellite cells to fuse into myofibers, so the higher expression of MyoD in the PCL – R group at a later time-point may indicate that cells are still trying to begin the fusion process. Jun and coworkers observed no differences in MyoD expression between cells on conductive and non-conductive scaffolds [7]. The largest difference in relative gene expression was seen for Myogenin, which is a marker of cell fusion. Expression of Myogenin was significantly lower on the 40% PPy-PCL-A and 20% PPy-PCL-A scaffolds than the TCP control. Myogenin expression may have been lower on these scaffolds due to the timing of the collection of mRNA for qPCR. By day 10 of the cell study, which was 7 days after differentiation media was first applied, the cells had plenty of opportunity to differentiate into myotubes. The myoblasts on the aligned scaffolds likely differentiated and fused into myotubes more quickly than the myoblasts on random scaffolds. The expression of Myogenin is highest when cells are actively fusing, and expression drops off after cell fusion is complete. Because the data were collected on day 10, the expression of Myogenin was much lower on the aligned scaffolds since those cells had already differentiated and fused whereas the cells on random scaffolds may have still been attempting to fuse. The lack of significant differences between groups for MHC may also be explained by the time-point that was used. The cells were no longer actively differentiating by this time, so relative expression levels of key genes were not in a state of flux. In contrast to these findings, Jun and coworkers found significantly higher

expression of Myogenin and MHC on conductive scaffolds compared with non-conductive scaffolds at 8 days in culture [7]. Our results seem to suggest that the media serum concentration had a larger effect on the expression of key myogenic genes than the scaffold, whereas the scaffold had a larger effect on the resulting cell morphology.

3.5 Conclusion

In this study, fibrous scaffolds made of a conductive copolymer, PPy-PCL, were fabricated via electrospinning, characterized, and evaluated for their ability to promote skeletal muscle regeneration. The addition of PPy-PCL to scaffolds with a base of pure PCL led to an increase in scaffold conductivity without increasing scaffold stiffness. It was found that the presence of aligned guidance cues and PPy-PCL were key factors in improving the attachment and differentiation of C2C12 myoblasts. However, there were not many significant differences in cell attachment or differentiation between scaffolds with three different levels of conductivity (resulting from three different concentrations of PPy-PCL). This study confirms previous research on scaffolds for skeletal muscle tissue engineering, but the results suggest that conductivity may not be a key factor in promoting myoblast differentiation. Instead, it seems that chemical moieties which promote cell attachment may explain the differences in myoblast growth and differentiation between conductive and non-conductive scaffolds. Future studies will further investigate the relationships between material choice, conductivity, mechanical properties, and myoblast attachment and differentiation in an effort to discover the optimal properties for regenerating skeletal muscle.

3.6 Acknowledgements

We are deeply grateful for the help of Dr. Nick Stebbins, formerly working under Dr. Kathryn Uhrich, who helped us work out the initial details of the copolymer synthesis reaction.

3.7 References

[1] Liao H, Zhou G-Q. Development and Progress of Engineering of Skeletal Muscle Tissue. Tissue Engineering Part B: Reviews 2009; 15(3): 319-331.
[2] Klumpp D, Horch RE, Kneser U, Beier JP. Engineering skeletal muscle tissue – new perspective *in vitro* and *in vivo*. Journal of Cellular and Molecular Medicine 2010; 14(11): 2622-2629.
[3] Morgan JE, Partridge TA. Muscle satellite cells. The International Journal of Biochemistry & Cell Biology 2003; 35(8): 1151-6.
[4] Koning M, Harmsen MC, van Luyn MJA, Werker PMN. Current opportunities and challenges in skeletal muscle tissue engineering. Journal of Tissue Engineering and Regenerative Medicine 2009; 3: 407-415.
[5] Sirivisoot S, Harrison BS. Skeletal myotube formation enhanced by electrospun polyurethane carbon nanotube scaffolds. International Journal of Nanomedicine 2011; 6: 2483-2497.
[6] Chen M-C, Sun Y-C, Chen Y-H. Electrically conductive nanofibers with highly oriented structures and their potential application in skeletal muscle tissue engineering. Acta Biomaterialia 2013; 9: 5562-5572.
[7] Jun I, Jeong S, Shin H. The stimulation of myoblast differentiation by electrically conductive sub-micron fibers. Biomaterials 2009; 30: 2038-2047.
[8] McKeon-Fischer KD, Freeman JW. Characterization of electrospun poly(L-lactide) and gold nanoparticle composite scaffolds for skeletal muscle tissue engineering. Journal of Tissue Engineering and Regenerative Medicine 2011; 5: 560-568.
[9] McKeon-Fischer KD, Flagg DH, Freeman JW. Coaxial electrospun poly(epsilon-caprolactone), multiwalled carbon nanotubes, and polyacrylic acid /polyvinyl alcohol scaffold for skeletal muscle tissue engineering. Journal of Biomedical Materials Research Part A 2011; 99A:493-499.
[10] Balint R, Cassidy NJ, Cartmell SH. Conductive Polymers: Towards a smart biomaterial for tissue engineering. Acta Biomaterialia 2014; 10(6): 2341-2353.
[11] Engler AJ, Griffin MA, Sen S, Bonnemann CG, Sweeney HL, Discher DE. Myotubes differentiate optimally on substrates with tissue-like stiffness. Journal of Cell Biology 2004; 166(6): 877-887.
[12] Gilbert PM, Havenstrite KL, Magnusson KEG, Sacco A, Leonardi NA, Kraft P, Nguyen NK, Thrun S, Lutolf MP, Blau HM. Substrate Elasticity Regulates Skeletal Muscle Stem Cell Self-Renewal in Culture. Science 2010; 329(5995): 1078-1081.
[13] Yoshimoto H, Shin YM, Terai H, Vacanti JP. A biodegradable nanofiber scaffold by electrospinning and its potential for bone tissue engineering. Biomaterials 2003; 24(12): 2077-2082.
[14] Kweon HY, Yoo MK, Park IK, Kim TH, Lee HC, Lee H-S, Oh J-S, Akaike T, Cho C-S. A novel degradable polycaprolactone networks for tissue engineering. Biomaterials 2003; 24(5): 801-808.
[15] Ghasemi-Mobarakeh L, Prabhakaran MP, Morshed M, Nasr-Esfahani, M-H, Ramakrishna S. Electrospun poly(epsilon-caprolactone)/gelatin nanofibrous scaffolds for nerve tissue engineering. Biomaterials 2008; 29(34): 4532-4539.
[16] Cui X, Wiler J, Dzaman M, Altschuler RA, Martin DC. In vivo studies of polypyrrole/peptide coated neural probes. Biomaterials 2003; 24(5): 777-787.

[17] Nguyen HT, Sapp S, Wei C, Chow JK, Nguyen A, Coursen J, Luebben S, Chang E, Ross R, Schmidt CE. Electric field stimulation through a biodegradable polypyrrole-co-polycaprolactone substrate enhances neural cell growth. J Biomed Mater Res Part A 2014; 102(8): 2554-2564.
[18] Pham QP, Sharma U, Mikos AG. Electrospinning of Polymeric Nanofibers for Tissue Engineering Applications: A Review. Tissue Engineering 2006; 12(5): 1197-1211.
[19] McKeon-Fischer KD, Browe DP, Olabisi RM, Freeman JW. Poly(3,4-ethylenedioxythiophene) nanoparticle and poly(epsilon-caprolactone) electrospun scaffold characterization for skeletal muscle regeneration. J Biomed Mater Res Part A 2015; 103A: 3633-3641.
[20] Chang HC, Sun T, Sultana N, Lim MM, Khan TH, Ismail AF. Conductive PEDOT:PSS coated polylactide (PLA) and poly(3-hydroxybutyrate-co-3-hydroxyvalerate) (PHBV) electrospun membranes: Fabrication and characterization. Materials Science and Engineering: C 2016; 61: 396-410.
[21] Lin M-F, Don T-M, Chang F-T, Huang S-R, Chiu W-Y. Preparation and Properties of Thermoresponsive and Conductive Composite Fibers with Core-Sheath Structure. Journal of Polymer Science, Part A: Polymer Chemistry 2016; 54: 1299-1307.
[22] Zhou X, Yang A, Huang Z, Yin G, Pu X, Jin J. Enhancement of neurite adhesion, alignment and elongation on conductive polypyrrole-poly(lactide acid) fibers with cell-derived extracellular matrix. Colloids and Surfaces B: Biointerfaces 2017; 149: 217-225.
[23] Wang L, Wu Y, Hu T, Guo B, Ma PX. Electrospun conductive nanofibrous scaffolds for engineering cardiac tissue and 3D bioactuators. Acta Biomaterialia 2017; 59: 68-81.
[24] Jeong SI, Jun ID, Choi MJ, Nho YC, Lee YM, Shin H. Development of Electroactive and Elastic Nanofibers that contain Polyaniline and Poly(L-lactide-co-epsilon-caprolactone) for the Control of Cell Adhesion. Macromolecular Bioscience 2008; 8: 627-637.
[25] Fung YC. Biomechanics: mechanical properties of living tissues. New York, USA: Springer-Verlag New York Inc.; 1993. page 568.
[26] Caiozzo VJ. Plasticity of Skeletal Muscle Phenotype: Mechanical Consequences. Muscle & Nerve 2002; 26(6): 740-768.
[27] Li M, Guo Y, Wei Y, MacDiarmid AG, Lelkes PI. Electrospinning polyaniline-contained gelatin nanofibers for tissue engineering applications. Biomaterials 2006; 27: 2705-2715.
[28] Gilmore KJ, Kita M, Han Y, Gelmi A, Higgins MJ, Moulton SE, Clark GM, Kapsa R, Wallace GG. Skeletal muscle cell proliferation and differentiation on polypyrrole substrates doped with extracellular matrix components. Biomaterials 2009; 30: 5292-5304.
[29] Mihardja SS, Sievers RE, Lee RJ. The effect of polypyrrole on arteriogenesis in an acute rat infarct model. Biomaterials 2008; 29: 4205-4210.
[30] Kotwal A, Schmidt CE. Electrical stimulation alters protein adsorption and nerve cell interactions with electrically conducting biomaterials. Biomaterials 2001; 22: 1055-1064.

CHAPTER 4: CHARACTERIZING THE IN VITRO RESPONSE AND EVALUATING THE EFFECT ON MYOBLAST DIFFERENTIATION OF COMBINED ELECTRICAL AND MECHANICAL STIMULATION PROVIDED WITH A CONTRACTILE, COMPOSITE SCAFFOLD

4.1 Introduction

The previous aims of this project have developed and optimized the two main components of a composite scaffold for regenerating skeletal muscle tissue while applying simultaneous electrical and mechanical stimulation. In the first aim, an ionic electroactive polymer was synthesized from poly(ethylene glycol) diacrylate and acrylic acid. This hydrogel actuator exhibited reversible and repeatable movement in an electric field and supported some myoblast cell growth. In the second aim, a conductive, fibrous scaffold was fabricated by electrospinning a mixture of polypyrrole-polycaprolactone copolymer and polycaprolactone. This fibrous scaffold provided a biocompatible environment for developing myoblasts, and the aligned guidance cues facilitated the development of myotubes, or immature muscle fibers. In this aim, the separate components previously developed are combined into a single composite scaffold. The hydrogel actuator component will expose cells to a cyclic stretch and elongation when electrical stimulation is applied. The fibrous scaffold will provide a highly biocompatible environment which will guide the formation of aligned muscle fibers. A schematic of the possible designs for this composite scaffold is provided in Figure 4.1.

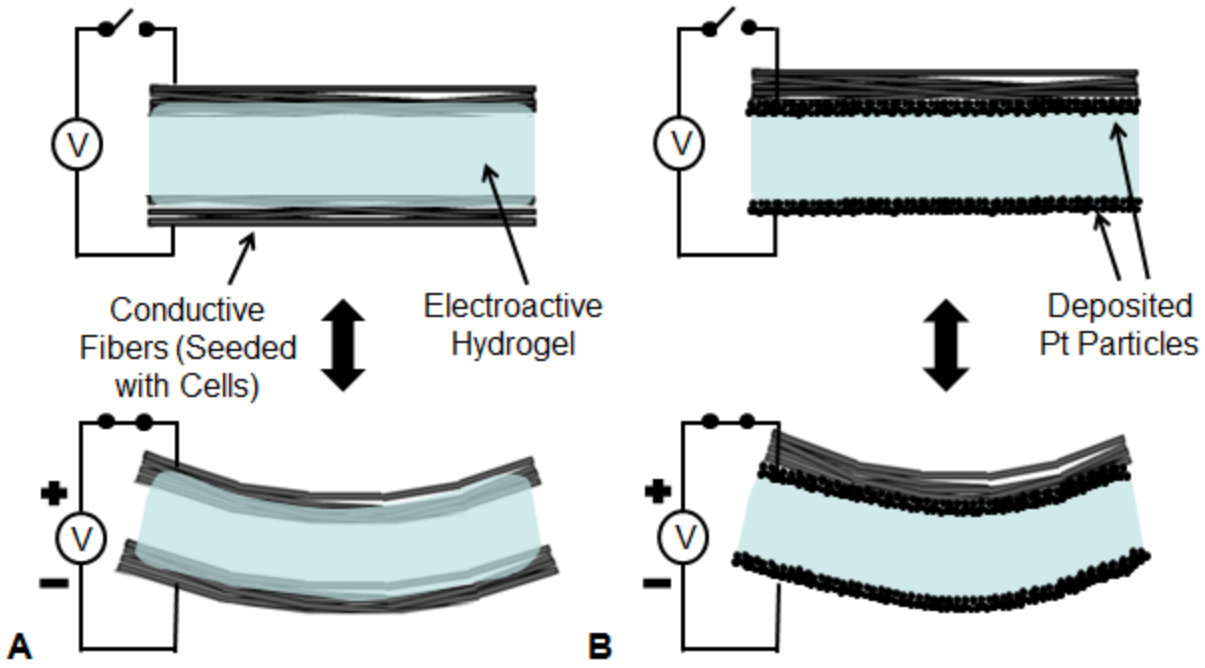

Figure 4.1: Composite scaffold diagram. The two possible designs of the contractile, composite scaffold. **A)** The conductive fibers function as the electrodes. **B)** Deposited Platinum (Pt) nanoparticles function as the electrodes.

There has been plenty of research into applying electrical stimulation to developing muscle cells and muscle tissue. Researchers have utilized electrical stimulation to model exercise or induce differentiation in culture [1-4]. Nikolic and coworkers applied electrical pulse stimulation to human myotubes as an *in vitro* model of exercise [1]. They applied 1) high-frequency stimulation of bipolar pulses at 100 Hz for 200 ms applied every 5th second at 30 V for 5-60 min and 2) chronic, low-frequency stimulation of single, bipolar pulses of 2 ms with 30 V and 1 Hz continuously for the last 24 or 48 hours of the differentiation period. Both stimulation patterns were found to be an adequate model to study the effects of exercise [1]. Fujita and coworkers employed electric pulse stimulation to manipulate the Calcium transients and sarcomere assembly in C2C12 myotubes [4]. They applied a stimulus of 0.667 V/mm at 1 Hz for 24 ms. They

were able to induce significant contractile activity in C2C12 myotubes within only 2 hours of the stimulation at 1 Hz. However, they did not notice any increase in contractility or sarcomere assembly with 10 Hz stimulation [4]. Donnelly and coworkers developed a cost-effective muscle electrical stimulation bioreactor to permit the application of physiologically relevant electrical stimulation patterns to monolayers and tissue-engineered constructs in culture [3]. This bioreactor allowed for the control of pulse amplitude, pulse width, pulse frequency, and work-to-rest ratio. They were able to culture C2C12 myoblasts under 100 Hz with 40x 0.3 ms pulses delivered in 400 ms trains with 3.6 s recovery for a total of 30 min per day. This resulted in a significant increase in the rate of protein synthesis and proving that the stimulation was an anabolic signal [3]. Finally, various studies have applied electrical stimulation to induce contraction of myotubes or thicker muscle constructs [5-9]. For instance, Dennis and coworkers stimulated muscle constructs using a range of voltages (3-40 V) and pulse widths (0.2 – 2.0 ms) [8]. They achieved supramaximal stimulation with a single 70 V and 4 ms pulse. They also measured the maximum isometric tetanic force by stimulating the muscle constructs at 40 V and 40 Hz with 1.20 ms pulses for a train duration of 2 s. It was also found that muscle construct force produced increased with increasing frequency from 5 Hz to 70 Hz [8]. These studies provide a useful reference for the electrical stimulation pattern employed in this set of experiments.

External mechanical stimulation of myoblasts and muscle tissue in culture has been studied comparatively less frequently than external electrical stimulation, and the results have been mixed. On a positive note, Haghighipour and coworkers were able to induce the differentiation of human mesenchymal stem cells into a myogenic lineage

using cyclic uniaxial stretch [10]. They applied a 10% cyclic uniaxial strain at 1 Hz to human mesenchymal stem cells grown on collagen-coated silicon membranes for 24 hours. The levels of MyoD and Myogenin mRNA increased significantly on cyclically loaded cells as compared to the unloaded control. These results showed that cyclic strain is a possible mechanism to induce myogenic differentiation [10]. However, other studies have shown negative results for externally applied mechanical stimulation [11, 12]. Akimoto and coworkers found that a cyclic mechanical stretch of 20% for 24 hours served as a down-regulatory signal for differentiation of C2C12 myoblasts [11]. In another case, Boonen and coworkers utilized a 2% uniaxial ramp stretch and intermittent dynamic stretch of 4% on C2C12 myoblasts in both 2D and 3D environments [12]. It was found that this protocol had a negative effect on cell differentiation and maturation in all cases as demonstrated by lower expression of differentiation markers, lower production of sarcomere proteins, and longer time to form cross striations [12]. Thus, it seems that externally applied mechanical stress is less tolerated by C2C12 cells than externally applied electrical stimulation. It may be the case that mechanical stimulation must be associated, or coupled, with electrical stimulation in order to bring about positive changes.

Combined external electrical and mechanical stimulation on developing myoblasts has rarely been studied. De Deyne built devices to study both mechanical stretch and electrical stimulation, but did not employ them simultaneously [13]. It was found that the application of passive uniaxial stretch had little effect on sarcomere structures either in a beneficial or detrimental way. However, electrical stimulation of 400 mV/mm with a field pulse of 2 ms and a frequency of 0.1 Hz increased sarcomere

assembly significantly [13]. Liao and coworkers investigated the effects of electromechanical stimulation on differentiation of skeletal myoblasts seeded on aligned polymer fibers [14]. They utilized a mechanical stimulation protocol of 5% cyclic strain applied 2 days post-differentiation and an electrical stimulation protocol of 20 V at 1 Hz applied 7 days post-differentiation. The synchronized stimulation profile significantly increased the amount of striation and the production of contractile proteins compared to unstimulated cells. However, the benefit of combined stimulation over single stimulation, either electrical or mechanical, was unclear [14]. This study provides proof of concept for the idea that combined electrical and mechanical stimulation can enhance the differentiation of muscle tissue. Interestingly, the timing of stimulation applied in this study was different for the mechanical and electrical portions, and the two types of stimulation were independent. In contrast, developing muscles are exposed to simultaneous and coupled electrical and mechanical stimulation. It may be possible to further enhance tissue maturation by exposing developing tissue to the proper coupled stimulation.

The purpose of this set of experiments is to provide proof of concept for using a composite scaffold while applying simultaneous electrical and mechanical stimulation to enhance myoblast differentiation. The electrical stimulation pattern chosen for this study was based on a combination of the previously mentioned results from the literature and the preliminary actuation experiments described in the methods section. The goal was to find an electrical stimulation pattern that would simultaneously cause hydrogel actuation and provide a beneficial stimulus to myoblasts (or at least not kill myoblasts). The parameters of the individual components of the composite scaffold have been optimized

in the earlier aims. Thus, hydrogel samples had a 1 to 4 ratio of poly(ethylene glycol) diacrylate to acrylic acid, and a 40% polypyrrole-polycaprolactone scaffold with aligned fibers was used. The main goals of this set of experiments were to 1) evaluate the feasibility of seeding myoblasts on the composite scaffold and measuring their proliferation and differentiation; and 2) provide a preliminary roadmap for future experimentation with this system by identifying favorable stimulation parameters.

Finally, to aid in achieving the previously mentioned objectives, a reporter cell line is developed to aid in the quantification of myoblast differentiation. Reporting of myosin light chain through a luciferase assay was used as a simple way to quantify differentiation. This method of quantifying differentiation is quicker and more cost effective than quantitative polymerase chain reaction or morphological analysis of fluorescent images. Thus, the development of this cell line significantly increases the given work that can be accomplished in a given amount of time and money for this experiment and for future work.

4.2 Materials and Methods

4.2.1 Cell Line Development

A reporter cell line was developed by transducing the myosin light chain (MLC) promoter with the luciferase gene into C2C12 cells. A plasmid was designed with the DNA of the MLC promoter and the luciferase gene along with resistance to Blasticidin. This plasmid was generously gifted to our lab by Dr. Emmanuel Ekwueme and Dr. Craig Neville from Massachusetts General Hospital-Harvard Medical School. The exact DNA sequence of the plasmid is shown in the appendix to this chapter. The plasmid was packaged into a lenti-virus and transduced into C2C12 myoblasts with the help of 1 μg/mL Polybrene. After 3 days in culture, the transduced cells were selected using media with 2 μg/mL Blasticidin changed every other day for a week. The surviving cells were grown up and frozen down for later use.

4.2.2 Cell Line Validation

In order to validate the cell line development, the transduced MLC reporting C2C12 myoblasts were seeded in 12-well plates at a density of 25,000 cells/cm^2 (purchased from ATCC). Three different groups (n = 4) were compared: 1) cells supplemented with 50 ng/mL IGF-1 meant to enhance myoblast differentiation, 2) cells supplemented with 40 μg/mL dexamethasone meant to deter myoblast differentiation, and 3) cells fed with the base media without any additives meant as a null control. During the initial proliferation phase (day 0 to day 2), all groups were fed with a base media of DMEM media with 10% Fetal Bovine Serum (FBS) and 1% Penicillin/Streptomycin (P/S) every other day. During the differentiation phase (day 3 to day 10), all samples

were fed with a base media of DMEM media with 1% FBS and 1% P/S with the corresponding additives appropriate for each group once per day.

A luciferase assay was performed at 1, 3, and 7 days after differentiation media was initially applied with a BioLux® Gaussia Luciferase Assay Kit (New England Biolabs, Ipswich, MA) according to the manufacturer's instructions. After the last time-point, all groups were fixed with a 4% paraformaldehyde solution to prepare for staining (n = 4). Cells were stained with NucBlue® fixed cell ReadyProbes® reagent (Thermo Fisher Scientific) for DNA (Blue) and Fluorescein Phalloidin (Thermo Fisher Scientific) for F-actin (Green).

A representative sample of five images for each group was used to quantify the morphology of the cells in the different groups. ImageJ software [version 1.46r/Java 1.6.0_25 (32-bit)] was used to quantify the total number of nuclei, the total number of myotubes, and the number of nuclei inside of myotubes for each image. Myotubes were defined as clearly distinguishable, linear structures which contained two or more nuclei. These parameters were used to calculate the fusion index (nuclei inside of myotubes/total number of nuclei).

4.2.3 Fabrication of Composites

All samples were cut to be approximately 20 mm by 5 mm. The hydrogel samples used in this set of experiments were fabricated as previously described in Aim 1. The hydrogel samples with a 1 to 4 ratio of poly(ethylene glycol diacrylate) to acrylic acid were used for all control samples (i.e. "hydrogel") and composites since these samples were determined to be the most biocompatible in Aim 1. Likewise the fibrous scaffolds used in this set of experiments were fabricated as previously described in Aim 2. The

copolymer scaffolds with a 40% concentration of polypyrrole-polycaprolactone copolymer in an aligned orientation were used for all composites since these samples were determined to enhance myoblast differentiation the most and have the highest conductivity in Aim 2.

The samples labeled “composite #1” were constructed with a hydrogel sample chemically bonded to a fibrous scaffold on one side. The fibrous scaffolds were placed in contact with the hydrogel samples and un-crosslinked hydrogel solution was administered at the interface. UV radiation was applied for 1 min at 365 nm to bind the fibrous scaffolds to the hydrogel samples.

The samples labeled “composite #2” were constructed with a hydrogel sample completely surrounded by a fibrous scaffold. The hydrogel samples were wrapped in just enough fibrous scaffold to completely cover their surface area. Then, the fibrous scaffold was adhered to itself using a sterile silicone glue, enveloping the hydrogel samples.

4.2.4 Actuation Experiments

Actuation experiments were performed to determine: 1) the degree to which the binding of the copolymer scaffolds impeded the movement of the hydrogel actuators, and 2) the movement that would be produced with more complex stimulation patterns than had been previously used. All actuation experiments were performed as previously described in Aim 1 with the exceptions of the groups tested for the first round of testing and the electrical stimulation pattern for the second round of testing. The first round of actuation testing was performed with three groups (n = 4) including plain hydrogel samples, composite #1, and composite #2. These samples were exposed to the same 20 V stimulus described in Aim 1. The second round of actuation tests was performed using a

signal generator (Keysight KT-33611A-33600A Series Waveform generator, 80 MHz, 1-channel) to administer a more complex electrical stimulation pattern. Two sets of parameters were used. In the first set of parameters, the frequency of the square wave was fixed at 2 Hz, and three different amplitudes were tested: 2.5 V, 5 V, and 10 V. In the second set of parameters, the amplitude of the square wave was fixed at 10 V, and three different frequencies were tested: 2 Hz, 10 Hz, and 50 Hz. Both sets of parameters were applied in a biphasic manner for one minute at a time on each polarity. Results were captured and analyzed as previously described in Aim 1.

4.2.5 Cell Study – Measuring Proliferation and Differentiation

The transduced MLC reporting C2C12 myoblasts were seeded onto four scaffold groups (n = 4) at a density of 50,000 cells/cm^2 (purchased from ATCC). The four groups included: 1) tissue culture plastic (TCP) control, 2) plain hydrogel samples, 3) composite #1, and 4) composite #2 (as previously described). Enough samples were used to accommodate a group size of four samples for each of three electrical stimulation patterns, as described in the following section. During the proliferation phase (day 0 to day 2), all samples were fed with DMEM media with 10% fetal bovine serum (FBS) and 1% penicillin/streptomycin (P/S) every other day. During the differentiation phase (day 3 to day 6), all samples were fed with DMEM media with 1% FBS and 1% P/S once per day. During the differentiation phase, electrical stimulation was applied once per day (see next section).

The metabolic activity and MLC production of the cells on the scaffold samples were measured using a PrestoBlue® cell viability assay and luciferase assay, respectively, on day 0 and day 3 after applying the differentiation media using the

instructions provided by the manufacturer (n = 4). Briefly, the media from the wells was aspirated, and PrestoBlue® cell viability reagent diluted to a ratio of 1:10 with differentiation media was applied for a 1 hour incubation period. The reagent-media mixture was removed at the end of the incubation period, and the absorbance was analyzed by a plate reader at a wavelength of 570 nm. After subtracting a blank control, the absorbance value produced by this assay is directly proportional to the metabolic activity of the cells on each sample. A luciferase assay was also performed at 0 and 3 days after differentiation media was initially applied with a BioLux® Gaussia Luciferase Assay Kit (New England Biolabs, Ipswich, MA) according to the manufacturer's instructions.

4.2.6 Electrical Stimulation Apparatus and Pattern

The apparatus for delivering electrical stimulation is shown below in Figure 4.2. Platinum wires were fixed to a 12-well plate at a distance of 1 cm apart spanning multiple wells. These wires could then be connected by wire to source of electrical stimulation. Samples were removed from their main wells and placed inside the electrical stimulation apparatus to apply stimulation. The wells of the apparatus were filled with differentiation media (DMEM with 1% FBS and 1% P/S while stimulation was taking place).

All electrical stimulation patterns were produced by a Keysight KT-33611A-33600A Series Waveform generator (80 MHz, 1-channel). There were three different stimulation groups used in this experiment: 1) no stimulation, 2) 5 V amplitude square wave at 50 Hz applied for 1 minute trains with 1 minute break between trains, and alternating trains were at opposite polarities, and 3) 10 V amplitude square wave at 50 Hz applied for 1 minute trains with 1 minute break between trains. Each stimulation pattern

was applied for 30 minutes once per day during the differentiation phase of the cell study (3 applications total).

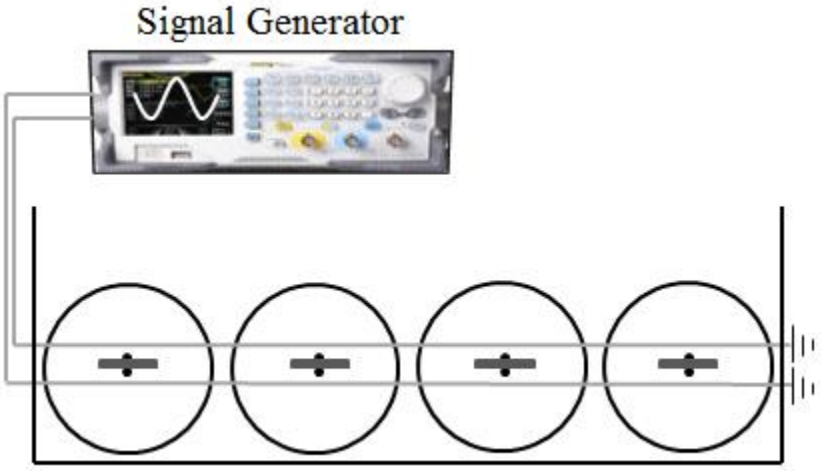

Figure 4.2: *In vitro* electrical stimulation apparatus. Schematic of the apparatus used to deliver electrical stimulation to myoblasts on the various scaffold groups. Two platinum wires were fixed inside of a 12-well plate at a separation of 1 cm across multiple wells, and these wires transmitted stimulation from a signal generator.

4.2.7 Data Analysis and Statistics

All data are expressed as the average for each group, and the error bars correspond to the standard deviation. The plot for survival ratio was produced by taking the individual sample values produced by the Presto Blue assay on day 3 and dividing them by the corresponding sample values produced by the Presto Blue assay from day 0. The plots for relative MLC production were produced by taking the individual sample values produced by the luciferase assay at each time-point and dividing them by the corresponding sample values from the Presto Blue assay at the corresponding time-point. The plot for differentiation ratio was produced by taking the individual sample values from the relative MLC production data on day 3 and dividing them by the corresponding

sample values from the relative MLC production data on day 0. Significance between groups was evaluated using a one-way ANOVA with a Tukey's post-hoc test. Significance was set at $\alpha = 0.05$ (denoted by * unless otherwise noted).

4.3 Results

4.3.1 Cell Line Validation

The results for the validation of the transduced MLC reporting C2C12 cell line with a luciferase assay are shown in Figure 4.3. On day 1, the group exposed to dexamethasone had significantly lower MLC production than the control group. On days 3 and 7, the group exposed to IGF-1 was significantly higher than the control group and the dexamethasone group was significantly lower than the control group. Over time, MLC production increased in the control group, MLC production increased at a faster rate in the IGF-1 group, and MLC production decreased over time in the dexamethasone group.

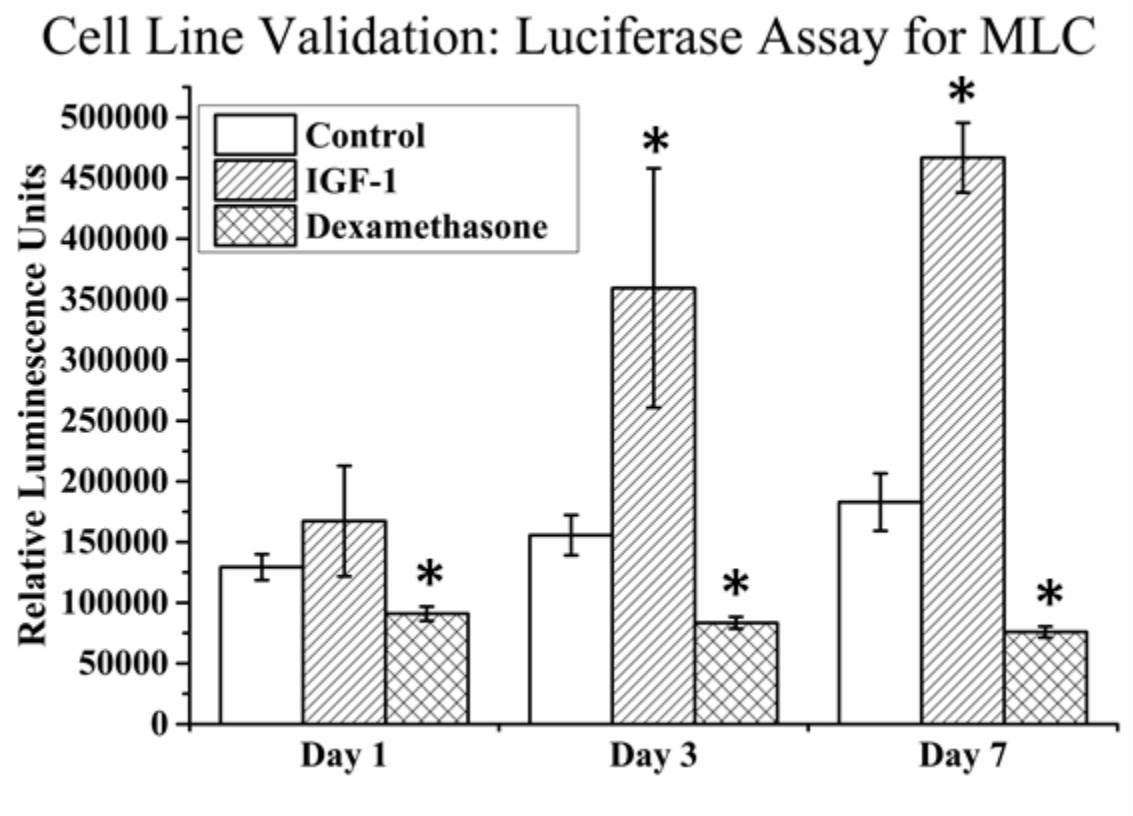

Figure 4.3: Cell line validation: Luciferase assay. Luciferase assay performed on days 1, 3, and 7 after applying differentiation media in the validation of the cell line development.

The results for the morphological analysis of the myoblasts for the cell line validation are shown in Figure 4.4. The number of myotubes produced and the fusion index was significantly greater in the cells treated with IGF-1 as compared to the control. Dexamethasone completely blocked the formation of myotubes, resulting in zero myotubes and a zero fusion index. Overall, the results of the morphological analysis correlate well to the results of the luciferase assay (Figure 4.3).

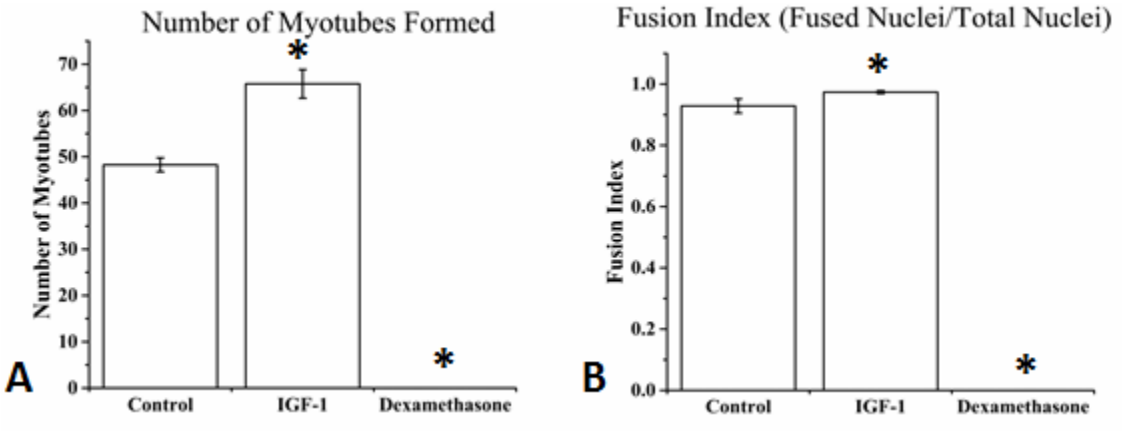

Figure 4.4: Cell line validation: Morphological analysis. Morphological analysis of the myoblasts used in the validation of the cell line on day 7 after application of differentiation media. **A)** Number of myotubes. **B)** Fusion index.

4.3.2 Actuation Experiments

The angular movement from the actuation experiment comparing hydrogel samples to the two composites is shown in Figure 4.5. There was no difference in the movement between the hydrogel group and the composite #1 group. Although, there was a slight trend of the composite #1 group preferring one direction over another. The

hydrogel group produced significantly more movement in the forward direction than the composite #2 group. The reverse movement was also lower but not significantly different.

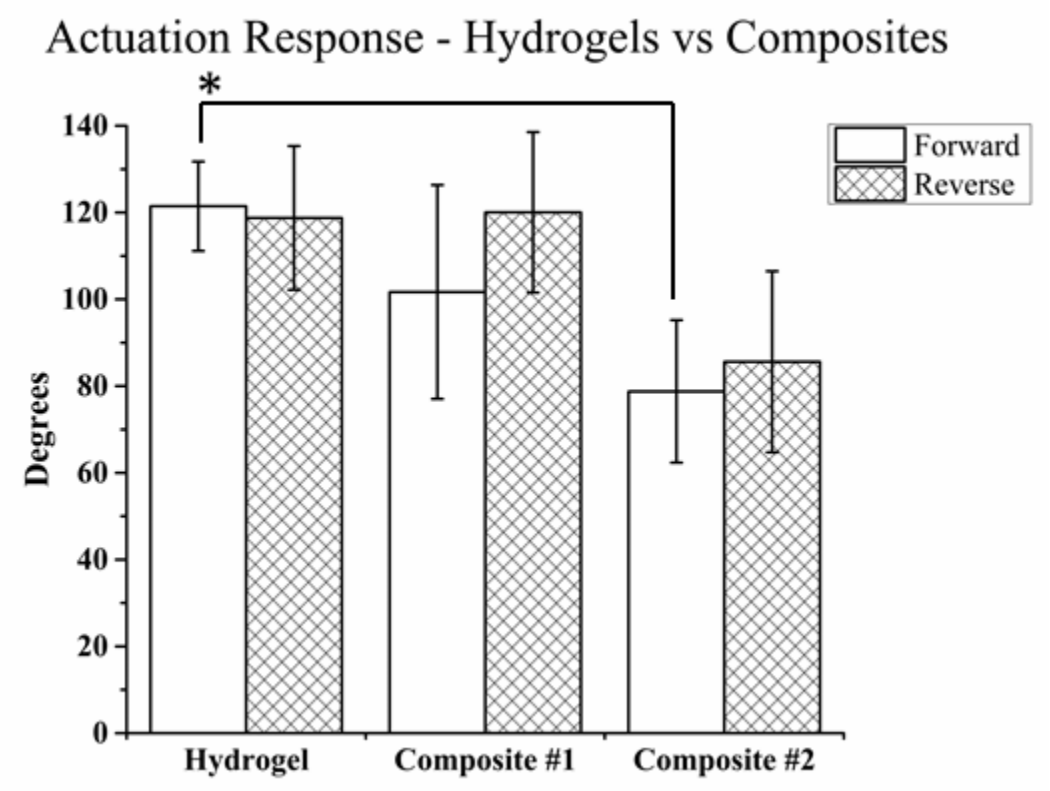

Figure 4.5: Actuation: Hydrogels vs. composites. The actuation response for pure hydrogel samples compared to both types of composite scaffolds.

The angular movement produced by the actuation experiment with a square wave stimulation pattern is shown in Figure 4.6. Angular movement was directly proportional to the amplitude of the square wave, with 10 V of stimulation producing significantly higher movement than 2.5 V of stimulation, as shown in Figure 4.6A. The overall magnitude of the angular movement was much lower than the angular movement produced by the previous stimulation pattern of constant 20 V applied for 1 minute (Figure 4.5). The frequency of the square wave in the range of 2 Hz to 50 Hz did not

significantly alter the actuation response, but there was a slight trend of more angular movement with a lower frequency.

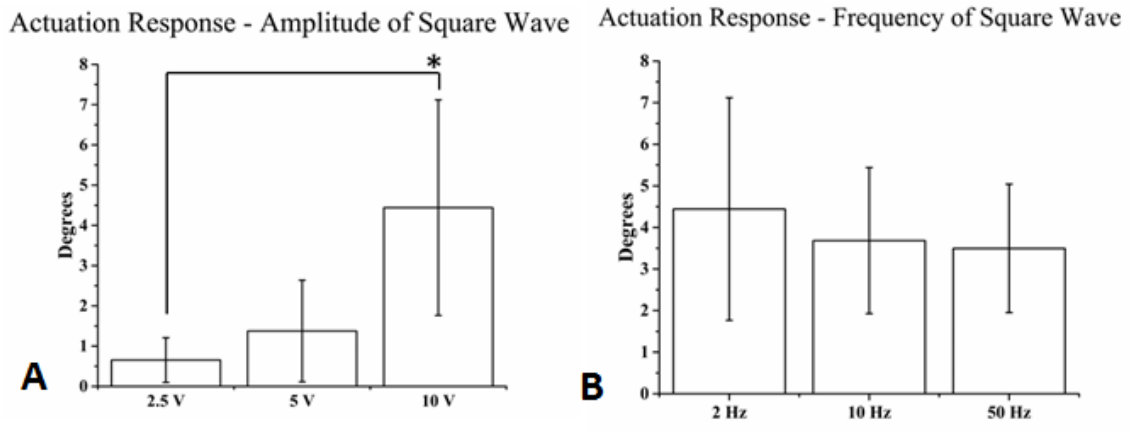

Figure 4.6: Actuation: Frequency and amplitude. The angular movement produced by actuation experiments with complex stimulation patterns. A) Varying amplitude of the square wave (2 Hz). B) Varying frequency of the square wave (10 V).

4.3.3 Cell Study – Measuring Proliferation and Differentiation

The results of the Presto Blue assay to measure metabolic activity are shown in Figure 4.7. In the groups that were not exposed to electrical stimulation, Figure 4.7A, the control TCP group and the composite #2 group maintained the same metabolic activity throughout the course of the study. In contrast, the hydrogel and composite #1 groups significantly dropped in metabolic activity by day 3. For both the electrical stimulation pattern #1 (Figure 4.7B) and electrical stimulation pattern #2 (Figure 4.7C), all groups had significantly lower metabolic activity on day 3 than on day 0.

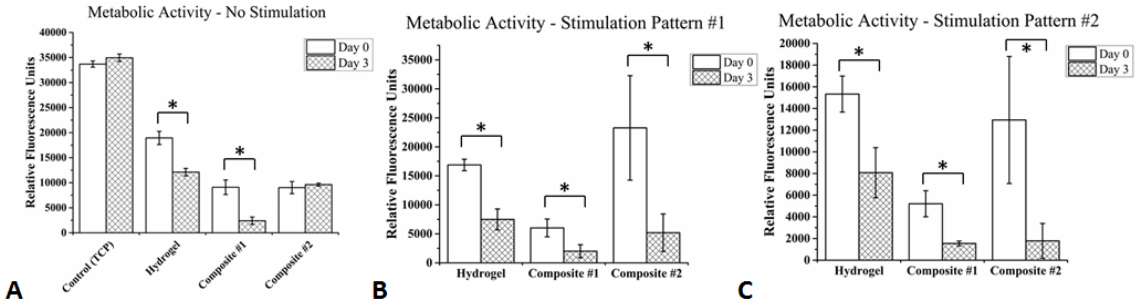

Figure 4.7: Metabolic activity: Electrical stimulation of composites. Metabolic activity as measured by a Presto Blue assay on days 0 and 3 for all groups and stimulation patterns. A) No stimulation. B) Stimulation Pattern #1 (5 V). C) Stimulation Pattern #2 (10 V).

The normalized metabolic activity data called the survival ratio is shown in Figure 4.8. The TCP control group and the composite #2 group with no stimulation both had a significantly higher survival ratio than the rest of the groups. The hydrogel group with no stimulation produced a higher survival ratio than all of the composite #1 groups. For the hydrogel and composite #1 groups, neither of the electrical stimulation patterns caused the metabolic activity to drop significantly more than the corresponding no stimulation group. However, both of the electrical stimulation patterns caused the metabolic activity to decrease significantly in the composite #2 group as compared to the no stimulation condition.

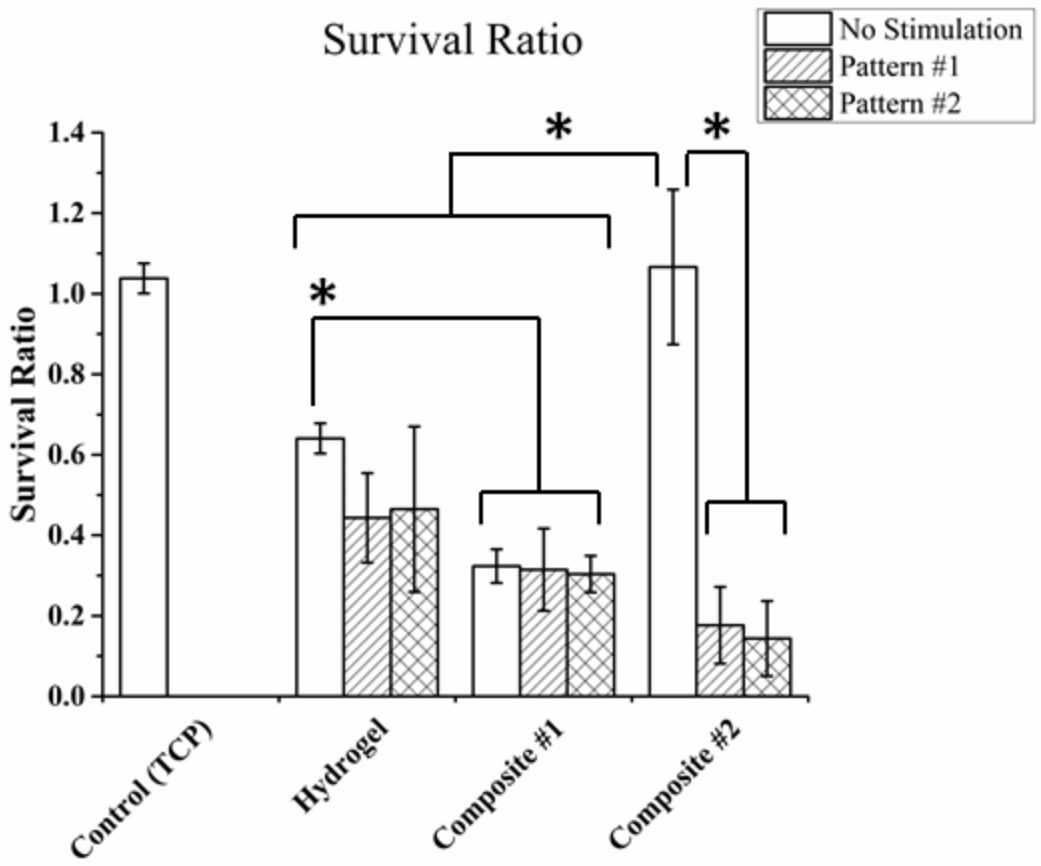

Figure 4.8: Survival ratio. Survival ratio for all groups and all stimulation patterns.

The relative MLC production as measured by the luciferase assay is shown in Figure 4.9 for all groups and conditions. For almost all groups and conditions, relative MLC production significantly increased from day 0 to day 3. The only exception was the composite #1 group for the electrical stimulation pattern #1 where relative MLC production increased but not significantly. The smallest relative MLC production for both day 0 and day 3 was found in the composite #2 group for all three stimulation patterns.

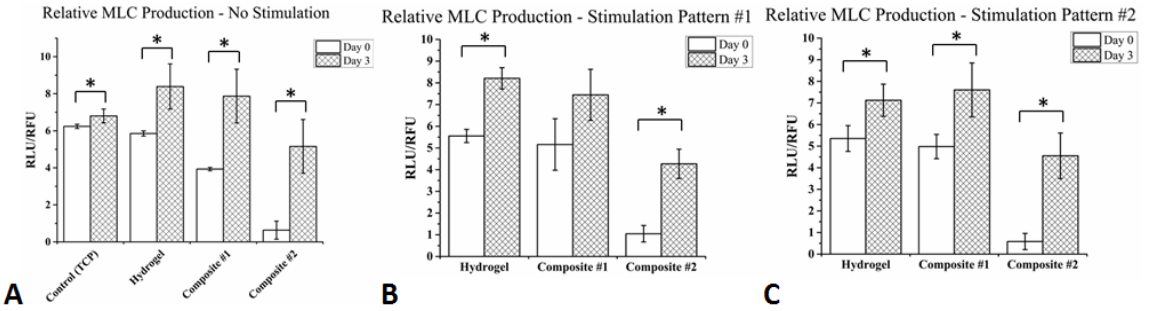

Figure 4.9: Luciferase assay: Electrical stimulation of composites. The relative MLC production as measured by luciferase assay and normalized to metabolic activity (cell number). A) No stimulation. B) Electrical stimulation pattern #1. C) Electrical stimulation pattern #2.

The data for the ratio of relative MLC production, termed the differentiation ratio, is shown in Figure 4.10. For all three groups, there was no significant difference in the differentiation ratio between the three stimulation patterns. However, the differentiation ratio for the composite #2 group was significantly greater than the differentiation ratio for the TCP control, hydrogel, and composite #1 groups for all stimulation patterns. The average differentiation ratio was between 1 and 2 for all stimulation conditions of the TCP control, hydrogel, and composite #1 groups. However, the average differentiation ratio was between 4 and 6 for all stimulation conditions of the composite #2 groups.

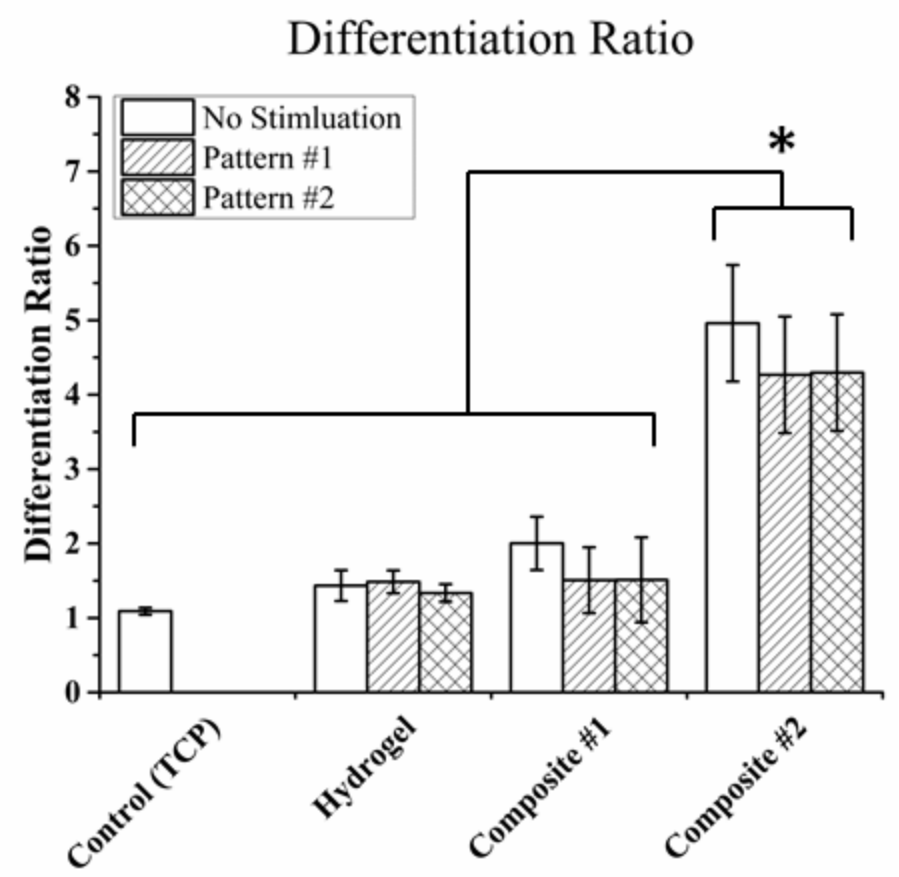

Figure 4.10: Differentiation ratio. Differentiation ratio for all groups and all stimulation conditions.

4.4 Discussion

This study attempted to provide a proof of concept for utilizing simultaneous, coupled electrical and mechanical stimulation for the development of myoblasts on a composite scaffold. This study is unique because the electrical and mechanical stimulation are coupled, and it utilizes an ionic electroactive polymer to deliver stimulation. This study may be the first to utilize ionic electroactive polymers for tissue engineering purposes. Due to the unique nature of this study, previous research can only provide vague guidelines for the specific parameters to use. The values chosen for the electrical stimulation pattern were based on a compromise between the literature and the previous results in this project. Such a compromise is bound to fall short in certain areas, and this study should be viewed as preliminary in nature.

The transduced MLC reporting C2C12 myoblasts were successfully validated by comparing the results of the luciferase assay to the morphological analysis of the same cells. The luminescence values reported by the luciferase assay, which measures the production of MLC, increased over time in the control group. Furthermore, the positive control group (media supplemented with IGF-1) produced higher values in the luciferase assay, and the negative control group (media supplemented with dexamethasone) produced lower values in the luciferase assay. These results are exactly what would be expected if the assay was running properly by associating MLC production with luciferase production. In addition, a morphological analysis of the same cells shows that the results of the luciferase assay can be used to successfully predict morphological differences in myotube formation in an easily quantifiable way. Overall, the production

of a MLC reporting cell line provides a quick, cost effective, and accurate way to quantify myoblast differentiation.

The actuation experiments in this study show that angular movement is somewhat impeded by the addition of other components to the hydrogel actuator or by implementing a high frequency electrical stimulation pattern (as compared to a constant voltage for the same time period). The samples in the composite #1 group move just as well as the hydrogel samples alone. Thus, the addition of a fibrous scaffold on one side of the hydrogel actuator does not significantly hamper movement. However, the samples in the composite #2 group caused significantly less movement in one direction and decreased movement in both directions as compared to the hydrogel samples alone. Thus, having the hydrogel actuator surrounded by a fibrous scaffold does hamper movement, but significant movement still occurs (80-90 degrees of movement on average for the composite #2 group). The type of electrical stimulation pattern had a much greater effect on the overall amount of movement observed in the hydrogels. Switching to a square wave pattern with a frequency of 2 Hz and an amplitude of 10 V produced only ~4.5 degrees of movement on average compared to ~120 degrees of movement on average with a constant application of 20 V for the same time period. This is likely due to the fact that constant ion flow in solution is needed for efficient hydrogel movement. The pulsating ion flow provided by a square wave pattern may be better overall for cells, but it dramatically reduces the extent and speed of hydrogel movement during actuation as compared to a constant voltage over the same time period. As expected, hydrogel movement remains directly proportional to the amplitude of the applied stimulation. In the range of 2 Hz to 50 Hz, the frequency does not seem to make a big difference in

actuation. We suspect that very low frequencies may produce more movement because a longer period of stimulation in a square wave pattern would more closely resemble a constant voltage (DC) stimulus.

The proliferation of myoblasts in this experiment was measured by a Presto Blue assay, which directly measures metabolic activity. It is important to note that metabolic activity is an indirect measure of cell proliferation since cells can become more or less metabolically active without changing in number. Cell proliferation decreased in almost all groups and stimulation conditions throughout the course of the study. The exceptions were the TCP control group and the composite #2 group with no stimulation. Looking at the survival ratio, it seems that the two stimulation patterns had anywhere from no effect to a large negative effect on cell survival/growth. One compounding factor was the integrity of the samples in the composite #1 group. Almost half of the samples in this group broke apart throughout the course of the study. This likely led to undesirable friction between the fibrous scaffold portion and the hydrogel actuation portion which may have contributed to cell death regardless of the stimulation pattern. This issue highlights the difficulty in attaching a material that changes in size (i.e. the hydrogel actuator, which can swell and contract as media concentration changes) to a material that does not change in size (i.e. the fibrous scaffold). Another compounding factor is the effect of removing the samples from their main wells to put them in the stimulation apparatus. This problem could possibly be avoided by turning each well plate into an apparatus for applying electrical stimulation. This can be achieved by fixing Platinum wires to each well plate or by designing an insert that can turn each well plate into an apparatus for delivering electrical stimulation. More data needs to be collected before a

definitive proclamation can be made regarding the ability of myoblasts to survive with these stimulation patterns.

The differentiation of myoblasts in this experiment was measured by a luciferase assay, which directly measures the production of MLC. As noted earlier, the production of MLC is correlated with morphological changes associated with myoblast differentiation. However, it is important to keep in mind that it possible for MLC to be produced without progress in the formation of myotubes. This could occur if a substrate somehow inhibits the formation of myotubes while leaving the cells alive in close proximity to one another. In any case, the production of MLC significantly increased from day 0 to day 3 on almost all groups and stimulation conditions. When looking at the differentiation ratio, neither of the stimulation patterns was able to cause the surviving cells to differentiate more than the corresponding group with no stimulation. It should also be noted that the results of the luciferase assay were normalized to metabolic activity (i.e. normalized to cell count). Thus, when considering the composite #2 group, both of the electrical stimulation patterns (#1 and #2) caused a significant decrease in the number of cells, and the cells that survived did not differentiate any more than with the no stimulation condition. The differentiation ratio was the biggest in the composite #2 group, but this is likely due to the fact that the MLC production started so much lower on day 0 for the composite #2 group. Finally, it remains difficult to properly evaluate the composite #1 group because almost half of the samples fell apart during the study.

Due to the unique nature of this study, it is difficult to make comparisons to the previous literature. The most relevant study was conducted by Liao and coworkers who investigated the effects of electromechanical stimulation on differentiation of skeletal

myoblasts seeded on aligned polymer fibers [14]. They applied both electrical and mechanical stimulation to the same samples, but these stimulation patterns did not overlap and were independent of one another. They did achieve superior results with the synchronized stimulation profile in terms of the amount of striation and the production of contractile proteins over unstimulated cells. However, the benefit of combined stimulation over single stimulation was not obvious [14]. This study falls short of the results reported by Liao and coworkers, but the system was very different. It is possible that similar results could be obtained by utilizing the electrical stimulation pattern used by Liao with the conductive, fibrous scaffolds developed in this project.

4.5 Conclusion

This study combined a hydrogel actuator and fibrous scaffold developed in earlier experiments and attempted to stimulate myoblasts on the resulting composite scaffold with simultaneous electrical and mechanical stimulation. A couple electrical stimulation patterns were chosen that elicited a minimal mechanical response. Although cells tolerated the electrical stimulation without completely dying, there was no measurable benefit to applying electrical stimulation in terms of improving differentiation. A potentially insightful set of future experiments might involve applying electrical stimulation to the conductive, fibrous scaffold alone without the hydrogel actuator. Those experiments would allow more flexibility with the electrical stimulation profile since the need to stimulate the hydrogel actuator would be eliminated. Although the results of this aim were mostly negative, the protocols developed in this study provide a baseline for measuring progress with future experiments.

4.6 Acknowledgements

We are very grateful for the help of Dr. Emmanuel Ekwueme, Dr. Craig Neville, and Dr. Rick Cohen in developing the cell line described earlier.

4.7 References

[1] Nikolic N, Bakke SS, Kase ET, Rudberg I, Halle IF, Rustan AC, Thoresen GH, Aas V. Electrical Pulse Stimulation of Cultured Human Skeletal Muscle Cells as an *In Vitro* Model of Exercise. PLoS ONE 2012; 7(3): e33203.
[2] Lambertucci RH, Silveira LDR, Hirabara SM, Curi R, Sweeney G, Pithon-Curi TC. Effects of Moderate Electrical Stimulation on Reactive Species Production by Primary Rat Skeletal Muscle Cells: Cross Talk Between Superoxide and Nitric Oxide Production. J. Cell. Physiol 2012; 227: 2511-2518.
[3] Donnelly K, Khodabukus A, Philp A, Deldicque L, Dennis RG, Baar K. A Novel Bioreactor for Stimulating Skeletal Muscle *In Vitro*. Tissue Engineering: Part C 2010; 16(4): 711-718.
[4] Fujita H, Nedachi T, Kanzaki M. Accelerated *de novo* sarcomere assembly by electric pulse stimulation in C2C12 myotubes. Experimental Cell Research 2007; 313: 1853-1865.
[5] Dennis RG, Kosnik PE, Gilbert ME, Faulkner JA. Excitability and contractility of skeletal muscle engineered from primary cultures and cell lines. Am. J. Physiol. Cell. Physiol 2001; 280: C288-C295.
[6] Borschel GH, Dennis RG, Kuzon WM. Contractile Skeletal Muscle Tissue-Engineered on an Acellular Scaffold. Plastic and Reconstructive Surgery 2004; 113(2): 595-602.
[7] Borschel GH, Dow DE, Dennis RG, Brown DL. Tissue-Engineered Axially Vascularized Contractile Skeletal Muscle. Plastic and Reconstructive Surgery 2006; 117(7): 2235-2242.
[8] Dennis RG, Kosnik PE. Excitability and Isometric Contractile Properties of Mammalian Skeletal Muscle Constructs Engineered *In Vitro*. In Vitro Cell. Dev. Biol. Animal 2000; 36: 327-335.
[9] Bajaj P, Reddy B, Millet L, Wei C, Zorlutuna P, Bao G, Bashir R. Patterning the differentiation of C2C12 skeletal myoblasts. Integrative Biology 2011; 3: 897-909.
[10] Haghighipour N, Heidarian S, Shokrgozar MA, Amirizadeh N. Differential effects of cyclic uniaxial stretch on human mesenchymal stem cell into skeletal muscle cell. Cell Biology International 2012; 36: 669-675.
[11] Akimoto T, Ushida T, Miyaki S, Tateishi T, Fukubayashi T. Mechanical stretch is a down-regulatory signal for differentiation of C2C12 myogenic cells. Materials Science and Engineering C 2001; 17: 75-78.
[12] Boonen KJM, Langelaan MLP, Polak RB, van der Schaft DWJ, Baaijens FPT, Post MJ. Effects of a combined mechanical stimulation protocol: Value for skeletal muscle tissue engineering. Journal of Biomechanics 2010; 43: 1514-1521.
[13] De Deyne PG. Formation of sarcomeres in developing myotubes: role of mechanical stretch and contractile activation. Am. J. Physiol. Cell. Physiol 2000; 279: C1801-C1811.
[14] Liao I-C, Liu JB, Bursac N, Leong KW. Effect of Electromechanical Stimulation on the Maturation of Myotubes on Aligned Electrospun Fibers. Cellular and Molecular Bioengineering 2008; 1(2-3): 133-145.

4.8 Appendix

MLC Promoter and Luciferase Plasmid DNA

ORIGIN

1 ttgtacaaag tggttgatat ccagcacagt ggcggccgct cgagtctaga gggcccgcgg

61 ttcgaaggta agcctatccc taaccctctc ctcggtctcg attctacgcg taccggttag

121 taatgatcga caatcaacct ctggattaca aaatttgtga aagattgact ggtattctta

181 actatgttgc tccttttacg ctatgtggat acgctgcttt aatgcctttg tatcatgcta

241 ttgcttcccg tatggctttc attttctcct ccttgtataa atcctggttg ctgtctcttt

301 atgaggagtt gtggcccgtt gtcaggcaac gtggcgtggt gtgcactgtg tttgctgacg

361 caacccccac tggttggggc attgccacca cctgtcagct cctttccggg actttcgctt

421 tccccctccc tattgccacg gcggaactca tcgccgcctg ccttgcccgc tgctggacag

481 gggctcggct gttgggcact gacaattccg tggtgttgtc ggggaagctg acgtcctttc

541 catggctgct cgcctgtgtt gccacctgga ttctgcgcgg gacgtccttc tgctacgtcc

601 cttcggccct caatccagcg gaccttcctt cccgcggcct gctgccggct ctgcggcctc

661 ttccgcgtct tcgccttcgc cctcagacga gtcggatctc cctttgggcc gcctccccgc

721 ctggcgatgg tacctaccgg gtaggggagg cgcttttccc aaggcagtct ggagcatgcg

781 ctttagcagc cccgctgggc acttggcgct acacaagtgg cctctggcct cgcacacatt

841 ccacatccac cggtaggcgc caaccggctc cgttctttgg tggccccttc gcgccacctt

901 ctactcctcc cctagtcagg aagttccccc ccgccccgca gctcgcgtcg tgcaggacgt

961 gacaaatgga agtagcacgt ctcactagtc tcgtgcagat ggacagcacc gctgagcaat

1021 ggaagcgggt aggcctttgg ggcagcggcc aatagcagct ttgctccttc gctttctggg

1081 ctcagaggct gggaaggggt gggtccgggg gcgggctcag gggcgggctc aggggcgggg

1141 cgggcgcccg aaggtcctcc ggaggcccgg cattctgcac gcttcaaaag cgcacgtctg

1201 ccgcgctgtt ctcctcttcc tcatctccgg gcctttcgac tctagacacg tgttgacaat

1261 taatcatcgg catagtatat cggcatagta taatacgaca aggtgaggaa ctaaaccatg

1321 gccaagcctt tgtctcaaga agaatccacc ctcattgaaa gagcaacggc tacaatcaac

1381 agcatcccca tctctgaaga ctacagcgtc gccagcgcag ctctctctag cgacggccgc

1441 atcttcactg gtgtcaatgt atatcatttt actgggggac cttgtgcaga actcgtggtg

1501 ctgggcactg ctgctgctgc ggcagctggc aacctgactt gtatcgtcgc gatcggaaat

1561 gagaacaggg gcatcttgag cccctgcgga cggtgccgac aggtgcttct cgatctgcat

1621 cctgggatca aagccatagt gaaggacagt gatggacagc cgacggcagt tgggattcgt

1681 gaattgctgc cctctggtta tgtgtgggag ggctaagcac aattcgagct cggtaccttt

1741 aagaccaatg acttacaagg cagctgtaga tcttagccac tttttaaaag aaaaggggg

1801 actggaaggg ctaattcact cccaacgaag acaagatctg ctttttgctt gtactgggtc

1861 tctctggtta gaccagatct gagcctggga gctctctggc taactaggga acccactgct

1921 taagcctcaa taaagcttgc cttgagtgct tcaagtagtg tgtgcccgtc tgttgtgtga

1981 ctctggtaac tagagatccc tcagaccctt ttagtcagtg tggaaaatct ctagcagtag

2041 tagttcatgt catcttatta ttcagtattt ataacttgca aagaaatgaa tatcagagag

2101 tgagaggaac ttgtttattg cagcttataa tggttacaaa taaagcaata gcatcacaaa

2161 tttcacaaat aaagcatttt tttcactgca ttctagttgt ggtttgtcca aactcatcaa

2221 tgtatcttat catgtctggc tctagctatc ccgcccctaa ctccgcccat cccgccccta

2281 actccgccca gttccgccca ttctccgccc catggctgac taatttttt tatttatgca

2341 gaggccgagg ccgcctcggc ctctgagcta ttccagaagt agtgaggagg ctttttgga

2401 ggcctaggga cgtacccaat tcgccctata gtgagtcgta ttacgcgcgc tcactggccg

2461 tcgttttaca acgtcgtgac tgggaaaacc ctggcgttac ccaacttaat cgccttgcag

2521 cacatccccc tttcgccagc tggcgtaata gcgaagaggc ccgcaccgat cgcccttccc

2581 aacagttgcg cagcctgaat ggcgaatggg acgcgccctg tagcggcgca ttaagcgcgg

2641 cgggtgtggt ggttacgcgc agcgtgaccg ctacacttgc cagcgcccta gcgcccgctc

2701 ctttcgcttt cttcccttcc tttctcgcca cgttcgccgg ctttccccgt caagctctaa

2761 atcgggggct ccctttaggg ttccgattta gtgctttacg gcacctcgac cccaaaaaac

2821 ttgattaggg tgatggttca cgtagtgggc catcgccctg atagacggtt tttcgccctt

2881 tgacgttgga gtccacgttc tttaatagtg gactcttgtt ccaaactgga acaacactca

2941 accctatctc ggtctattct tttgatttat aagggatttt gccgatttcg gcctattggt

3001 taaaaaatga gctgatttaa caaaaattta acgcgaattt taacaaaata ttaacgctta

3061 caatttaggt ggcacttttc ggggaaatgt gcgcggaacc cctatttgtt tatttttcta

3121 aatacattca aatatgtatc cgctcatgag acaataaccc tgataaatgc ttcaataata

3181 ttgaaaaagg aagagtatga gtattcaaca tttccgtgtc gcccttattc cctttttgc

3241 ggcattttgc cttcctgttt ttgctcaccc agaaacgctg gtgaaagtaa aagatgctga

3301 agatcagttg ggtgcacgag tgggttacat cgaactggat ctcaacagcg gtaagatcct

3361 tgagagtttt cgccccgaag aacgttttcc aatgatgagc acttttaaag ttctgctatg

3421 tggcgcggta ttatcccgta ttgacgccgg gcaagagcaa ctcggtcgcc gcatacacta

3481 ttctcagaat gacttggttg agtactcacc agtcacagaa aagcatctta cggatggcat

3541 gacagtaaga gaattatgca gtgctgccat aaccatgagt gataacactg cggccaactt

3601 acttctgaca acgatcggag gaccgaagga gctaaccgct tttttgcaca acatggggga

3661 tcatgtaact cgccttgatc gttgggaacc ggagctgaat gaagccatac caaacgacga

3721 gcgtgacacc acgatgcctg tagcaatggc aacaacgttg cgcaaactat taactggcga

3781 actacttact ctagcttccc ggcaacaatt aatagactgg atggaggcgg ataaagttgc

3841 aggaccactt ctgcgctcgg cccttccggc tggctggttt attgctgata aatctggagc

3901 cggtgagcgt gggtctcgcg gtatcattgc agcactgggg ccagatggta agccctcccg

3961 tatcgtagtt atctacacga cggggagtca ggcaactatg gatgaacgaa atagacagat

4021 cgctgagata ggtgcctcac tgattaagca ttggtaactg tcagaccaag tttactcata

4081 tatactttag attgatttaa aacttcattt ttaatttaaa aggatctagg tgaagatcct

4141 ttttgataat ctcatgacca aaatccctta acgtgagttt tcgttccact gagcgtcaga

4201 ccccgtagaa aagatcaaag gatcttcttg agatcctttt tttctgcgcg taatctgctg

4261 cttgcaaaca aaaaaaccac cgctaccagc ggtggtttgt ttgccggatc aagagctacc

4321 aactcttttt ccgaaggtaa ctggcttcag cagagcgcag ataccaaata ctgttcttct

4381 agtgtagccg tagttaggcc accacttcaa gaactctgta gcaccgccta catacctcgc

4441 tctgctaatc ctgttaccag tggctgctgc cagtggcgat aagtcgtgtc ttaccgggtt

4501 ggactcaaga cgatagttac cggataaggc gcagcggtcg ggctgaacgg ggggttcgtg

4561 cacacagccc agcttggagc gaacgaccta caccgaactg agatacctac agcgtgagct

4621 atgagaaagc gccacgcttc ccgaagggag aaaggcggac aggtatccgg taagcggcag

4681 ggtcggaaca ggagagcgca cgagggagct tccagggga aacgcctggt atctttatag

4741 tcctgtcggg tttcgccacc tctgacttga gcgtcgattt ttgtgatgct cgtcaggggg

4801 gcggagccta tggaaaaacg ccagcaacgc ggccttttta cggttcctgg ccttttgctg

4861 gccttttgct cacatgttct ttcctgcgtt atcccctgat tctgtggata accgtattac

4921 cgcctttgag tgagctgata ccgctcgccg cagccgaacg accgagcgca gcgagtcagt

4981 gagcgaggaa gcggaagagc gcccaatacg caaaccgcct ctccccgcgc gttggccgat

5041 tcattaatgc agctggcacg acaggtttcc cgactggaaa gcgggcagtg agcgcaacgc

5101 aattaatgtg agttagctca ctcattaggc accccaggct ttacacttta tgcttccggc

5161 tcgtatgttg tgtggaattg tgagcggata acaatttcac acaggaaaca gctatgacca

5221 tgattacgcc aagcgcgcaa ttaaccctca ctaaagggaa caaaagctgg agctgcaagc

5281 ttaatgtagt cttatgcaat actcttgtag tcttgcaaca tggtaacgat gagttagcaa

5341 catgccttac aaggagagaa aaagcaccgt gcatgccgat tggtggaagt aaggtggtac

5401 gatcgtgcct tattaggaag gcaacagacg ggtctgacat ggattggacg aaccactgaa

5461 ttgccgcatt gcagagatat tgtatttaag tgcctagctc gatacataaa cgggtctctc

5521 tggttagacc agatctgagc ctgggagctc tctggctaac tagggaaccc actgcttaag

5581 cctcaataaa gcttgccttg agtgcttcaa gtagtgtgtg cccgtctgtt gtgtgactct

5641 ggtaactaga gatccctcag acccttttag tcagtgtgga aaatctctag cagtggcgcc

5701 cgaacaggga cttgaaagcg aaagggaaac cagaggagct ctctcgacgc aggactcggc

5761 ttgctgaagc gcgcacggca agaggcgagg ggcggcgact ggtgagtacg ccaaaaattt

5821 tgactagcgg aggctagaag gagagagatg ggtgcgagag cgtcagtatt aagcgggggga

5881 gaattagatc gcgatgggaa aaaattcggt taaggccagg gggaaagaaa aaatataaat

5941 taaaacatat agtatgggca agcagggagc tagaacgatt cgcagttaat cctggcctgt

6001 tagaaacatc agaaggctgt agacaaatac tgggacagct acaaccatcc cttcagacag

6061 gatcagaaga acttagatca ttatataata cagtagcaac cctctattgt gtgcatcaaa

6121 ggatagagat aaaagacacc aaggaagctt tagacaagat agaggaagag caaaacaaaa

6181 gtaagaccac cgcacagcaa gcggccgctg atcttcagac ctggaggagg agatatgagg

6241 gacaattgga gaagtgaatt atataaatat aaagtagtaa aaattgaacc attaggagta

6301 gcacccacca aggcaaagag aagagtggtg cagagagaaa aaagagcagt gggaatagga

6361 gctttgttcc ttgggttctt gggagcagca ggaagcacta tgggcgcagc gtcaatgacg

6421 ctgacggtac aggccagaca attattgtct ggtatagtgc agcagcagaa caatttgctg

6481 agggctattg aggcgcaaca gcatctgttg caactcacag tctggggcat caagcagctc

6541 caggcaagaa tcctggctgt ggaaagatac ctaaaggatc aacagctcct ggggatttgg

6601 ggttgctctg gaaaactcat ttgcaccact gctgtgcctt ggaatgctag ttggagtaat

6661 aaatctctgg aacagatttg gaatcacacg acctggatgg agtgggacag agaaattaac

6721 aattacacaa gcttaataca ctccttaatt gaagaatcgc aaaaccagca agaaaagaat

6781 gaacaagaat tattggaatt agataaatgg gcaagtttgt ggaattggtt taacataaca

6841 aattggctgt ggtatataaa attattcata atgatagtag gaggcttggt aggtttaaga

6901 atagtttttg ctgtactttc tatagtgaat agagttaggc agggatattc accattatcg

6961 tttcagaccc acctcccaac cccgagggga cccgacaggc ccgaaggaat agaagaagaa

7021 ggtggagaga gagacagaga cagatccatt cgattagtga acggatctcg acggtatcga

7081 ttaactttta aaagaaaagg ggggattggg gggtacagtg caggggaaag aatagtagac

7141 ataatagcaa cagacataca aactaaagaa ttacaaaaac aaattacaaa aattcaaaat

7201 tttatcgatg tcgacgttaa cgctagtgat atcaactttg tatagaaaag ttggctccga

7261 attcgccctt ggatccgagc tttaagatac aatttatttt ttccatgtgg aaaggtttag

7321 tgaaaggaca agacaaggga gagggatgag agaaagaaga agagtaggaa agagaagagc

7381 ccgccatgag catgtgaaga gaaggggagg ggagtgggga gagaagggac aaaaggggaa

7441 aaggggagga gcaagagtta agacacaatt taagtctcca gttaaataat aatttcattt

7501 ctaaaaagaa ataaattttt atatgcttag acttcaaatg tcattttgag acaaaaaaat

7561 cagcacataa tgtattttgt gaggaaggta acttgaagat ggtttaaaaa caaacttgaa

7621 aatatttgct tatacagcac aggcttttga aaagttattt ttaaaagatg aggaattagg

7681 cacctgttgc ttcgccagct ggtggggatt ttaaaaatga cgatcactct tctgcctgcg

7741 cagctccatt tttgcacctg ctgcgacttg agttatgagc ggttcacaca tggtaattta

7801 ataaggttag gtcccatgac agtgtgctga agttagcccg tggggacagt taaagcacta

7861 ttataaaatc ttgagaggaa agcgttatac acaaggctca aaacgaacaa tttataccgc

7921 acagacatca tgcttttcta tcttgaaaaa aatgtaaaga catgtacacc acagatcaaa

7981 aaaaaaaaaa aaagagccct ctataattaa gactacgtgt agcagtcatt ttctctacac

8041 tgtgaccttt atgcttctga aaatactttt attttagaga gggggcaggg cttctcgtgt

8101 aatgtctgtc ctggaactct ttctgtagag taggtagcct caaactcaga gatacatctt

8161 cctctggctt ccaagggctc tgggattaat agcggatcct ctagagtcga ggaattcaat

8221 tccatactca gaacccatta atgtgaaaga agagctgtag cttcacgcag ttgtcctctg

8281 acatccacat gcaaactgta cccacacgtg tgcattgcac aaacacacac acatacatac

8341 acacatacaa ctgtgatgat tgataattat tatataataa ttaatgatga taatactatt

8401 taaatggcta ttaacaaacg ttagaatgac actggacgat aatagaattt caataccctc

8461 tctggtgaaa cttgtcactt aggaacttat aaccactggt tttcatgagt tgctttttag

8521 cttgttttca aggcagggtc tcagttggta gctcaggctg tcctgaaact cacttgtaga

8581 ccagactgac cttgaactca cagagaagcc gtttgtctct gacccaggta ctgggattaa

8641 agatatacac aaatacaccc agttttgggt ttcatatatt actttatatg agtctaacct

8701 tgcaaactgg aaaccaagga caaaactaag aaaaaacaaa tatcaaattg ccagcaaaac

8761 atgcacagta ttgataatta cgtctttttt aaattatttc cctaaaaatg tatttgtccc

8821 tctagcatgg atataagatt aaggagacaa ataattctat ttcatgtcat ttagaagaca

8881 atgggctaat tgcagactca atcaaaaact aatttaccat tcttcattaa attgtacaga

8941 aaaatcaggt tataggaaat aatttaaatt ttaaatttag ttttctttag catagggaca

9001 cagacataga gggaggcaag gagagacaga ctgtactccc tagaaaggaa agcacattag

9061 acctggtgga ctttccttat acgtctgctt tttatttta aacactacca gtgacctctt

9121 tgctgaccaa cattttcttg caaatcatgg ccaaggaggg agggcatgag ccgtgaagaa

9181 gctgggtgaa agttggtaat gcctcagcca agatccaagt tgaaattgaa ccggtaaagt

9241 ttcttaggaa ggaaaaaaaa aaaaagattt acagcttcaa cagaactgta attctaccaa

9301 gaaaaaggta cgtctatcag ctgtcaccaa accaaccatg gctggctttg tcgtgcttct

9361 ttttccttta tagatagaag tggaggggaa gaagaaagaa aaaaaaaaag agagagagag

9421 aagaagaagc aagaggcatt caaaaaactt aaggaagccc tgacccttta gactccattt

9481 atagtctgag cccgaatgcc acccccctgg acaagtgaac cgtccaatcc agccgcgtgt

9541 gtcaaggttc tattaggcac taagagaaat atatatgcat gcccttatac cattcaacac

9601 tctgggtcca ccctccagac gctgggctgc gggtcaagcg agccaccact gctcttccaa

9661 gtgtcatttt gacaggttct tctggaggag atccttcttt tgttccaagg gcgaattcga

9721 cccaagtttg tacaaaaaag caggctccgc ggccgccccc ttcaccatgg gagtcaaagt

9781 tctgtttgcc ctgatctgca tcgctgtggc cgaggccaag cccaccgaga acaacgaaga

9841 cttcaacatc gtggccgtgg ccagcaactt cgcgaccacg gatctcgatg ctgaccgcgg

9901 gaagttgccc ggcaagaagc tgccgctgga ggtgctcaaa gagatggaag ccaatgcccg

9961 gaaagctggc tgcaccaggg gctgtctgat ctgcctgtcc cacatcaagt gcacgcccaa

10021 gatgaagaag ttcatcccag gacgctgcca cacctacgaa ggcgacaaag agtccgcaca

10081 gggcggcata ggcgaggcga tcgtcgacat tcctgagatt cctgggttca aggacttgga

10141 gcccatggag cagttcatcg cacaggtcga tctgtgtgtg gactgcacaa ctggctgcct

10201 caaagggctt gccaacgtgc agtgttctga cctgctcaag aagtggctgc cgcaacgctg

10261 tgcgaccttt gccagcaaga tccagggcca ggtggacaag atcaaggggg ctggtggtga

10321 cgcggccgct actaattttt cattattaaa gcaagcagga gatgttgaag aaaatcccgg

10381 gcccatggtg agcaagggcg aggagctgtt caccggggtg gtgcccatcc tggtcgagct

10441 ggacggcgac gtaaacggcc acaagttcag cgtgtccggc gagggcgagg gcgatgccac

10501 ctacggcaag ctgaccctga agttcatctg caccaccggc aagctgcccg tgccctggcc

10561 caccctcgtg accaccctga cctacggcgt gcagtgcttc agccgctacc ccgaccacat

10621 gaagcagcac gacttcttca agtccgccat gcccgaaggc tacgtccagg agcgcaccat

10681 cttcttcaag gacgacggca actacaagac ccgcgccgag gtgaagttcg agggcgacac

10741 cctggtgaac cgcatcgagc tgaagggcat cgacttcaag gaggacggca acatcctggg

10801 gcacaagctg gagtacaact acaacagcca caacgtctat atcatggccg acaagcagaa

10861 gaacggcatc aaggtgaact tcaagatccg ccacaacatc gaggacggca gcgtgcagct

10921 cgccgaccac taccagcaga acacccccat cggcgacggc cccgtgctgc tgcccgacaa

10981 ccactacctg agcacccagt ccgccctgag caaagacccc aacgagaagc gcgatcacat

11041 ggtcctgctg gagttcgtga ccgccgccgg gatcactctc ggcatggacg agctgtacaa

11101 gtacccatac gatgtccctg attatgcttg ataatagaag ggtgggcgcg ccgacccagc

11161 tttc

CHAPTER 5: CONCLUSIONS AND FUTURE PROSPECTUS

5.1 Project Summary

This project explored the feasibility of engineering a biocompatible actuator for regenerating skeletal muscle tissue. The project was approached in three main phases: 1) identifying a potentially biocompatible, electroactive material and optimizing the movement of that material, 2) developing a set of conductive guidance cues with a low overall stiffness to augment the biocompatibility of the actuator, and 3) testing the feasibility of the composite scaffold for promoting the proliferation and differentiation of myoblasts under electrical stimulation. This section will give a succinct summary of the achievements and limitations of the project.

In the preliminary experiments for Aim 1, we tested a variety of materials in an array of combinations to produce a viable electroactive actuator. The combination of poly(ethylene glycol) (PEGDA) and acrylic acid (AA) produced an actuator that displayed reversible and repeatable movement. We build an apparatus and developed a protocol to quantify the movement of these hydrogels while applying a constant 20 V of stimulation under various conditions. We were able to optimize the movement speed and contractile force of these hydrogels with respect to concentration, ratio of components, and geometry of the samples. However, the maximum contractile stress produced, 297 Pa to 821 Pa, fell short of the estimated contractile stress of native muscle fibers, 60 kPa to 380 kPa [1-4]. In addition, the results of the biocompatibility tests were less than optimal. While myoblast cells survived on the hydrogel samples with lower relative concentrations of acrylic acid, the myoblasts failed to fuse into myotubes in a reasonable timeframe. This result motivated the development of conductive guidance cues in Aim 2.

In similar fashion to Aim 1, we had investigated a large variety of materials to form a conductive, fibrous scaffold that would provide guidance cues for differentiating myoblasts in Aim 2. The criterion for selecting a suitable material included the feasibility of electrospinning, conductivity, mechanical properties (stiffness) and biocompatibility. We decided to synthesize a copolymer of polycaprolactone (PCL) and polypyrrole (PPy) based on favorable properties for both components: PCL has a relatively low stiffness and is easy to electrospun; PPy is a conductive polymer that has good reported biocompatibility. This copolymer was combined with pure PCL and electrospun into fibrous scaffolds with various properties depending on the relative concentration of copolymer. The addition of the PPy-PCL copolymer did not significantly change the stiffness of the resulting fibrous scaffolds when compared to a scaffold of pure PCL. Although the scaffolds made from PPy-PCL exhibited lower conductivity than expected, the cell studies indicated that myoblasts have a clear preference for scaffolds with PPy-PCL compared with scaffolds made from only PCL. Myoblasts exhibited higher attachment, more proliferation, higher numbers of myotubes formed, and a higher fusion index on scaffolds made with PPy-PCL as compared with scaffolds made of PCL. In the context of the overall project, the conductivity of these scaffolds was too low to use them as “biocompatible electrodes”. However, the excellent biocompatibility and relatively low stiffness of the PPy-PCL scaffolds made them suitable for the purposes of Aim 3.

In Aim 3, the goal was to combine the actuator from Aim 1 and the biocompatible fibers from Aim 2 to produce an actuator which could easily support cell attachment, proliferation, and differentiation. The produced composite scaffold could be seeded with myoblasts, and electrical stimulation could be applied while the myoblasts are

developing. The working hypothesis was that there is an electrical stimulation pattern which will produce movement in the actuator portion of the composite while providing beneficial electrical stimulation to the developing myoblasts. Further, it was our hypothesis that this combined electrical and mechanical stimulation would have a positive impact on the differentiation of myoblasts. Two different versions of the composite scaffold were fabricated, and two different electrical stimulation patterns were selected based on the minimal stimulation needed for the hydrogel portion to move and previous studies in the literature (see Aim 3). The electrical stimulation patterns seemed to have a net negative effect on the survival of myoblasts on all groups, but enough cells survived to evaluate their differentiation. Based on the results of using a cell line which reports on the production of myosin light chain (associated with differentiation), there was no difference in the progress of differentiation between groups exposed to electrical stimulation and the control groups which received no stimulation. Further, the hydrogel samples and composite structures exhibited very little movement under these electrical stimulation patterns. Thus, it seems that the set of electrical stimulation patterns that produce actuation in this hydrogel and the set of electrical stimulation patterns which are ideal for stimulating myoblasts are either mutually exclusive or there is very little overlap between them. However, there may be a viable set of experiments to evaluate the effect of electrical stimulation on cells growing on the conductive, fibrous scaffolds alone.

5.2 Next Steps for Progress of the Project

This project has developed a set of protocols to evaluate the potential of materials to serve as biocompatible actuators to aid in the regeneration of muscle tissue. Perhaps the simplest way to improve this project is to find or generate a new material to produce

actuation in an electric field. It may be possible to achieve this by duplicating the key elements of an ionic electroactive polymer in a novel way. Ionic electroactive polymers are characterized by side chains with a highly polar or charged entity attached to the main polymer backbone. We achieved this configuration by chemically binding acrylic acid to a poly(ethylene glycol) backbone. The carboxylic acid groups on the acrylic acid molecules provided the highly polar entities which allowed movement to occur. It may be possible to synthesize a new ionic electroactive polymer with highly charged side chains capable of facilitating stronger and faster movement. This line of experimentation will likely require the help of an experienced chemist, but the protocol for evaluating and comparing the movement of various actuators has already been developed.

In contrast, it is possible that the movement strength and speed of the actuator can be improved by developing a more sophisticated way to bind a "biocompatible electrode" to the hydrogel samples. The movement speed of ionic electroactive polymers is proportional to the strength of the electric field, which can be enhanced by increasing the voltage or reducing the distance through which the voltage is applied. While increasing the voltage is less than ideal because it hampers biocompatibility, it may be possible to reduce the distance through which the voltage is applied by fusing a biocompatible electrode to the surface of the ionic electroactive polymer. This concept has already been proved with the use of ionic polymer-metal composites (IPMCs). IPMCs are essentially composed of an ionic electroactive polymer with deposited metal particles on the surface. The electric field can then be applied directly to the metal particles on the surface of the construct, and the electric field strength is greatly enhanced. It may be possible to develop a type of "biocompatible electrode" made of a highly conductive polymer which

can be fixed to the outside of an ionic electroactive polymer and function in a similar way. We originally thought that this was a possibility, but the conductivity of the PPy-PCL copolymer scaffolds was too low to function as an electrode. Thus, this domain of experimentation would have to explore the use of new conductive materials.

Another possibility for progress in this project is to develop a new conductive polymer with relatively high conductivity and low enough stiffness to move with the composite actuator. Most strategies for enhancing the conductivity of scaffolds also significantly increase scaffold stiffness. For the purposes of this project, relatively high scaffold stiffness is undesirable because the stiffness would impede the movement of the composite actuator. The use of polymer synthesis techniques may be required to make a new copolymer with suitable conductivity and mechanical properties.

Finally, this project may benefit from the use of more sophisticated electrical stimulation patterns. We were somewhat limited in the electrical stimulation patterns that we could use by the limits of our function generator. In this project, we utilized a simplified version of stimulation patterns from the literature, which was sufficient for a proof of concept experiment. However, in the future, more sophisticated stimulation patterns may be necessary to properly stimulation the myoblasts while the composite actuator moves. Previous studies have devoted significant resources just to building a device with such capabilities [5], and it may be necessary to achieve better results in this project.

5.3 Challenges with Clinical Applicability

A number of challenges remain to be addressed before this project can approach clinical relevance. The biggest obstacle to overcome likely involves the application of

voltage within the human body. Electrolysis is the decomposition of water molecules into molecules of hydrogen and oxygen gas, and this process can occur with as little as 1.23 V of electricity. While human cells can tolerate electrolysis reasonably well *in vitro*, the production and build-up of gases in a closed area of the human body is dangerous. In order to avoid electrolysis, all internal application of voltage must be run with less than 1.23 V, or the electrical stimulation must be delivered from the outside of the body. All of the experiments completed in this project indicate that 1.23 V is too low to cause significant movement of an ionic electroactive polymer. Thus, significant improvements in the design of the actuator and/or composite, as detailed earlier, need to occur before internal stimulation can be considered during clinical use. External stimulation may be a viable alternative for some patients, especially after the commercialization of various electronic muscle stimulation (EMS) products. However, these products rarely work for obese patients due to the high impedance of fat tissue. Also, scar tissue may complicate the process by increasing impedance in some patients.

In its current form, this project proposes a composite scaffold made of multiple biodegradable materials, but this may not be ideal for producing homogeneous muscle tissue. The PEGDA/AA hydrogel and PPy-PCL copolymer are composed of biodegradable components, but these components may degrade at different rates. It is not clear that the composite scaffold will facilitate uniform muscle fiber development across its surface. A more uniform scaffold would be more likely to produce homogenous muscle tissue as it degrades, but a uniform scaffold may not be possible to implement with the desired functionality.

Another issue related to scaffold degradation is the simultaneous optimization of contractile strength and degradation rate. In theory, this composite scaffold is designed to degrade over time as new muscle tissue forms. However, contractile strength will also diminish as the composite degrades. It may be the case that contractile strength needs to be diminished to provide the appropriate degradation rate, or vice versa. A robust scaffold that has a high contractile strength may be more appropriate as an exoskeleton designed to augment muscle contractile force from outside the body rather than as an implant.

Like all implants, this scaffold must eventually address the issues of proper vascularization and innervation over time. New vascularization needs to grow rather quickly after implantation to avoid a lack of oxygen and nutrients for developing muscle fibers. In addition, the newly formed muscle tissue must be properly innervated to allow for conscious control with the nervous system. It is possible that innervation can be achieved by ion impulses spreading from neighboring muscle depending on the size of the muscle defect, but steps will at least need to be taken to ensure proper vascularization.

Despite the previously mentioned challenges, there is some evidence that implantable scaffolds which provide guidance cues to proliferating satellite cells (myoblasts) can regenerate muscle tissue. Decellularized urinary bladder tissue from pigs (xenografts) has been implemented successfully in clinical trials [6]. The study achieved functional improvements in 60% of the human patients treated. This study provides proof for the concept of implantable scaffolds providing the framework for cells to attach. Since decelluarized tissue is not conductive, it seems that conductivity is not required for the regeneration of skeletal muscle tissue. The more important factors for regenerating

skeletal muscle tissue are likely facilitating cell attachment and providing very precise scaffolding for forming muscle fibers.

5.4 Potential Side Projects Stemming from this Work

Progress in academia is often non-linear. Projects can be unsuccessful, but the results can spur the start of new projects. In that spirit, there are a few "side projects" that can stem from this work and be of use in other domains.

The detached power supply developed in the lab of Dr. Najafizadeh, mostly by Yi Huang, can be used to power other types of implants [7]. Most implantable electronic devices, such as pacemakers, are powered by batteries which must be continually replaced with additional surgeries. Providing a power source that can recharge devices through the skin would be immensely beneficial by saving on the costs of recurring surgeries.

Another interesting domain of inquiry involves the relationship between the conductivity of a substrate and the cell-material interaction. It would be interesting to determine the lowest concentration of conductive particles (percolation threshold) needed to enhance cell attachment. This information could inform future scaffold design for both muscle and nervous tissue. In addition, it would be useful to discover what cell processes are activated when cells come into contact with a conductive polymer as opposed to a nonconductive polymer. It is possible that all the interactions are confined to the cell surface, but knowing the signal transduction pathway activated by a conductive substrate would be useful for the domain of scaffold research.

The "soft" actuator developed in this project may have other purposes as well. Light-weight actuators are more useful for certain applications than heavier mechanical

actuators. Possible applications for “soft” actuators include biomimetic sensors, actuators for light-weight robotics, and animated toys.

The cell line developed in this project as a myosin light chain reporter can be used by other researchers studying various types of muscle. The cell line can evaluate other scaffolds and treatments for regenerating muscle tissue in a quick and cost effective way. The best use of the cell line is likely as a screening tool to quickly evaluate potential treatments/conditions for further study. However, the stability and longevity of the cell line will have to be quantified before widespread use.

5.5 Final Thoughts

The results of the experiments performed for this project provide a baseline to be improved upon in future iterations. This project also provides a set of protocols to evaluate scaffolds and actuators for regenerating skeletal muscle tissue. A potential guiding principal for the future development of these ideas is to reduce complexity wherever possible. Each additional component to a system adds new complexity and potential issues. It is telling that a successful clinical trial for muscle regeneration utilized a decellularized xenograft scaffold with little processing [6]. Sometimes simple ideas provide a better solution.

5.6 References

[1] Close RI. Dynamic properties of fast and slow skeletal muscle of the rat after nerve cross-union. J. Physiol. (London) 1969; 204: 331-46.
[2] Burke RE, Tsairis P. Anatomy and innervation ratios in the motor units in cat gastrocnemius. J. Physiol 1973; 234: 769-5.
[3] Lannergren J, Westerblad H. The temperature dependence of isometric contraction of single, intact fibres dissected from a mouse foot muscle. J. Physiol 1987; 390: 285-93.
[4] Kanda K, Hashizume K. Factors causing difference in force output among motor units in the rat medial gastrocnemius muscle. J. Physiol 1992; 448: 677-95.

[5] Donnelly K, Khodabukus A, Philp A, Deldicque L, Dennis RG, Baar K. A Novel Bioreactor for Stimulating Skeletal Muscle *In Vitro*. Tissue Engineering: Part C 2010; 16(4): 711-718.
[6] Sicari BM, Rubin JP, Dearth CL, Wolf MT, Ambrosio F, Boninger M, Turner NJ, Weber DJ, Simpson TW, Wyse A, Brown EHP, Dziki JL, Fisher LE, Brown S, Badylak SF. An Acellular Biologic Scaffold Promotes Skeletal Muscle Formation in Mice and Humans with Volumetric Muscle Loss. Science Translational Medicine 2014; 6(234): 234-258.
[7] Huang Y, Browe D, Freeman J, Najafizadeh L. A Wirelessly Tunable Electrical Stimulator for Ionic Electroactive Polymers. IEEE Sensors Journal 2018; 18(5): 1930-1939.